Transportation Consortium of South-Central States

Solving Emerging Transportation Resiliency, Sustainability, and Economic Challenges through the Use of Innovative Materials and Construction Methods: From Research to Implementation

Toward Non-Corrosion and Highly Sustainable Structural Members by Using Ultra-High-Performance Materials for Transportation Infrastructure

Project No. 18STUTA01

Lead University: University of Texas at Arlington

Final Report

September 2019

Disclaimer

The contents of this report reflect the views of the authors, who are responsible for the facts and the accuracy of the information presented herein. This document is disseminated in the interest of information exchange. The report is funded, partially or entirely, by a grant from the U.S. Department of Transportation's University Transportation Centers Program. However, the U.S. Government assumes no liability for the contents or use thereof.

Acknowledgments

The high-strength basalt fiber-reinforced polymer (BFRP), glass fiber-reinforced polymer (GFRP), and steel bars used in this research were donated by New Energy Materials Corp., Composite Rebar Technologies, and MMFX, respectively. Their help is greatly appreciated.

TECHNICAL DOCUMENTATION PAGE

1. Project No.	2. Government Accession No.	3. Recipient's Catalog No.
18STUTA01		

4. Title and Subtitle	5. Report Date
Toward Non-Corrosion and Highly Sustainable Structural Members by Using Ultra-High-Performance Materials for Transportation Infrastructure	Sept. 2019
	6. Performing Organization Code
7. Author(s)	**8. Performing Organization Report No.**
PI: Shih-Ho Chao https://orcid.org/0000-0003-2679-7364 GRA: Ashish Karmacharya https://orcid.org/0000-0001-7517-7693	
9. Performing Organization Name and Address	**10. Work Unit No. (TRAIS)**
Transportation Consortium of South-Central States (Tran-SET) University Transportation Center for Region 6 3319 Patrick F. Taylor Hall, Louisiana State University, Baton Rouge, LA 70803	**11. Contract or Grant No.** 69A3551747106
12. Sponsoring Agency Name and Address	**13. Type of Report and Period Covered**
United States of America Department of Transportation Research and Innovative Technology Administration	Final Research Report Mar. 2018 – Mar. 2019
	14. Sponsoring Agency Code

15. Supplementary Notes

Report uploaded and accessible at Tran-SET's website (http://transet.lsu.edu/).

16. Abstract

This research focused on investigating a highly sustainable and efficient reinforced concrete structural member for future infrastructure by utilizing emerging high-performance materials. These materials include ultra-high-performance fiber-reinforced concrete (UHP-FRC) and corrosion-resistant high-strength fiber-reinforced polymer (FRP) bars. Four reduced scale UHP-FRC specimens were tested under large displacement reversals to prove the proposed new ductile-concrete strong-reinforcement (DCSR) design concept by fully utilizing these ultra-high-performance materials. Micro steel fibers were incorporated into three specimens and ultra-high molecular weight polyethylene fibers were blended into the fourth specimen. One specimen with ASTM A1035 MMFX high-strength steel rebars, one with high-strength glass fiber reinforced polymer (GFRP) rebars, and two with high-strength basalt fiber reinforced plastic (BFRP) rebars were tested. The beams had a reinforcement ratio of 14% to 15%. The test results concluded that the beams could sustain very large cyclic drift ratios without major damage in the UHP-FRC material, which provided ample shear strength and confinement to the reinforcement throughout the testing. Even with the high amount of reinforcement, UHP-FRC's superior ductility provided a very stable cyclic behavior up to some very large drift ratios. Because of the DCSR design, all specimens also exhibited a self-centering ability, which considerably reduces the residual displacement after being subjected to large displacement reversals. The test results also show that the high damage-resistance and self-centering characteristics of the proposed UHP-FRC flexural members can provide excellent resilience for building structures.

17. Key Words	18. Distribution Statement
UHP-FRC, FRP rebars, Self-centering, Ductility, Sustainability	No restrictions. This document is available through the National Technical Information Service, Springfield, VA 22161.

19. Security Classif. (of this report)	20. Security Classif. (of this page)	21. No. of Pages	22. Price
Unclassified	Unclassified	102	

Form DOT F 1700.7 (8-72) **Reproduction of completed page authorized.**

SI* (MODERN METRIC) CONVERSION FACTORS

APPROXIMATE CONVERSIONS TO SI UNITS

Symbol	When You Know	Multiply By	To Find	Symbol
		LENGTH		
in	inches	25.4	millimeters	mm
ft	feet	0.305	meters	m
yd	yards	0.914	meters	m
mi	miles	1.61	kilometers	km
		AREA		
in^2	square inches	645.2	square millimeters	mm^2
ft^2	square feet	0.093	square meters	m^2
yd^2	square yard	0.836	square meters	m^2
ac	acres	0.405	hectares	ha
mi^2	square miles	2.59	square kilometers	km^2
		VOLUME		
fl oz	fluid ounces	29.57	milliliters	mL
gal	gallons	3.785	liters	L
ft^3	cubic feet	0.028	cubic meters	m^3
yd^3	cubic yards	0.765	cubic meters	m^3
		NOTE: volumes greater than 1000 L shall be shown in m^3		
		MASS		
oz	ounces	28.35	grams	g
lb	pounds	0.454	kilograms	kg
T	short tons (2000 lb)	0.907	megagrams (or "metric ton")	Mg (or "t")
		TEMPERATURE (exact degrees)		
^oF	Fahrenheit	5 (F-32)/9 or (F-32)/1.8	Celsius	^oC
		ILLUMINATION		
fc	foot-candles	10.76	lux	lx
fl	foot-Lamberts	3.426	$candela/m^2$	cd/m^2
		FORCE and PRESSURE or STRESS		
lbf	poundforce	4.45	newtons	N
lbf/in^2	poundforce per square inch	6.89	kilopascals	kPa

APPROXIMATE CONVERSIONS FROM SI UNITS

Symbol	When You Know	Multiply By	To Find	Symbol
		LENGTH		
mm	millimeters	0.039	inches	in
m	meters	3.28	feet	ft
m	meters	1.09	yards	yd
km	kilometers	0.621	miles	mi
		AREA		
mm^2	square millimeters	0.0016	square inches	in^2
m^2	square meters	10.764	square feet	ft^2
m^2	square meters	1.195	square yards	yd^2
ha	hectares	2.47	acres	ac
km^2	square kilometers	0.386	square miles	mi^2
		VOLUME		
mL	milliliters	0.034	fluid ounces	fl oz
L	liters	0.264	gallons	gal
m^3	cubic meters	35.314	cubic feet	ft^3
m^3	cubic meters	1.307	cubic yards	yd^3
		MASS		
g	grams	0.035	ounces	oz
kg	kilograms	2.202	pounds	lb
Mg (or "t")	megagrams (or "metric ton")	1.103	short tons (2000 lb)	T
		TEMPERATURE (exact degrees)		
^oC	Celsius	1.8C+32	Fahrenheit	^oF
		ILLUMINATION		
lx	lux	0.0929	foot-candles	fc
cd/m^2	$candela/m^2$	0.2919	foot-Lamberts	fl
		FORCE and PRESSURE or STRESS		
N	newtons	0.225	poundforce	lbf
kPa	kilopascals	0.145	poundforce per square inch	lbf/in^2

TABLE OF CONTENTS

LIST OF FIGURES

LIST OF TABLES

ACRONYMS, ABBREVIATIONS, AND SYMBOLS

a	Depth of equivalent rectangular stress block
AASHTO	American Association of State Highway and Transportation Officials
ACI	American Concrete Institute
A_{sc}	Total area of non-prestressed compression longitudinal reinforcement
A_{st}	Total area of non-prestressed tension longitudinal reinforcement
ASTM	American Society for Testing and Materials
A615/A615M	Standard Specification for Deformed and Plain Carbon-Steel Bars for Concrete Reinforcement
A706/A706M	Standard Specification for Low-Alloy Steel Deformed and Plain Bars for Concrete Reinforcement
A1035/A1035M	Standard Specification for Deformed and Plain, Low-carbon, Chromium, Steel Bars for Concrete Reinforcement
b	Width of compression face
β_1	Factor relating depth of equivalent rectangular compressive stress block to depth of neutral axis.
BFRP	Basalt Fiber-Reinforced Polymer
c	Distance from extreme compression fiber to neutral axis
c_c	Clear cover of reinforcement
$C_{concrete}$	Compression force provided by concrete
CELB	Civil Engineering Laboratory Building
$C_{reinforcement}$	Compression force provided by reinforcement.
d	Distance from extreme compression fiber to centroid of longitudinal tension reinforcement
D	Drift ratio (%)
DAQ	Data Acquisition
DCSR	Ductile Concrete Strong Reinforcement

E_s	Modulus of elasticity of reinforcement
ε_{st}	Ultimate compressive strain of concrete
$\varepsilon_{rupture}$	Ultimate reinforcement rupture strain
ε_t	Net tensile strain in extreme layer of longitudinal tension reinforcement at nominal strength
ε_{ty}	Value of net tensile strain in the extreme layer of longitudinal tension reinforcement used to define a compression-controlled section
$f_c^{'}$	Compressive strength
f_{fu}	Tensile stress at rupture
FRP	Fiber-Reinforced Polymer
f_y	Reinforcement yield stress
GFRP	Glass Fiber-Reinforced Polymer
LVDT	Linear Variable Differential Transformer
M	Applied moment (kips-in.)
MAST	Multi-Axial Sub-assemblage Testing
MMFX	Martensitic Microcomposite Formable Steel
MTS	Material Testing System
P	Applied load (lbf)
PE	Ultra-high-molecular-weight Polyethylene
S	Distance from extreme compression fiber to centroid of longitudinal compression reinforcement.
S	Effective span (in.)
UHP-FRC	Ultra-High-Performance Fiber-Reinforced Concrete
UTA	University of Texas at Arlington
V	Net vertical displacement of the specimen (in.)

EXECUTIVE SUMMARY

The research objective is to develop highly sustainable and efficient reinforced concrete structural members for future infrastructure by utilizing emerging high-performance materials. These materials include ultra-high-performance fiber-reinforced concrete (UHP-FRC) and corrosion resistant high-strength fiber-reinforced polymer (FRP) bars and high-strength steel rebars. The new type of UHP-FRC flexural members were designed based on a newly developed design concept, ductile-concrete strong-reinforcement (DCSR), in which the ductile component is the concrete and the elastic component is the reinforcement. The advantages of using such design is to fully utilize the high compressive strength and ductility of UHP-FRC and minimize the cracking by reducing the elongation of reinforcement, thereby maintaining high stiffness of the members. Four specimens were tested under reversed cyclic loading. The proposed UHP-FRC flexural members have much larger stiffness and strength than conventional reinforced concrete members and can sustain very large drift ratios under reversed cyclic loading without major damage in the material. Because of the DCSR design concept, the reinforcement remains elastic thus providing a self-centering capability. This allows a very sustainable and resilient future structures subjected to major earthquake loadings. Four pilot UHP-FRC reduced scale flexural members, one with corrosion resistant high-strength steel rebars (100 ksi as per ASTM A1035), one with non-corrosive high-strength GFRP (glass, 90 ksi) rebars, and two with non-corrosive high-strength BFRP (Basalt, 147 ksi) rebars were tested at UT Arlington under large displacement reversals to prove the resilience of the proposed new DCSR design concept. All flexural members had a reinforcement ratio of 14%. The last two specimens were designed to have a smaller length-to-depth ratio to increase the shear force demand. Ultra-high-molecular-weight-polyethylene (UHMWPE) fibers (13 mm in length and 0.0015 mm in diameter with a tensile strength of 375 ksi) were used for specimen # 3. Meanwhile micro steel fibers (13 mm in length and 0.2 mm in diameter with a tensile strength of 399 ksi) were used for the other three specimens. Experimental results show that all flexural members sustained very large cyclic displacements without major damage to the UHP-FRC material, which provided ample shear strength and confinement to the reinforcement throughout the testing. Even with the high amount of reinforcement, UHP-FRC's superior ductility provided a very stable cyclic behavior up to very large drift ratios. All specimens also exhibited a self-centering ability, which considerably reduces the residual displacement (and resultant potential of collapse) after being subject to large displacements. This pilot testing also verified that very high damage resistant and self-centering characteristics of the proposed columns made of high-performance materials and designed by the DCSR concept can provide excellent resilience (which requires no repair work after major earthquakes) for building structures in earthquake-prone areas. Structural members such as columns are the most critical structural members providing collapse prevention and assuring the resilience of buildings in earthquake-prone areas. Their resilience and damage resistance against multiple strong excitations are critical to the resilience of earthquake-prone buildings and society. If successfully implemented, the results from this project are expected to directly impact society through enhanced safety of buildings that would otherwise collapse under earthquakes, hurricanes, and other life-threatening natural and manmade disasters. Consumers can also benefit from the short- and long-term cost savings gained by improving structural resiliency and extending the structures' lifetime. On a day-to-day basis, annual savings can be realized through reduced construction time, as well as fewer repairs and maintenance costs.

1. INTRODUCTION

Ultra-high-performance fiber-reinforced concrete (UHP-FRC) is a new generation of fiber-reinforced concrete which has ultra-high compressive strength (18–30 ksi; 10 to 12 ksi after 24 hours.) and ductility. A concrete with only ultra-high compressive strength is not suitable for structural application, even reinforced with mild reinforcing steel, as the very brittle nature can cause potential issues such as abrupt unpredictable failures and a minimum capability of stress redistribution. UHP-FRC was developed by changing the porous nature of conventional concrete through reducing dimensions of microcracking (or defects) in the concrete. This is achieved in UHP-FRC through a very low water to cementitious materials ratio (0.18 to 0.25) and a dense particle packing, which leads to almost no shrinkage or creep, making it very suitable for concrete members under long-term compression. The consequences of a very dense microstructure and low-water ratio results in enhanced compressive strength *(1)* and delayed liquid ingress *(2)*. Furthermore, the addition of steel or synthetic fibers (typically less than 3% by volume of concrete) improves the brittle nature of concrete by increasing the tensile cracking resistance, post-cracking strength, ductility, and energy absorption capacity. In terms of corrosion resistance, research has indicated that UHP-FRC has a much greater durability than conventional concrete due to its very dense microstructure *(3)*. This dense microstructure impedes the conductive chloride ions from coming into direct contact with the steel reinforcing bars, which protects the reinforcing bars from corrosion. Table 1 provides a comparison between typical conventional concrete and UHP-FRC.

Table 1. Comparison of typical conventional concrete and UHP-FRC (all data from UT Arlington research except Rapid Chloride Penetration Test).

Properties of Concrete	Conventional Concrete	UHP-FRC
Ultimate Compressive Strength	< 8,000 psi (55 MPa)	18,000 to 30,000 psi (124 to 207 MPa)
Early (24-hour) compressive strength	< 3000 psi (21 MPa)	10,000 – 12,000 psi (69 to 83 MPa)
Flexural Strength	< 670 psi (4.6 MPa)	2,500 to 6,000 psi (17 to 41 MPa)
Shear strength	< 180 psi (1.2 MPa)	> 600 psi (4.1 MPa)
Direct Tension	< 450 psi (3 MPa)	up to 1,450 psi (10 MPa)
Rapid Chloride Penetration Test ***(3)***	2000-4000 Coulombs passed	Negligible (< 100 Coulombs passed)
Ductility	Negligible	High ductility
Ultimate Compressive Strain, ε_{cu}	0.003	0.015 to 0.03
Confining	Negligible	High confining capability

Addition of fibers to the UHPC matrix decreases the brittleness and increases the compressive strength and maximum usable compressive strain. The UHP-FRC mix with 3% micro steel fibers *(4)* showed ultimate compressive strength at a strain of approximately 1.2-1.4% as shown in Figure 1 below.

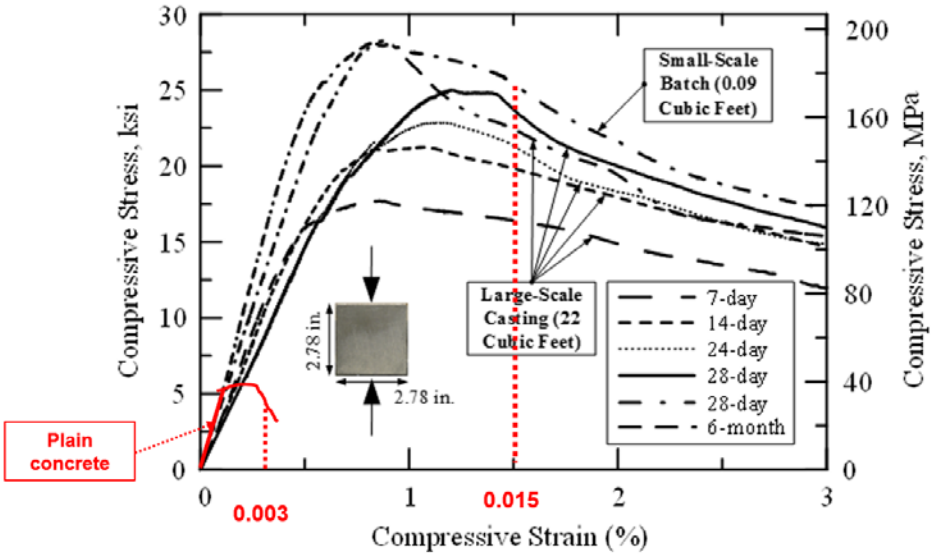

Figure 1. Compressive stress-strain behavior of UHP-FRC *(4)*.

Fiber-reinforced concrete (FRC) has been used for many decades; however, conventional FRC only enhances the post-cracking ductility, and its compressive strength is close to that of plain concrete (5 to 8 ksi). In other words, conventional FRC does not fundamentally change the micro-structure of concrete, but it has a greater residual tensile capacity and ductility after cracking. Research *(5)* shows that even a high-performance FRC column (an FRC with tensile strain-hardening behavior) has essentially the same failure mode as that of an RC column after FRC is crushed, which eventually leads to rebar buckling and fracture (Figure 2).

Figure 2. Failure pattern of RC column (left) *(6)* and HPFRC Column (right) *(6)* with a specified compressive strength of 8 ksi.

2. OBJECTIVES

The research objective is to develop highly sustainable and efficient reinforced concrete structural members for future infrastructure by utilizing emerging high-performance materials. These materials include ultra-high-performance fiber-reinforced concrete (UHP-FRC) and corrosion resistant high-strength fiber-reinforced polymer (FRP) and MMFX bars. The next generation structural members will have the sustainability and resiliency that are not previously available.

3. LITERATURE REVIEW

3.1. High Strength Steel Reinforcement

ASTM A1035 reinforcement has low carbon content and high chromium content as compared to ASTM A615/A615M steel. This makes the ASTM A1035 reinforcements high-strength and more corrosion resistant *(7)*. This reinforcement has seen its major use in bridge decks subjected to de-icing salts *(8)*.

Tensile Properties: The stress-strain curves for ASTM A1035/A1035M bars in Grades 100 (690) and 120 (830), ASTM A615/A615M bars in Grades 60 (420) and 75 (520) and ASTM A706/A706M bars are shown in the Figure 3.

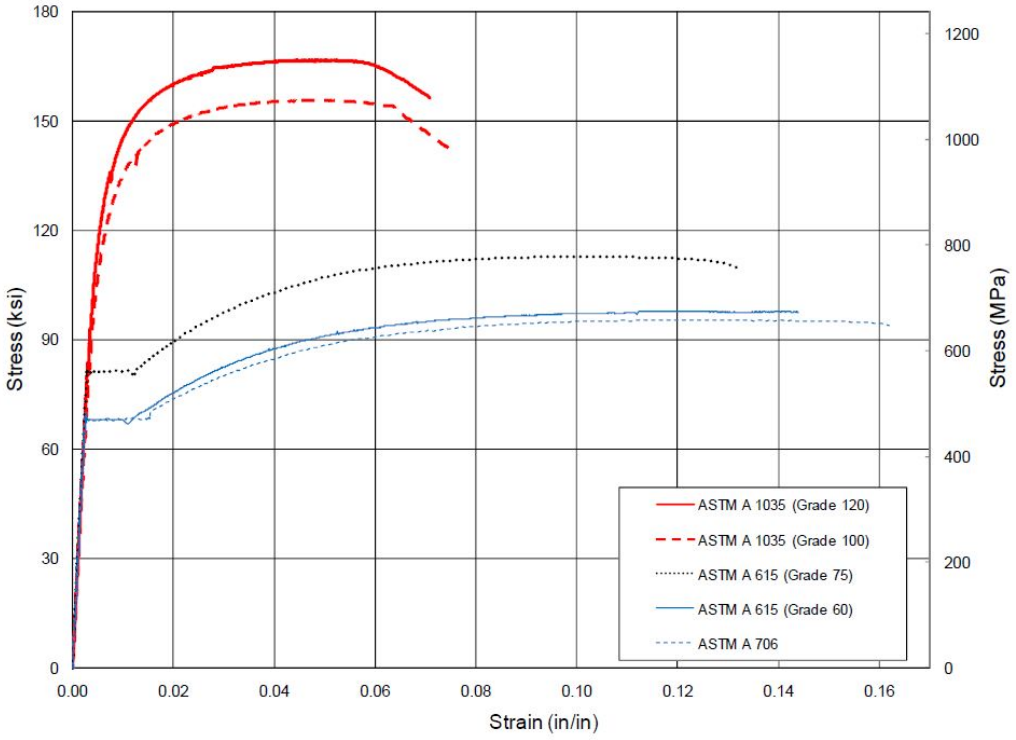

Figure 3. Stress-strain curves for different grades of steel reinforcing bars *(9)*.

ASTM A1035/A1035M bars have higher tensile strength but no well-defined yield point. The proportionate limit of ASTM 1035/A1035M bars is at a stress of 60,000 to 80,000 psi (410 to 550 MPa) which is similar to the yield stress of ASTM A615/A615M Grade 60 (420) and ASTM 706/A706M bars *(9)*. The strain at peak tensile stress for ASTM A615/A615M Grade 60 (420) steel lies at 0.07 to 0.10, and for ASTM A706/A706M steel is within 0.10 to 0.14. For ASTM A1035/A1035M steel, the ultimate strain at fracture ranges from 0.08 to 0.13, while for ASTM A615/A615M Grade 60 (420) and ASTM A706/A706M steel ranges from 0.09 to 0.12 and 0.14 to 0.20 respectively. The modulus of elasticity is observed to be 29,000 ksi (200,000 MPa) for ASTM A1035/A1035M bars similar to the other steel *(9)*. From actual

testing, the yield strength of the ASTM A1035/A1035M bars obtained from 0.2% offset method (Figure 4) is more than 115,000 psi (790 MPa) for Grade 100 (690) bars and 125,000 psi (850 MPa) for Grade 120 (830) bar.

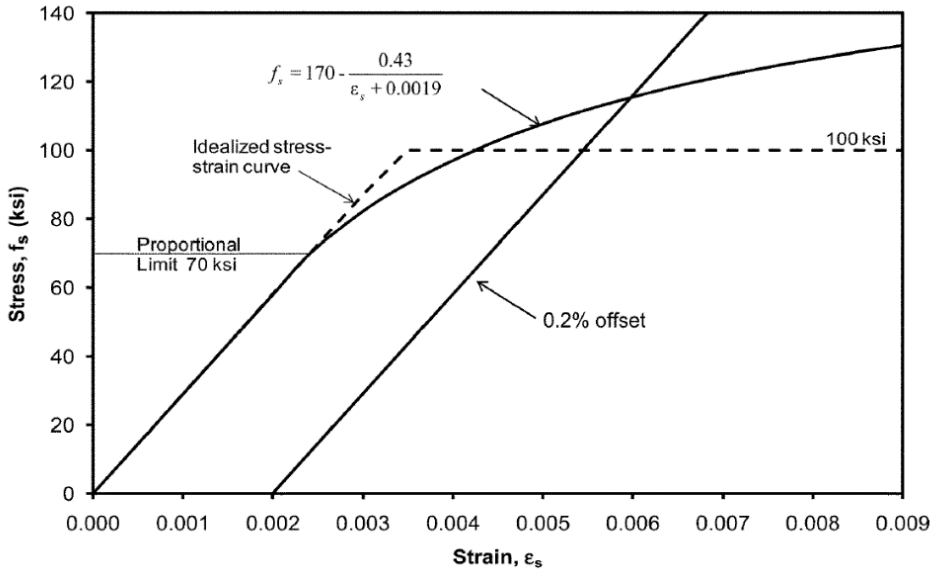

Figure 4. Approximated nonlinear stress-strain relationship of ASTM A1035/A1035M Grade 100 (690) steel and idealized bilinear elastic-plastic stress-strain relationship for simplified design *(7)*.

The tensile strength for ASTM A1035/A1035M Grade 100 (690) bar and Grade 120 (830) bar exceeds 155,000 psi (1070 MPa) and 160,000 psi (1100 MPa) respectively. The following Equations 1 to 3 are based on a proportional limit of 70,000 psi (480 MPa) and an assumed tensile strength of 150,000 psi (1030 MPa) at a strain of 0.02.

Approximate lower bound of stress-strain curves of Grade 100 (690) are represented by following equations:

$$f_s = 29{,}000\varepsilon_s \ \text{(ksi)} \qquad \text{for } 0 \le \varepsilon_s \le 0.0024 \qquad [1]$$

$$f_s = 170 - \frac{0.43}{\varepsilon_s + 0.0019} \ \text{(ksi)} \qquad \text{for } 0.0024 \le \varepsilon_s \le 0.02 \qquad [2]$$

$$f = 150 \ \text{(ksi)} \qquad \text{for } 0.02 \le \varepsilon_s \le 0.06 \qquad [3]$$

Aforementioned equations in SI units:

$$f_s = 200{,}000\varepsilon_s \ \text{(MPa)} \qquad \text{for } 0 \le \varepsilon_s \le 0.0024 \qquad [1M]$$

$$f_s = 1170 - \frac{2.96}{\varepsilon_s + 0.0019} \ \text{(MPa)} \qquad \text{for } 0.0024 \le \varepsilon_s \le 0.02 \qquad [2M]$$

$$f = 1040 \ \text{(MPa)} \qquad \text{for } 0.02 \le \varepsilon_s \le 0.06 \qquad [3M]$$

Table 2. Specified tensile and yield strengths *(7)*.

Bar type	Tensile strength, minimum, psi (MPa)	Yield strength[a], minimum, psi (MPa)	Yield strength[a], maximum, psi (MPa)	Stress corresponding to prescribed strain, minimum stress, psi (MPa)	Stress corresponding to prescribed strain, strain, %
ASTM A615/A615M Grade 60	90,000 (620)	60,000 (420)	-	60,000 (420)[b]	0.35[b]
ASTM A615/A615M Grade 75	100,000 (690)	75,000 (520)	-	75,000 (520)[b]	0.35[b]
ASTM A615/A615M Grade 80	105,000 (725)	80,000 (550)	-	80,000 (550)[b]	0.35[b]
ASTM A706/A706M Grade 60	80,000 (550)[c]	60,000 (420)	78,000 (540)	60,000 (420)[b]	0.35[b]
ASTM A706/A706M Grade 80	100,000 (690)[c]	80,000 (550)	98,000 (675)	80,000 (550)[b]	0.35[b]
ASTM A1035/A1035M Grade 100	150,000 (1030)	100,000 (690)	-	80,000 (550)	0.35
ASTM A1035/A1035M Grade 120	150,000 (1030)	120,000 (830)	-	90,000 (620)	0.35

[a] Observed yield point for ASTM A615/A615M and ASTM A706/A706M bars, and yield strength according to 0.2% offset method for ASTM A1035/A1035M bars.
[b] Applicable to ASTM A615/A615M and ASTM A706/706M bars only when steel bar tested does not exhibit a well-defined yield point.
[c] Tensile strength for ASTM A706/A706M bars should also be not less than 1.25 times actual yield strength.

Table 3. Representative chemical composition of rebar.

Element	ASTM A1035/A 1035M Maximum content, %	ASTM A615/A615M Maximum content, %	ASTM A706/A706M Maximum content, %
Carbon	0.15	b	0.30
Chromium	8.0 to 10.9[a]	-	-
Manganese	1.50	b	1.50[c]
Nitrogen	0.05	-	-
Phosphorus	0.035	0.06	0.035
Sulphur	0.045	b	0.045
Silicon	0.50	-	0.50

Flexural Design: ACI ITG-6R-10 *(7)* suggests limiting the strain developed in the ASTM A1035 longitudinal reinforcement to 0.015 to prevent excessive cracking and deflection. A

practical design can be performed through a nonlinear flexural analysis by considering force equilibrium and strain compatibility using Equations 1 and 2 and considering the limiting strain of 0.015. A simplified flexural design method for ASTM A1035/A1035M bars was put forward by Mast et al. *(10)*. He proposed using stress-strain behavior comprising of a linear elastic portion followed by a plastic yield plateau (Figure 5) similar to ASTM A615/A615M Grades 60 (420) and 75 (520) bars.

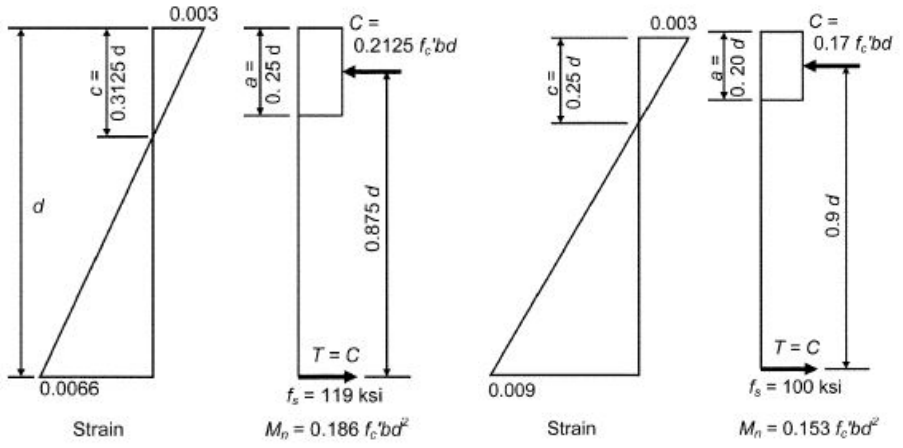

(a) **(b)**

Figure 5. (a) Behavior based on Equation, and (b) Behavior based on simplified method (Tension-controlled strain limits with $f_c' = 5$ ksi and $\beta_1 = 0.8$).

Table 4. Comparison of design methods using ASTM A 1035/A1035M Grade 100 (690) steel (in.-lb units) *(7)* .

Attribute	Using Equation 1 and 2	Simplified method
Tension-controlled strain limit	0.0066	0.009
Steel tensile stress f_s, ksi	119	100
Neutral axis depth c, in.	0.3125d	0.25d
Stress block depth $a = \beta_1 c$, in.	$0.3125\beta_1 d$	$0.25\beta_1 d$
Compression force C, kip	$0.85 f_c' ab$	$0.85 f_c' ab$
Steel area $A_s = C / f_s$, in.^{2}	$0.85(f_c'/119)(0.3125\beta_1 d)b$	$0.85(f_c'/100)(0.25\beta_1 d)b$
Tension-controlled reinforcement ratio $\rho_t = A_s / bd$	$0.002232 f_c' \beta_1$	$0.002125 f_c' \beta_1$
$T = C = A_s f_s = \rho_t bd f_s$, kip	$0.2656 f_c' \beta_1 bd$	$0.2125 f_c' \beta_1 bd$
Lever arm = $d - a/2$, in.	$d(1-0.156\beta_1)$	$d(1-0.125\beta_1)$
M_n for $f_c' = 22$ ksi; $\beta_1 = 0.8$, kip-in.	$0.232 f_c' bd^2$	$0.191 f_c' bd^2$

Table 5. Comparison of design methods using ASTM A 1035/A1035M Grade 100 (690) steel (SI units) *(7)*.

Attribute	Using Equation 1 and 2	Simplified method
Tension-controlled strain limit	0.0066	0.009
Steel tensile stress f_s, MPa	820	690
Neutral axis depth c, mm	0.3125d	0.25d
Stress block depth $a = \beta_1 c$, mm	$0.3125\beta_1 d$	$0.25\beta_1 d$
Compression force C, N	$0.85 f_c' ab$	$0.85 f_c' ab$
Steel area $A_s = C / f_s$, mm²	$0.85(f_c' / 820)(0.3125\beta_1 d)b$	$0.85(f_c' / 690)(0.25\beta_1 d)b$
Tension-controlled reinforcement ratio $\rho_t = A_s / bd$	$0.0003239 f_c' \beta_1$	$0.0003079 f_c' \beta_1$
$T = C = A_s f_s = \rho_t bdf_s$, N	$0.2656 f_c' \beta_1 bd$	$0.2125 f_c' \beta_1 bd$
Lever arm = $d - a/2$, mm	$d(1-0.156\beta_1)$	$d(1-0.125\beta_1)$
M_n for f_c' = ksi; $\beta_1 = 0.8$, N-mm	$0.232 f_c' bd^2$	$0.191 f_c' bd^2$

Tension and Compression Control: ACI 318 defines tension-controlled sections as the flexural members having a net tensile strain of 0.05 in the extreme tension reinforcement. This is based on the ASTM A615/A615M Grade 60 (420) and Grade 75 (720) bars. Behavior similar to the members designed using ACI 318 with Grades 60 (420) and 75 (720) was found using the simplified model for ASTM A1035/A1035M bar at a tension-controlled strain limit of 0.0066 *(10)*. The strain limit was modified to 0.009 to balance for the actual stress at nominal strength being higher than the assumed 100,000 psi (690 MPa).

ACI 318 defines compression-controlled sections as the flexural members having the net tensile strain at balanced strain condition. For a yield strength of 100,000 psi (690 MPa) and modulus of elasticity of 29,000 ksi (200,000 MPa), the compression-controlled strain limit is 0.00345 *(7)*.

3.2. Fiber-Reinforced Polymer (FRP) Reinforcement

Corrosion is a major concern in mild steel and prestressing steel in reinforced concrete and prestressed concrete structures exposed to aggressive environments. Composite materials such as fiber-reinforced polymer (FRP) bars are a suitable alternative to steel reinforcing bars when reinforced concrete is exposed to deicing salts, built in or close to seawater, subjected to other corrosive agents, required to maintain low electric conductivity or electromagnetic neutrality, or required to meet weight limits (FRP is about 75% lighter than steel). Fiber reinforced polymers uses a polymeric resin system reinforced with fibers. Hence. the properties of FRP is a combination of the properties of the resin matrix and the fibers used (Figure 6). Fibers are typically aramid, basalt, carbon or glass and the polymer is usually an epoxy, phenol formaldehyde resin, polyester thermosetting plastic or vinyl ester.

Aramid fiber reinforced polymer (ARFP), carbon fiber reinforced polymer (CFRP) and glass fiber reinforced polymer (GFRP) are the most commonly used FRP composites. Aramid fibers are a synthetic aromatic-polyamide material. Aramid fibers are lighter than carbon and glass fibers with similar mechanical properties and are more suitable for prestressed concrete

structures than for reinforced concrete ones. Carbon fibers are manufactured by heat treatment processes such as carbonization and graphiting. CFRP shows suitable mechanical properties; in spite of this, the fibers are electrically conductive which might result in the formation of galvanic cells on contact with a metallic substrate. Glass fibers are manufactured by extruding silica dioxide and exhibit favorable mechanical properties; however, they are vulnerable to creep- and moisture-induced damage. Basalt fibers are a mineral-based inorganic product and were recently introduced to the structural engineering community *(11)*. Basalt fibers are chemically inert and demonstrate good acidic and thermal resistance. The properties and costs of basalt fibers are similar to those of glass fibers.

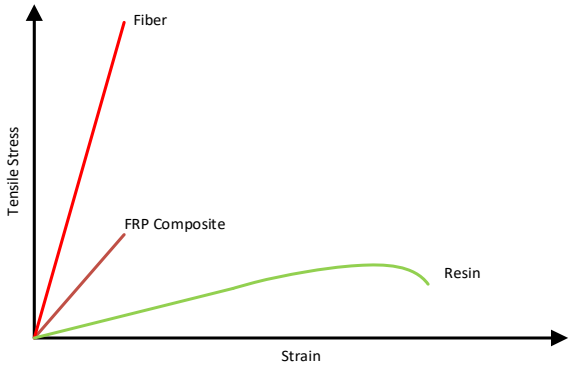

Figure 6. Properties of FRP composite *(12)*.

3.2.1. Tensile and Compressive Behavior

The tensile behavior of FRP bars are controlled by the properties of the fiber and resin, fiber volume fraction and the fiber geometry and orientation within the matrix *(12)*. FRP materials are anisotropic in nature and show pure elastic behavior until failure. As a result, this lack of ductility should be taken into consideration when designing concrete structures reinforced with FRP bars. Figure 7 shows the typical behavior of the FRP bars. FRP bars show higher tensile strength than typical steel bars but the tensile modulus of FRP bars is significantly lower than steel counterparts, as small as 20% *(13)*. Typical mechanical properties of FRP bars are presented in Table 6.

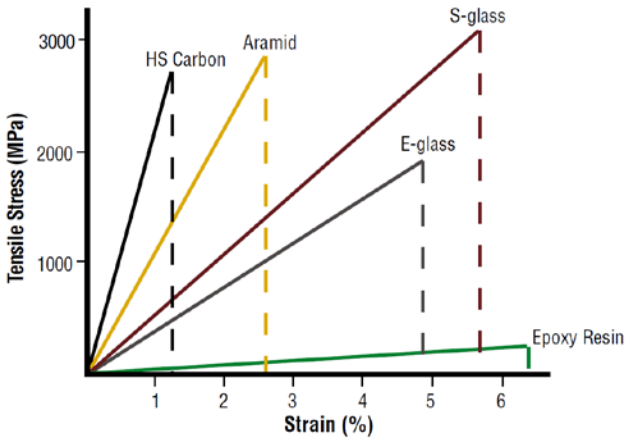

Figure 7. Tensile stress strain relationship for FRP bars *(12)*.

Table 6. Typical mechanical properties of FRP bars *(11)*.

Type	Density lb/in^3 (g/cm^3)	Tensile strength ksi (MPa)	Tensile modulus ksi (GPa)	Elongation at break (%)
Aramid	0.052 (1.45)	525-533 (3,600-3,620)	18,000-19,000 (127-131)	2.5-2.8
Carbon	0.064-0.078 (1.77-2.16)	275-640 (1,900-4,410)	32000-110,000 (220-758)	0.32-2.0
Glass	0.09-0.092 (2.49-2.54)	500-625 (3,450-4,300)	10,500-12,600 (72.4-86.9)	4.8-5.0

3.2.2. Flexural Design

Design of reinforced concrete members with FRP reinforcements is similar to the design of steel-reinforced concrete members. However, unlike steel, FRP bars do not exhibit ductility. Hence, the failure of a reinforced concrete member due to rupture of FRP bars before concrete crushing is sudden, destructive and not desirable. It is preferable for FRP-reinforced concrete members to fail in compression rather than the rupture of FRP bars *(14)*. Neither of the above-mentioned method of failure for FRP-reinforced structural members; tension-controlled or compression-controlled failure, will provide ductility to the member. Therefore, in the absence of ductility, ACI 440.1R (2015) suggests a more conservative design for FRP-reinforced members than for the steel-reinforced members. If high strength concrete is used with the FRP reinforcement bars, stiffness of the cracked section is increased but it reduces the deformability of the flexural member compared to normal strength concrete *(13)*. The balanced FRP reinforcement ratio can be computed from Equation 4.

$$\rho_{fb} = 0.85\beta_1 \frac{f_c^{'}}{f_{fu}} \frac{E_f \varepsilon_{cu}}{E_f \varepsilon_{cu} + f_{fu}} \qquad [4]$$

For compression-control: $\rho_f < \rho_{fb}$

For tension-controlled: $\rho_f > \rho_{fb}$

Equilibrium equations and strain compatibility can be used for the calculation of the nominal flexural strength of FRP-reinforced concrete flexural members (Figure 8).

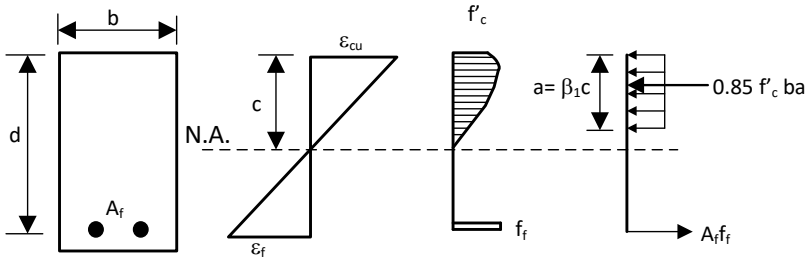

(a) Failure governed by concrete crushing

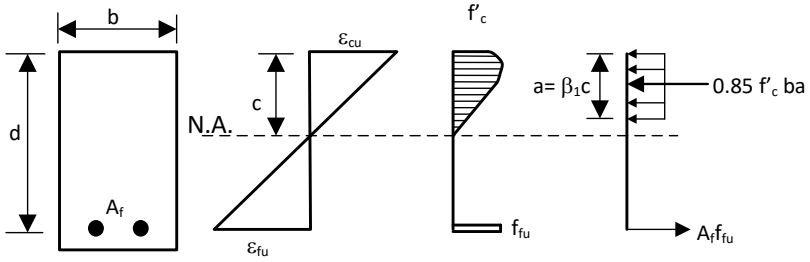

(b) Balanced failure condition

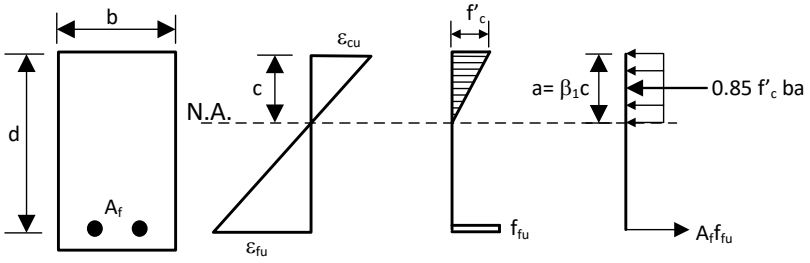

(c) Failure governed by FRP rupture (concrete stress maybe nonlinear)

Figure 8. Stress-strain distribution at ultimate conditions *(16)*.

3.2.3. Nominal Flexural Strength

Compression-controlled ($\rho_f > \rho_{fb}$): Crushing of concrete is the controlling limit state. In this case, the stress distribution in the concrete can be approximated with the ACI rectangular stress block. Equation 5 tis used to calculate nominal flexural strength.

$$M_n = A_f f_f \left(d - \frac{a}{2} \right) \qquad [5]$$

Tension-controlled ($\rho_f < \rho_{fb}$): Rupture of FRP reinforcement is the controlling limit state. Equation 6 is used to calculate nominal flexural strength.

$$M_n = A_f f_{fu} \left(d - \frac{a}{2} \right) \qquad [6]$$

3.2.4. Shear Design

The shear design for FRP-reinforced concrete members is similar to the steel-reinforced concrete members. However, issues related to FRP reinforcements such as low modulus of elasticity, low transverse shear resistance, and lack of ductility need to be considered. ACI 440 suggests using a strength reduction factor of 0.75 for FRP reinforcement similar to steel-reinforced concrete. The nominal shear strength of the reinforced concrete section is the sum of the shear resistance provided by the concrete and the shear reinforcement *(15)*.

Due to the lower axial stiffness for the FRP reinforcement, a cross section with FRP flexural reinforcement after cracking has a smaller depth of neutral axis as compared to the steel-reinforced section with equal areas of longitudinal reinforcement. The depth of the compression zone is reduced, and the crack width are wider. This reduces the contribution of the aggregate interlock and compression zone in the shear resistance. Earlier research on shear capacity of flexural concrete members without shear reinforcement has shown that shear strength of concrete depends on stiffness of flexural reinforcement *(16-19)*. There is lack of study regarding the involvement of FRP reinforcement bars in the dowel action. However, it can be assumed that the contribution is less than comparable area of steel owing to the lower axial stiffness of the FRP rebars.

3.2.5. High Strength to Weight Ratio

Specific weight of FRP is less than 2.00 g/cm^3 *(12)* compared to nearly 8.00 g/cm^3 for steel (Figure 9). This makes FRP 75% lighter than steel. This results in the FRP having a very high strength to weight ratio compared to metals. FRP's light weight facilitates construction and reduce the overall weight of the structure.

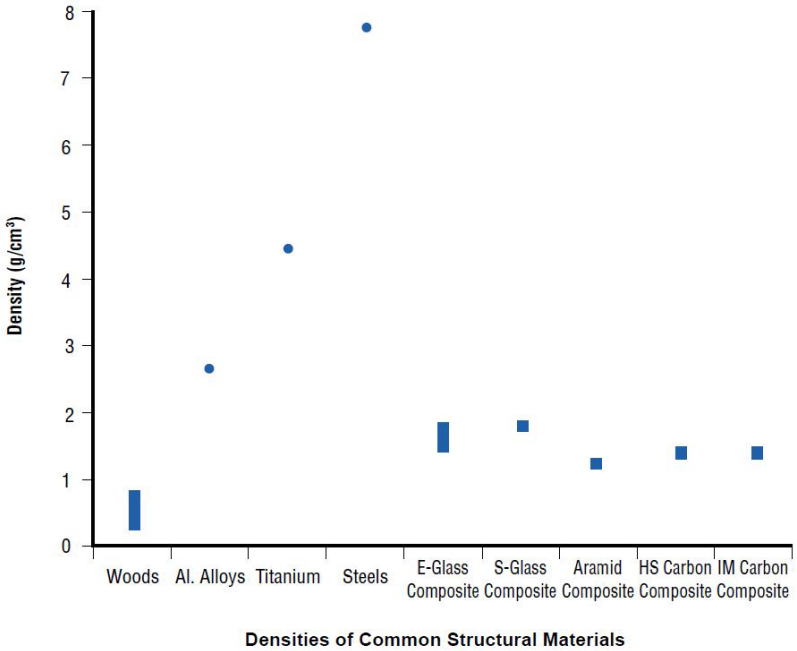

Figure 9. Densities of common structural materials *(12)*.

3.3. Prior Research UHP-FRC Structural Members Subjected to Earthquake Loadings

The potential of using the superior mechanical properties of UHP-FRC to improve the low damage resistant ability of conventional concrete was demonstrated in a pilot study where a full-scale ACI 318-compliant RC column *(15)* and a UHP-FRC column were tested under large axial load and displacement reversals up to failure *(20, 21)*. Both columns had the same reinforcement details with ASTM A706 Grade 60 rebars. Although the UHP-FRC column could have had a smaller cross section by utilizing its high compressive strength, a column's cross-sectional dimension is usually controlled by the stiffness requirement of the structure; therefore, both column specimens used the same dimensions. Both columns were fabricated at UT Arlington's Civil Engineering Laboratory Building (CELB) and tested at the MAST laboratory at the University of Minnesota (Figure 10). The UHP-FRC material used in the experiment was developed at UT Arlington based on a dense particle-packing concept *(4)*.

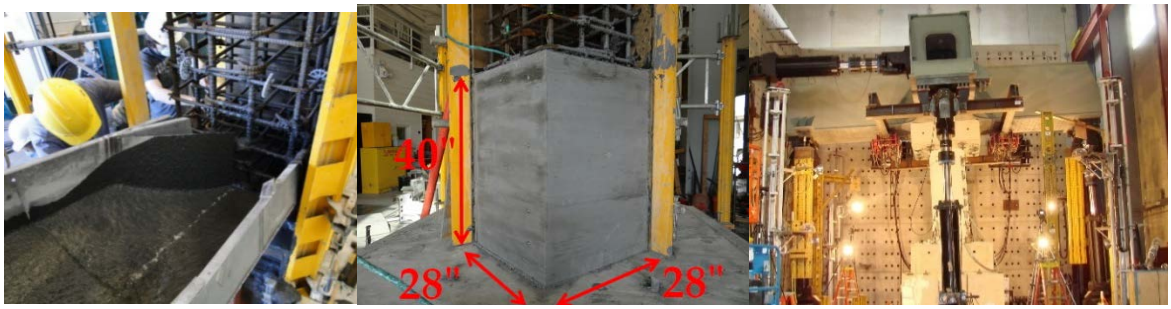

(a) **(b)** **(c)**

Figure 10. (a) UHP-FRC casting at UT Arlington CELB, (b) completed UHP-FRC at the plastic hinging zone of the specimen, and (c) experimental testing at MAST laboratory at the University of Minnesota.

The hysteresis responses for both column specimens are shown in Figure 11a. For the RC column with normal strength concrete (5 ksi), the first observable flexural cracks were seen at 0.5% drift ratio, and the first longitudinal bar yielded at 0.75% drift ratio. The failure of the RC column started with concrete crushing at the corners of the columns at 1.0% drift ratio. Soon after the crushing, a decrease in strength was observed at 1.38% drift ratio. As the cyclic reversals continued, the concrete cover was eventually lost, followed by the bulging and opening of the transverse reinforcement, and then the buckling and fracture of the longitudinal reinforcement. This deterioration resulted in a significant decrease in strength and eventual failure of the RC column. On the other hand, the UHP-FRC column-maintained strength up to nearly 4% drift ratio. Note that ACI 374-13 *(22)* requires that for frame buildings, the maximum story drift ratio should be kept within 4% to meet the "Collapse Prevention" performance level requirement. To meet the "Life Safety" performance level requirement, a structure should not have a strength degradation of up to 2% story drift ratio. Figure 11a shows that the UHP-FRC column was able to maintain nearly full peak strength up to 4% story drift ratio, and it had no strength degradation up to approximately 2.5% story drift ratio. Note that while the axial load ratio ($P_u/A_g f'_c$) for the RC column was 0.3, it dropped to 0.06 for the UHP-FRC column due to the high compressive strength of UHP-FRC. This smaller axial load ratio in the UHP-FRC column minimized the influence of the axial load effect at the post-elastic stage, which is very beneficial for columns.

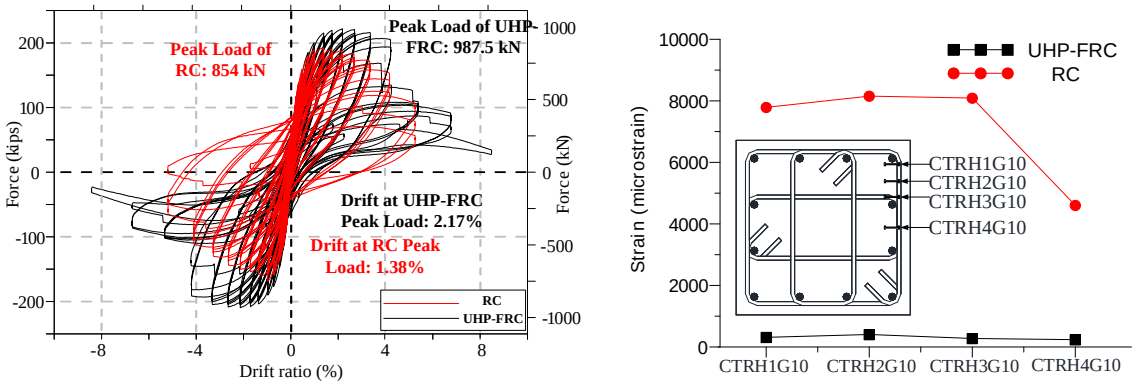

(a) **(b)**

Figure 11. Comparison of UHP-FRC and RC columns: (a) hysteresis loops and (b) confinement characteristic.

The use of UHP-FRC significantly changes the failure mechanism observed in conventional RC columns due to its high strength and high compressive ductility. There was no visible concrete damage observed in the plastic hinge region of the UHP-FRC column throughout the test (Figure 12). This allowed longitudinal reinforcement to be fully utilized to its ultimate tensile capacity without buckling. Furthermore, strain data of transverse reinforcement in the UHP-FRC region only indicated minor strains of less than 50% yielding, suggesting that transverse reinforcement may be significantly reduced in UHP-FRC columns allowing for less congestion and greater ease of construction. Figure 11 compares both specimens, at the same lateral load of 190 kips, with embedded concrete gauges at a cross-section10 inches above the footing. It shows that the measured concrete tensile strains in the UHP-FRC column is significantly lower than those in the RC column, which illustrates the great confinement provided by UHP-FRC material. Figure 12 compares both columns at 2.75% and 5.25% drift ratios showing significant concrete crushing and bar buckling in the RC column with no visible damage detected in the UHP-FRC column. The ultimate failure of the UHP-FRC column was due to the low-cycle fatigue of the longitudinal reinforcement at the interface between the footing and the column section. Inside the UHP-FRC column, ultrasonic tomography showed that the internal cracking of the UHP-FRC column was much less than that of RC column *(23)*. The pilot testing shows the great resilience capability of columns made of UHP-FRC materials.

(a) **(b)**

Figure 12. Experimental test results: (a) Conventional Reinforced Concrete Column (left) and UHP-FRC Column (right) at 2.75% drift ratio and (b) Conventional Reinforced Concrete Column (left) and UHP-FRC Column (right) at 5.25% drift ratio *(21)*.

3.4. Ductile-Concrete Strong-Reinforcement (DCSR) Design Concept

The research objective is to develop highly sustainable and efficient reinforced concrete structural members. UHP-FRC offers a new way to design reinforced concrete flexural members due to its superior mechanical properties as compared to conventional concrete. For plain concrete, the compressive strain at this level of stress is 0.003. AASHTO LRFD *(24)* and ACI 318 *(15)* uses 0.003 as the design maximum strain at the crushing of concrete (Figure 13). Due to this small strain capacity of plain concrete, only a small amount of longitudinal reinforcement could be used to ensure that the flexural member is tension-controlled. For a tension-controlled beam section, the tensile strain in the extreme tension reinforcement (closest to the tension face) is sufficiently large (≥ 0.005); therefore, the beam shows a large deflection as a warning before failure occurs.

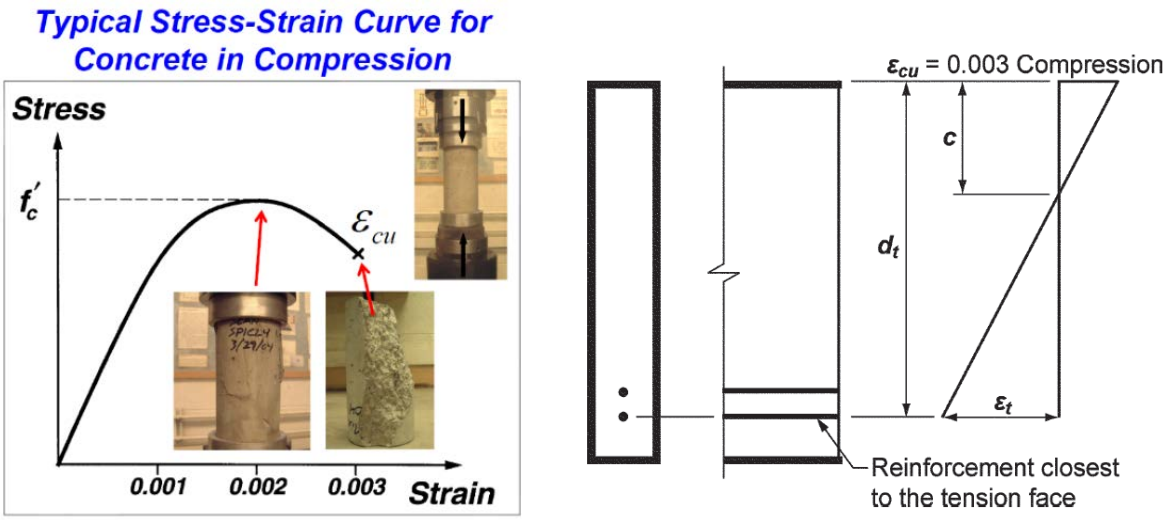

Figure 13. Typical compressive stress-strain response of conventional concrete and maximum usable strain allowed by AASHTO and ACI 318.

Figure 14 shows typical compressive and tensile stress-strain relations of UHP-FRC materials *(4)*. The maximum usable compressive strain (at a post-peak stress of approximately 80% of the peak stress), ε_{cu}, is approximately 0.015. If the concrete compressive strain can be five times greater, the beam could be more efficiently utilized by placing a considerably higher amount of longitudinal reinforcement while still maintaining tension-controlled behavior.

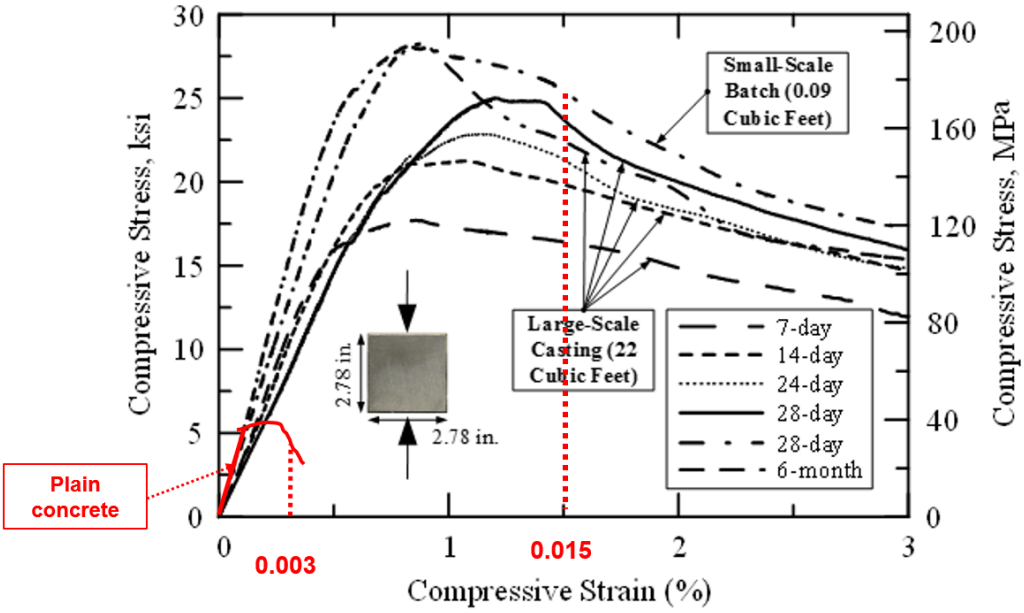

Figure 14. Compressive stress-strain response of UHP-FRC *(4)*.

The proposed DCSR design concept is to use UHP-FRC as the ductile element and fiber-reinforced polymer (FRP) bars as the elastic element, which is opposite to conventional RC where the steel bars are the ductile element and the concrete is the brittle element. Using high-strength FRP bars can reduce reinforcement congestion, while achieving high structural efficiency in members (that is, high flexural strength with a relatively smaller cross-section). Keeping FRP bars elastic will also reduce the bond demand and the residual deformation (i.e., self-centering) once a member experiences large deformation under overloading. In addition, FRP bars are a suitable alternative to steel reinforcing bars when reinforced concrete is exposed to deicing salts, built in or close to seawater, subjected to other corrosive agents, required to maintain low electric conductivity or electromagnetic neutrality, or required to meet weight limits (FRP is about 75% lighter than steel). The high shear strength of UHP-FRC allows partial or total elimination of shear reinforcement.

ACI 440 (2015) suggests a very conservative design for concrete members reinforced with FRP bars because both concrete and FRP bars are brittle materials. However, combining UHP-FRC (very ductile) and FRP bars can provide an excellent solution for concrete structures, which require both ductility and corrosion-free characteristics. Two beam specimens were designed and tested and described as follows.

Beam Details (Monotonic Loading): In the previous test *(28)* two beams were tested verify the new DCSR design concept. One UHP-FRC beam reinforced with BFRP (basalt) bars were tested along with an RC specimen with conventional steel. The BFRP bars had an ultimate tensile strength of approximately 125 ksi and an ultimate tensile strain of 0.017 to 0.025. The RC beam was designed to have the highest amount of longitudinal reinforcement while still maintaining tension-controlled behavior, according to ACI 318 and AASHTO LRFD provisions. Thus, the extreme tensile reinforcement reached 0.005 strain when the maximum concrete strain was 0.003 (Figure 15a). This led to the use of nine Grade 60 No. 5 rebars. Design compressive strength of the RC beams was 5,000 psi. For the UHP-FRC beam, the

design compressive strength of UHP-FRC was 22,000 psi, and the maximum usable compressive strain, ε_{cu}, was taken as 0.015. A lower bound BFRP rupture strain of 0.014 was used for design (Figure 15b). This led to a higher amount of high-strength reinforcement. No shear reinforcement was used in UHP-FRC beam (Figure 16). Design summary is given in Table 7.

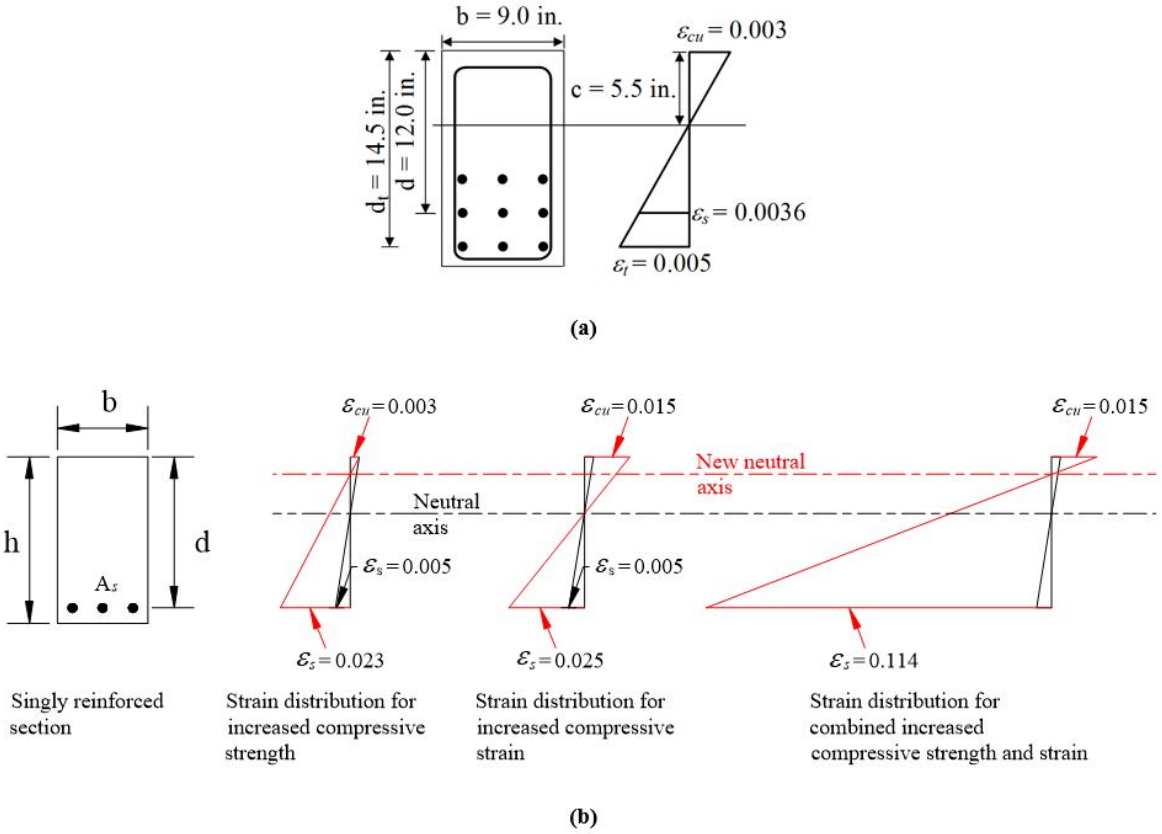

Figure 15. Strain profile of (a) RC (Gr. 60 steel rebars); (b) UHP-FRC (BFRP bars).

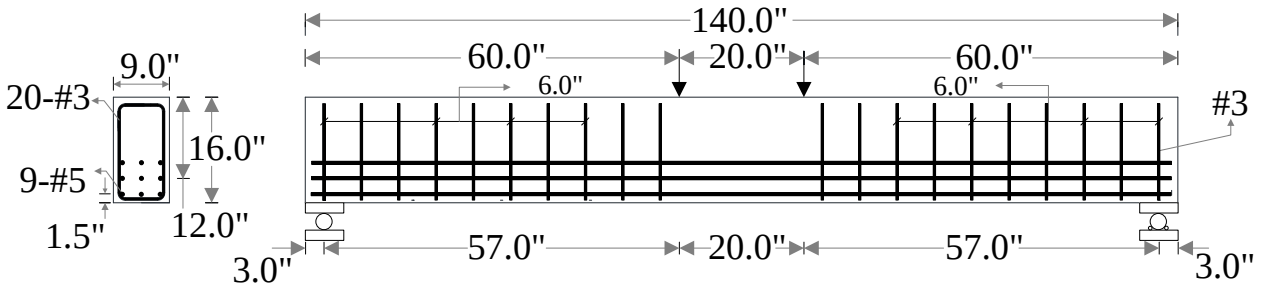

(a) RC (Gr. 60 mild steel rebars)

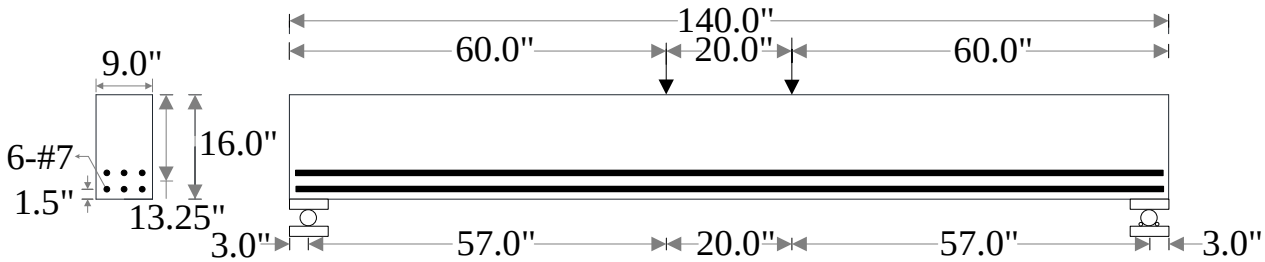

(b) UHP-FRC (BFRP bars; no shear reinforcement)

Figure 16. Reinforcement details: (a) conventional RC beam; (b) UHP-FRC beam with BFRP bars (no shear reinforcement).

Table 7. Design summary of RC and UHP-FRC beams.

Specimen	Effective depth (d) in. (mm)	a/d	ρ (%)	β_1	Target Compressive Strength psi (MPa)	Measured compressive strength psi (MPa)
RC #1 (Grade 60 steel)	12 (305)	4.75	2.58	0.8	5000 (35)	5000 (35)
UHP-FRC #4 (BFRP)	13.25 (336.55)	4.3	3.02	0.65	22000 (152)	18500 (128)

Figure 17 shows the test results which indicate that the UHP-FRC beam has a much higher stiffness and a strength three times that of conventional RC beam. The UHP-FRC beam also have an excellent ductility, allowing a large deformation or warning sign to occur before failure. As shown in Figure 28, compared to RC beam, UHP-FRC beam shows high damage resistant capability even beyond ultimate loads. UHP-FRC beam's behavior was controlled by flexure even no shear reinforcement was used.

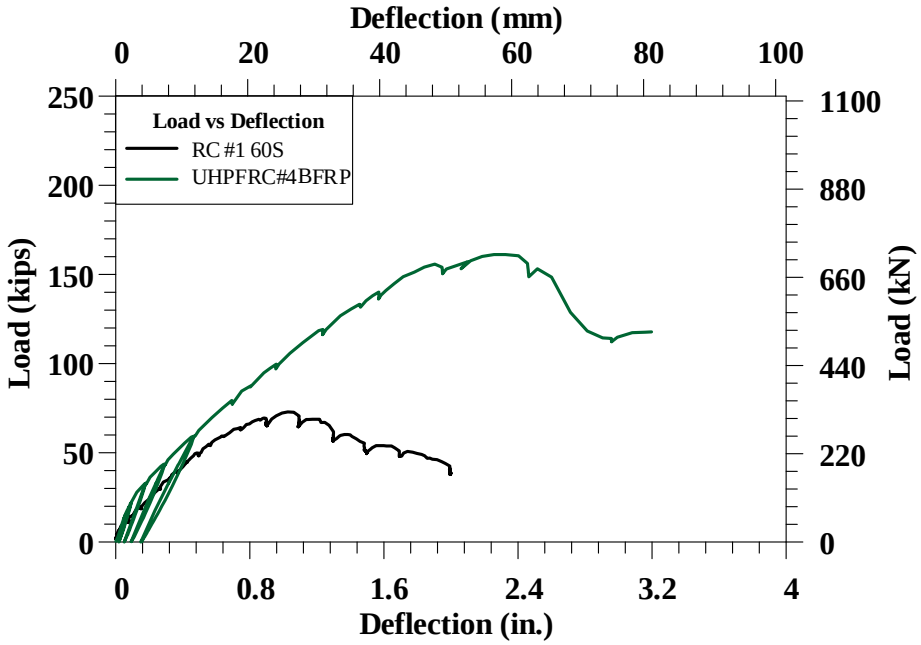

Figure 17. Responses of RC and UHP-FRC beam with FRP bars.

(a) **(b)**

Figure 18. Damage at end of testing: (a) RC beam; (b) UHP-FRC (with BFRP bars) beam without shear reinforcement.

4. METHODOLOGY

The primary purpose of this research is to develop the next generation highly corrosive-resistant and structurally efficient structural members by utilizing the high durability, compressive ductility, cracking resistance, and shear strength of UHP-FRC as well as the corrosion resistant high-strength fiber-reinforced polymer (FRP) bars. The research focused on using high-strength reinforcement to reduce reinforcement congestion while achieving a high structural efficiency in members (that is, high flexural strength with a relative smaller cross section).

ACI 440 *(13)* suggests a very conservative design for concrete members reinforced with FRP bars because both concrete and FRP bars are brittle materials. However, combining UHP-FRC (very ductile) and FRP bars can provide an excellent solution for concrete structures, which require both ductility and corrosion-free characteristics. Four beam specimens were designed and tested as a part of the experimental program. Main parameters to be investigated include: 1) type of FRP bars (glass fiber, carbon fiber, and basalt fiber). Glass fibers are manufactured by extruding silica dioxide and exhibit favorable mechanical properties; however, they are vulnerable to creep- and moisture-induced damage. Basalt fibers are a mineral-based inorganic product and were recently introduced to the structural engineering community *(12)*. Basalt fibers are chemically inert and demonstrate good acidic and thermal resistance. The properties and costs of basalt fibers are similar to those of glass fibers. 2) fiber types for UHP-FRC: high-strength micro steel fibers and ultra-high-molecular-weight polyethylene (PE) fibers (Figure 19 and Table 8), and 3) shear reinforcement (steel, FRP).

Figure 19. Micro steel fiber (left) and ultra-high molecular weight polyethylene fiber (right).

Table 8. Mechanical properties of the fibers used.

Fiber type	Length (mm)	Diameter (mm)	Tensile strength (ksi)
Micro steel fiber	13	0.2	399
UHMW Polyethylene fiber	13	0.0015	375

4.1. Beam Details – Fully Reversed Cyclic Loading

A total of four beams were designed and their design parameters are presented in Table 9. All UHP-FRC specimens were tested under large displacement reversals to prove the proposed new DCSR design concept by fully utilizing these ultra-high-performance materials. Micro steel fibers were used for three specimens and ultra-high molecular weight polyethylene fibers was used for one specimen. One specimen with high strength corrosion resistant MMFX steel rebars (100 ksi as per ASTM A1035, 2016), one with high-strength GFRP (glass, 90 ksi) rebars and two with BFRP (basalt, 145.8 ksi) (Table 10) were tested. The beams had a reinforcement ratio of 14% to 15%. The cross-section details along with the detailed side view of the specimens are presented below from Figure 20 to Figure 24.

Table 9. Design summary of specimens.

Specimen	Effective depth (d), in. (mm)	Width of compression face (b), in. (mm)	ρ (%)	Reinforcement type	Fiber type	Effective span, in. (mm)
UHP-FRC #1	4.311 (109)	6 (152)	15.5	MMFX	Steel	49.5 (1257)
UHP-FRC #2	6.375 (162)	6 (152)	13.9	GFRP	Steel	49.5 (1257)
UHP-FRC #3	5.35 (136)	8 (203)	14.8	BFRP	PE	34 (864)
UHP-FRC #4	5.35 (136)	8 (203)	14.8	BFRP	Steel	34 (864)

Table 10. Reinforcement details.

Reinforcement type	Diameter in. (mm)	Tensile strength ksi (MPa)
MMFX	1.125 (29)	100 (690)
GFRP	0.75 (19)	90 (620)
BFRP	1.00 (25)	147 (1014)

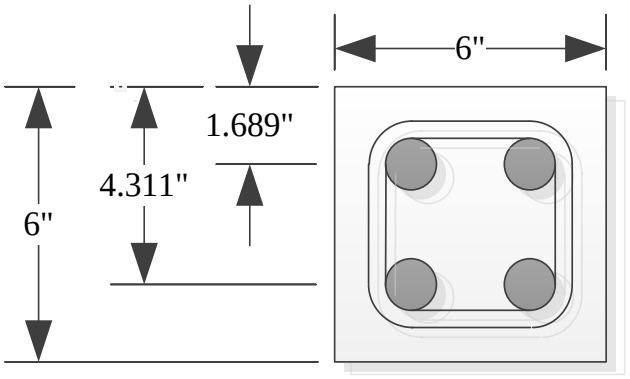

Figure 20. Cross section of MMFX Beam (UHP-FRC #1).

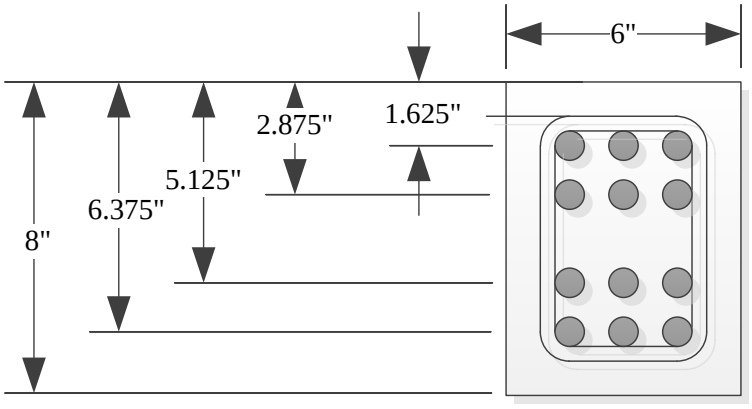

Figure 21. Cross section of GFRP Beam (UHP-FRC #2).

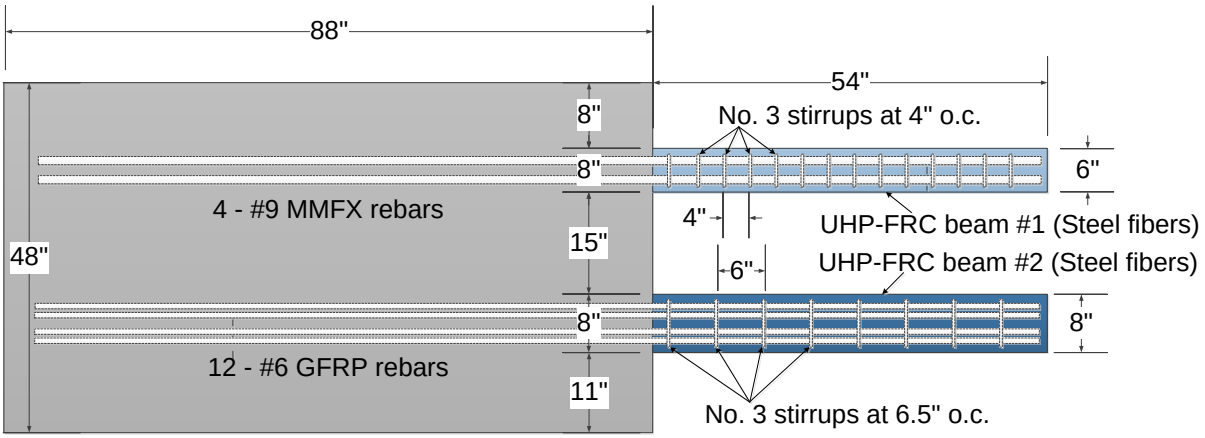

Figure 22. Detailed side view of the specimen showing specimens UHP-FRC #1 and #2.

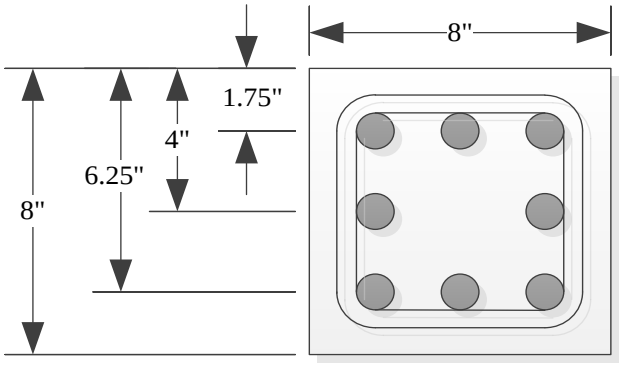

Figure 23. Cross section of BFRP Beam (UHP-FRC #3 and #4).

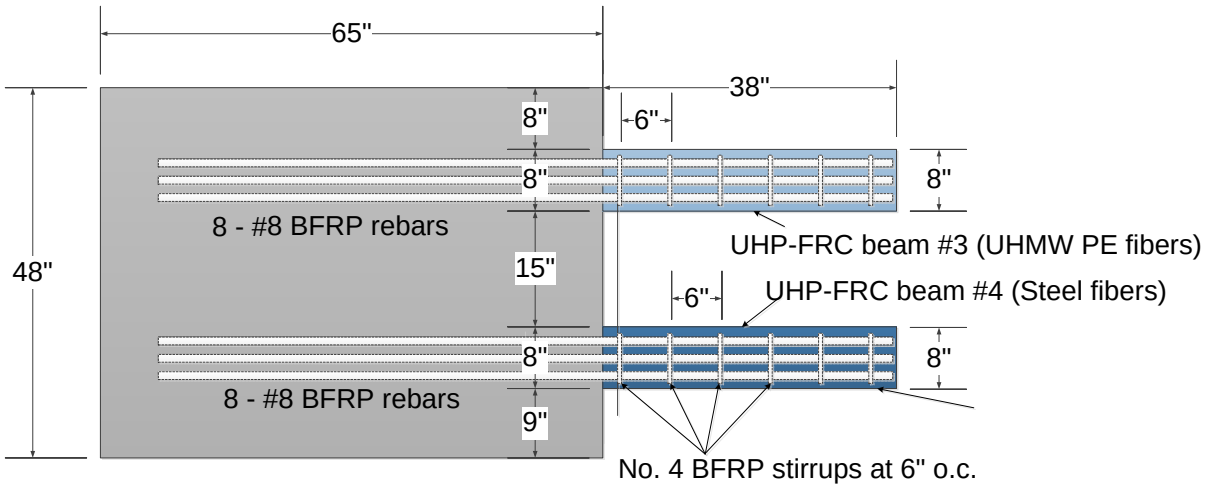

Figure 24. Detailed side view of the specimen showing specimens UHP-FRC #1 and #2.

The detailed design procedure of the four specimens is presented in the next section.

4.1.1. Specimen UHP-FRC #1 Design Calculations

The first beam was design with UHP-FRC with micro short steel fibers. The fiber content for the UHP-FRC beam was 3% by volume. High strength MMFX bars confirming to ASTM A1035/A10355M was used as flexural reinforcements. The design calculations are presented below:

$f_c' = 22$ ksi , $\beta_1 = 0.65$

$f_y = 100$ ksi

$E_s = 29,000$ ksi

$\varepsilon_y = 0.009$

$b = 6$ in.

$d = 4.311$ in.

$d_c = 1.689$ in.

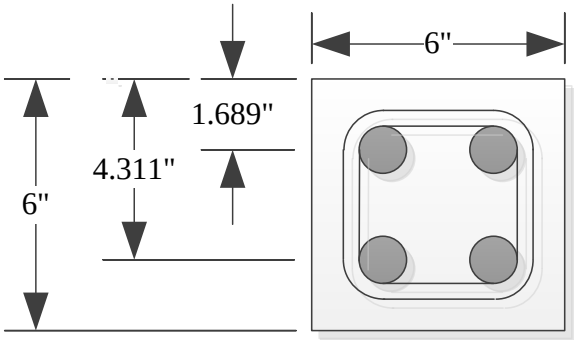

Figure 25. Cross section of UHP-FRC #1.

Based on the strain compatibility:

$$a = \beta_1 c \ ;$$

$$c = \frac{a}{\beta_1}$$

$$\frac{\varepsilon_{sc}}{\varepsilon_{cu}} = \frac{c - d_c}{c} \text{ or } \varepsilon_{sc} = \frac{c - d_c}{c} \times \varepsilon_{cu}$$

$$\frac{\varepsilon_{st}}{\varepsilon_{cu}} = \frac{d - c}{c} \text{ or } \varepsilon_{st} = \frac{d - c}{c} \times \varepsilon_{cu}$$

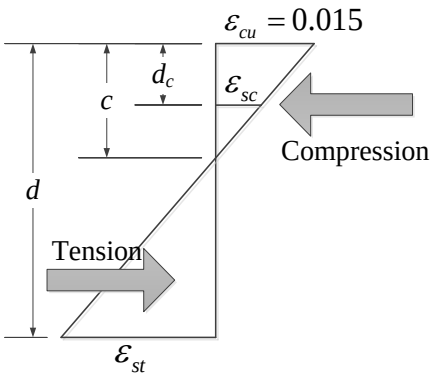

Figure 26. Strain compatibility diagram.

Compression force:

$$C = C_{concrete} + C_{reinforcement}$$

$$C_{concrete} = 0.85 f_c' (ab - A_{sc})$$

$$C_{reinforcement} = A_s f_{sc}$$

where:

$$f_{sc} = \min \begin{Bmatrix} f_{fu} \\ E_s \times \varepsilon_{sc} \end{Bmatrix}$$

Tension force:

$$T = A_{st} f_{st}$$

where:

$$f_{st} = \min \begin{Bmatrix} f_{fu} \\ E_s \times \varepsilon_{st} \end{Bmatrix}$$

Assuming that the MMFX rebars yield in tension but do not yield in compression:

$$f_{sc} = E_s \times \varepsilon_{sc} = E_s \times \frac{c - d_c}{c} \times \varepsilon_{cu}$$

$$f_{st} = 100 \text{ ksi}$$

This results in:

$$C = C_{concrete} + C_{reinforcement}$$

$$C = 0.85 f_c' \left(ab - A_s \right) + A_s f_{sc}$$

$$C = 0.85 f_c' \left(ab - A_s \right) + A_s \times E_s \times \left(\frac{c - d_c}{c} \right) \times \varepsilon_{cu}$$

$$C = 0.85 f_c' \left(ab - A_s \right) + A_s \times E_s \times \left(\frac{\frac{a}{\beta_1} - d_c}{\frac{a}{\beta_1}} \right) \times \varepsilon$$

Tension force:

$$T = A_{st} \times f_{st} = A_{st} \times 100$$

Based of equilibrium of forces:

(C) = Tension force (T), or

$C_{concrete} + C_{reinforcement} = T$, or

$$0.85 f_c' \left(ab - A_s \right) + A_s \times E_s \times \left(\frac{\frac{a}{\beta_1} - d_c}{\frac{a}{\beta_1}} \right) \times \varepsilon_{cu} = A_{st} \times 100 \text{, or}$$

$$0.85 \times 22 \times \left(a \times 6 - 2 \times 1 \right) + \left(2 \times 1 \right) \times 29000 \times \left(\frac{\frac{a}{0.65} - 1.689}{\frac{a}{0.65}} \right) \times 0.015 = (2 \times 1) \times 100$$

Solving for *a*:

$a = 1.238$ in.

$$c = \frac{a}{\beta_1} = \frac{1.238}{0.65} = 1.905 \text{ in.}$$

Strain in tension longitudinal reinforcement:

$$\varepsilon_{st} = \frac{d - c}{c} \varepsilon_{cu} = \frac{4.311 - 1.905}{1.905} \times 0.015 = 0.019 > 0.009$$

Strain in compression longitudinal reinforcement:

$$\varepsilon_{sc} = \frac{c - d_c}{c} \varepsilon_{cu} = \frac{1.905 - 1.689}{1.905} \times 0.015 = 0.0017 < 0.009$$

Stress in tension longitudinal reinforcement:

$$f_{st} = 100 \text{ ksi}$$

Stress in compression longitudinal reinforcement:

$$f_{sc} = E_s \varepsilon_{sc} = 29000 \times 0.0017 = 49.3 \text{ ksi}$$

For the compression and tension forces:

$$C_c = 0.85 f_c' \left(ab - A_{sc} \right) = 0.85 \times 22 \times \left(1.238 \times 6 - 2 \times 1 \right) = 101.5 \text{ kips}$$

$$C_s = A_{sc} f_{sc} = \left(2 \times 1 \right) \times 49.3 = 98.6 \text{ kips}$$

$$T = A_{st} f_{st} = 2 \times 1 \times 100 = 200 \text{ kips}$$

Nominal Moment:

$$M_n = C_c \left(d - \frac{a}{2} \right) + C_s \left(d - d_c \right)$$

$$M_n = 101.5 \times \left(4.311 - \frac{1.238}{2} \right) + 98.6 \times \left(4.311 - 1.689 \right)$$

$$M_n = 633.27 \text{ kip-in.} = 52.77 \text{ kip-ft}$$

Considering the strain hardening of the reinforcement:

$$M_{nF} = 1.25 \times M_n = 1.25 \times 633.27 = 791.59 \text{ kip-in.} = 65.97 \text{ kip-ft}$$

For development length *(ACI 318-14:25.4.2)*:

$$l_d = \left(\frac{3 f_y \Psi_t \Psi_e}{40 \lambda \sqrt{f_c'}} \right) d_b \text{ for No. 7 and larger bars}$$

$$l_{bhf} = \left(\frac{3 \times 100000 \times 1 \times 1}{40 \times 1 \times \sqrt{22000}} \right) \times 1.125 = 56.9 \text{ in.}$$

Effective span of the beam considered:

$$L = 49.5 \text{ in.}$$

$$\text{Shear span to depth ratio} = \frac{49.5}{6} = 8.25$$

Ultimate shear:

$$V_u = \frac{M_n}{L} = \frac{65.97 \text{ kip-ft}}{\frac{49.5}{12} \text{ ft}} = 16 \text{ kips}$$

Nominal shear strength provided by concrete:

$$\phi V_c = 0.75 \times 600 \text{ psi} \times bd = 0.75 \times 600 \times 6 \times 4.311 = 11.64 \text{ kips}$$

For the shear reinforcements, No. 3 Grade 60 deformed rebars are used where:

Area of shear reinforcements:

$$A_v = 2 \times 0.11 = 0.22 \text{ in.}^2$$

For spacing (s) of shear reinforcements:

$$s = \frac{0.75 \times A_v \times f_y \times d}{V_u - \phi V_c} = \frac{0.75 \times 0.22 \times 60 \times 4.311}{16 - 11.64} = 9.79 \text{ in.}$$

According to ACI 318-14; Table 9.7.6.2.2 for maximum spacing of shear reinforcement:

$$4\sqrt{f_c'} b_w d = 4 \times \sqrt{22000} \times 6 \times 4.311 = 15.35 \text{ kips}$$

$$V_s = \frac{V_u - \phi V_c}{\phi} = \frac{16 - 11.64}{0.75} = 5.81 \text{ kips} < 4\sqrt{f_c'} b_w d = 15.35 \text{ kips}$$

Hence, maximum spacing:

$$s_{\max} = \frac{d}{2} = \frac{4.311}{2} = 2.16 \text{ in.} < 24 \text{ in.}$$

However, as the cross-sectional dimensions of the beam was small, a transverse reinforcement spacing of 4 in. was considered.

Therefore, for transverse reinforcements #3 Grade 60 deformed stirrups @ 4 in. o.c. was taken.

4.1.2. Specimen UHP-FRC #2 Design Calculations

The second beam was designed with UHP-FRC with micro short steel fibers. The fiber content for the UHP-FRC beam was 3% by volume. High-strength GFRP (Glass, 104 ksi) rebars was used as flexural reinforcements. The design calculations are presented below:

$f_c' = 22 \text{ ksi}$, $\beta_1 = 0.65$

$f_{fu} = 104 \text{ ksi}$

$\varepsilon_{rupture} = 0.018$

$E_f = 5800 \text{ ksi}$

$b = 6 \text{ in.}$

$d = 5.75 \text{ in.}$

$d_c = 1.625 \text{ in.}$

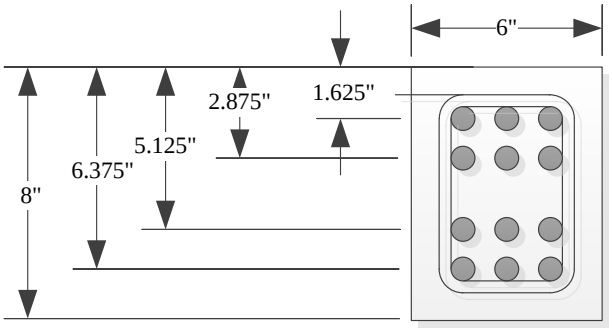

Figure 27. Cross section of UHP-FRC #2.

For the balanced reinforcement ratio *(ACI 440.1R-15: 7.2.1b)*:

$$\rho_{fb} = 0.85\beta_1 \frac{f_c'}{f_{fu}} \frac{E_f \varepsilon_{cu}}{E_f \varepsilon_{cu} + f_{fu}} = 0.85 \times 0.65 \times \frac{22000}{91000} \times \frac{5800 \times 0.015}{5800 \times 0.015 + 91}$$

$$\rho_{fb} = 0.0653$$

For compression control:

$$\rho_f > \rho_{fb} = 0.0653$$

Taking #12 GFRP rebars in a section as shown in the cross section:

$$\rho_f = \frac{A_{st}}{bd} = \frac{6 \times 0.442}{6 \times 5.75} = 0.077 > \rho_{fb}$$ [Compression controlled]

Based on strain compatibility:

$$a = \beta_1 c; \quad c = \frac{a}{\beta_1}$$

$$\frac{\varepsilon_{sc}}{\varepsilon_{cu}} = \frac{c - d_c}{c} \text{ or } \varepsilon_{sc} = \frac{c - d_c}{c} \times \varepsilon_{cu}$$

$$\frac{\varepsilon_{st}}{\varepsilon_{cu}} = \frac{d - c}{c} \text{ or } \varepsilon_{st} = \frac{d - c}{c} \times \varepsilon_{cu}$$

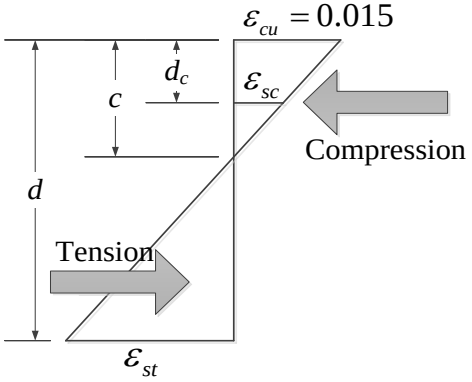

Figure 28. Strain compatibility diagram.

Compression force:

$$C = C_{concrete} + C_{reinforcement}$$

$$C_{concrete} = 0.85 f_c'(ab - A_{sc})$$

$$C_{reinforcement} = A_s f_{sc}$$

where:

$$f_{sc} = \min\left\{\begin{matrix} f_{fu} \\ E_s \times \varepsilon_{sc} \end{matrix}\right\}$$

Tension force:

$$T = A_{st} f_{st}$$

where:

$$f_{st} = \min\left\{\begin{matrix} f_{fu} \\ E_s \times \varepsilon_{st} \end{matrix}\right\}$$

Assuming that the GFRP rebars do not rupture in both tension and compression:

$$f_{sc} = E_s \times \varepsilon_{sc} = E_s \times \frac{c - d_c}{c} \times \varepsilon_{cu}$$

$$f_{st} = E_s \times \varepsilon_{st} = E_s \times \frac{d - c}{c} \times \varepsilon_{cu}$$

Therefore, compression force is now:

$$C = C_{concrete} + C_{reinforcement}$$

$$C = 0.85 f_c' \left(ab - A_s\right) + A_s f_{sc}$$

$$C = 0.85 f_c' \left(ab - A_s\right) + A_s \times E_s \times \left(\frac{c - d_c}{c}\right) \times \varepsilon_{cu}$$

$$C = 0.85 f_c' \left(ab - A_s\right) + A_s \times E_s \times \left(\frac{\frac{a}{\beta_1} - d_c}{\frac{a}{\beta_1}}\right) \times \varepsilon$$

Tension force:

$$T = A_{st} \times \varepsilon_{st} = A_{st} \times E_s \times \left(\frac{d - c}{c}\right) \times \varepsilon_{cu}$$

$$T = A_{st} \times E_s \times \left(\frac{d - \frac{a}{\beta_1}}{\frac{a}{\beta_1}}\right) \times \varepsilon_{cu}$$

Based of equilibrium of forces:

Compression force (C) = Tension force (T)

$$C_{concrete} + C_{reinforcement} = T$$

$$0.85 f_c' \left(ab - A_s\right) + A_s \times E_s \times \left(\frac{\frac{a}{\beta_1} - d_c}{\frac{a}{\beta_1}} \right) \times \varepsilon_{cu} = A_{st} \times E_s \times \left(\frac{d - \frac{a}{\beta_1}}{\frac{a}{\beta_1}} \right) \times \varepsilon_{cu}$$

$$0.85 \times 22 \times \left(a \times 6 - 3 \times 0.442\right) + \left(3 \times 0.442\right) \times 5800 \times \left(\frac{\frac{a}{0.65} - 1.625}{\frac{a}{0.65}} \right) \times 0.015 =$$

$$(6 \times 0.442) \times 5800 \times \left(\frac{5.75 - \frac{a}{0.65}}{\frac{a}{0.65}} \right) \times 0.015$$

Solving for *a*:

$$a = 1.921 \text{ in.}$$

$$c = \frac{a}{\beta_1} = \frac{1.921}{0.65} = 2.955 \text{ in.}$$

Strain in tension longitudinal reinforcement is now:

$$\varepsilon_{st} = \frac{d - c}{c} \varepsilon_{cu} = \frac{5.75 - 2.955}{2.955} \times 0.015 = 0.014 < 0.018$$

Strain in extreme tension longitudinal reinforcement:

$$\varepsilon_{st,\max} = \frac{d_t - c}{c} \varepsilon_{cu} = \frac{6.325 - 2.955}{2.955} \times 0.015 = 0.0171 < 0.018$$

Strain in compression longitudinal reinforcement:

$$\varepsilon_{sc} = \frac{c - d_c}{c} \varepsilon_{cu} = \frac{2.955 - 1.625}{2.955} \times 0.015 = 0.00675 < 0.018$$

Stress in tension longitudinal reinforcement:

$$f_{st} = E_s \varepsilon_{st} = 5800 \times 0.014 = 81.2 \text{ ksi}$$

Stress in extreme tension longitudinal reinforcement:

$$f_{st,\max} = E_s \varepsilon_{st,\max} = 5800 \times 0.0171 = 99.18 \text{ ksi}$$

Stress in compression longitudinal reinforcement:

$$f_{sc} = E_s \varepsilon_{sc} = 5800 \times 0.00675 = 39.15 \text{ ksi}$$

For the compression and tension forces:

$$C_c = 0.85 f_c' \left(ab - A_{sc}\right) = 0.85 \times 22 \times \left(1.921 \times 6 - 3 \times .442\right) = 190.74 \text{ kips}$$

$$C_s = A_{sc} f_{sc} = \left(3 \times 0.442\right) \times 39.15 = 51.91 \text{ kips}$$

$$T = A_{st} f_{st} = 6 \times 0.442 \times 81.2 = 215.34 \text{ kips}$$

Nominal Moment:

$$M_n = C_c \left(d - \frac{a}{2}\right) + C_s \left(d - d_c\right)$$

$$M_n = 190.74 \times \left(5.75 - \frac{1.921}{2}\right) + 51.91 \times \left(5.75 - 1.625\right)$$

$$M_n = 1127.68 \text{ kip-in.} = 93.97 \text{ kip-ft}$$

For development length *(ACI 440.1R-15:10.2b)*:

$$l_{bhf} = \frac{f_{fu}}{37.5} \frac{d_b}{\sqrt{f_c'}} \text{ for } 75000 \text{ psi} < f_{fu} < 150,000 \text{ psi}$$

$$l_{bhf} = \frac{104000}{37.5} \frac{0.75}{\sqrt{22000}} = 14.02 \text{ in.}$$

Effective span of the beam considered:

$$L = 49.5 \text{ in.}$$

$$\text{Shear span to depth ratio} = \frac{49.5}{6} = 8.25$$

Ultimate shear:

$$V_u = \frac{M_n}{L} = \frac{93.97 \text{ kip-ft}}{\frac{49.5}{12} \text{ ft}} = 22.78 \text{ kips}$$

Nominal shear strength provided by concrete:

$$\phi V_c = 0.75 \times 600 \text{ psi} \times bd = 0.75 \times 600 \times 6 \times 5.75 = 15.53 \text{ kips}$$

For the shear reinforcements, No. 3 BFRP rebars are used where:

Area of shear reinforcements:

$$A_v = 2 \times 0.11 = 0.22 \text{ in.}^2$$

For spacing (s) of shear reinforcements:

$$s = \frac{0.75 \times A_v \times f_y \times d}{V_u - \phi V_c} = \frac{0.75 \times 0.22 \times 60 \times 5.75}{22.78 - 15.53} = 7.85 \text{ in.}$$

According to ACI 318-14; Table 9.7.6.2.2 for maximum spacing of shear reinforcement:

$$4\sqrt{f_c'}b_w d = 4\times\sqrt{22000}\times 6\times 5.75 = 20.47 \text{ kips}$$

$$V_s = \frac{V_u - \phi V_c}{\phi} = \frac{20.76 - 15.53}{0.75} = 6.97 \text{ kips} < 4\sqrt{f_c'}b_w d = 20.47 \text{ kips}$$

Hence, maximum spacing:

$$s_{\max} = \frac{d}{2} = \frac{5.75}{2} = 2.88 \text{ in.} < 24 \text{ in.}$$

However, as the cross-sectional dimensions of the beam was small, a transverse reinforcement spacing of 6.5 in. was considered. Therefore, for transverse reinforcements #3 steel stirrups @ 6.5 in. o.c. was taken.

4.1.3. Specimen UHP-FRC #3 Design Calculations

UHP-FRC #3 and #4 had a span-depth ratio much shorter than that of UHP-FRC #1 and #2. The selected span-depth ratio is closer to that of an actual column. In addition, a short span-depth ratio imposes greater shear demand which examine the shear performance of UHP-FRC flexural members.

The beam was designed with UHP-FRC with ultra-high molecular weight polyethylene fiber. The fiber content for the UHP-FRC beam was 0.75% by volume. High-strength GFRP (Glass, 104 ksi) rebars was used as flexural reinforcements. The design calculations are presented below:

$f_c' = 20$ ksi , $\beta_1 = 0.65$

$f_{fu} = 145.8$ ksi

$\varepsilon_{rupture} = 0.024$

$E_f = 6141$ ksi

$b = 8$ in.

$d = 5.35$ in.

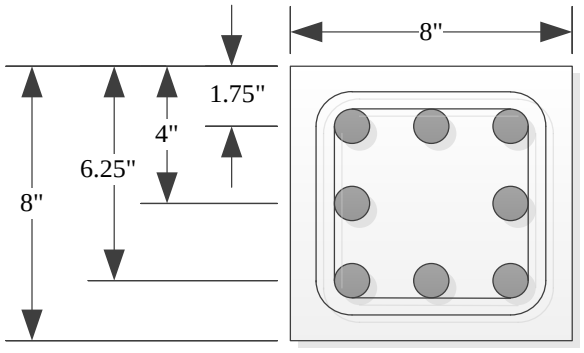

Figure 29. Cross section of UHP-FRC #3.

For the balanced reinforcement ratio *(ACI 440.1R-15: 7.2.1b)*:

$$\rho_{fb} = 0.85\beta_1 \frac{f_c^{'}}{f_{fu}} \frac{E_f \varepsilon_{cu}}{E_f \varepsilon_{cu} + f_{fu}} = 0.85 \times 0.65 \times \frac{20000}{145800} \times \frac{6141 \times 0.015}{6141 * 0.015 + 145.8}$$

$$\rho_{fb} = 0.0293$$

For compression control:

$$\rho_f > \rho_{fb} = 0.0293$$

Taking #8 BFRP rebars in a section:

$$\rho_f = \frac{A_{st}}{bd} = \frac{5 \times 0.79}{8 \times 5.35} = 0.0923 > \rho_{fb}$$ (Compression controlled)

Based on strain compatibility:

$$a = \beta_1 c\ ;\ \ c = \frac{a}{\beta_1}$$

$$\frac{\varepsilon_{sc}}{\varepsilon_{cu}} = \frac{c - d_c}{c} \text{ or } \varepsilon_{sc} = \frac{c - d_c}{c} \times \varepsilon_{cu}$$

$$\frac{\varepsilon_{st}}{\varepsilon_{cu}} = \frac{d - c}{c} \text{ or } \varepsilon_{st} = \frac{d - c}{c} \times \varepsilon_{cu}$$

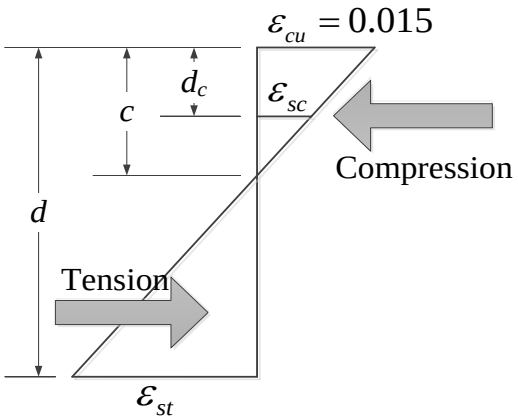

Figure 30. Strain compatibility diagram.

Compression force:

$$C = C_{concrete} + C_{reinforcement}$$

$$C_{concrete} = 0.85 f_c' (ab - A_{sc})$$

$$C_{reinforcement} = A_s f_{sc}$$

where:

$$f_{sc} = \min\left\{\begin{matrix} f_{fu} \\ E_s \times \varepsilon_{sc} \end{matrix}\right\}$$

Tension force:

$$T = A_{st} f_{st}$$

where:

$$f_{st} = \min\left\{\begin{matrix} f_{fu} \\ E_s \times \varepsilon_{st} \end{matrix}\right\}$$

Assuming that the BFRP rebars do not rupture in both tension and compression:

$$f_{sc} = E_s \times \varepsilon_{sc} = E_s \times \frac{c - d_c}{c} \times \varepsilon_{cu}$$

$$f_{st} = E_s \times \varepsilon_{st} = E_s \times \frac{d - c}{c} \times \varepsilon_{cu}$$

Compression force is now:

$$C = C_{concrete} + C_{reinforcement}$$

$$C = 0.85 f_c' \left(ab - A_s\right) + A_s f_{sc}$$

$$C = 0.85 f_c' \left(ab - A_s\right) + A_s \times E_s \times \left(\frac{c - d_c}{c}\right) \times \varepsilon_{cu}$$

$$C = 0.85 f_c' \left(ab - A_s\right) + A_s \times E_s \times \left(\frac{\frac{a}{\beta_1} - d_c}{\frac{a}{\beta_1}}\right) \times \varepsilon$$

Tension force:

$$T = A_{st} \times \varepsilon_{st} = A_{st} \times E_s \times \left(\frac{d - c}{c}\right) \times \varepsilon_{cu}$$

$$T = A_{st} \times E_s \times \left(\frac{d - \frac{a}{\beta_1}}{\frac{a}{\beta_1}}\right) \times \varepsilon_{cu}$$

Based of equilibrium of forces:

Compression force (C) = Tension force (T)

$$C_{concrete} + C_{reinforcement} = T$$

$$0.85 f_c' \left(ab - A_s\right) + A_s \times E_s \times \left(\frac{\frac{a}{\beta_1} - d_c}{\frac{a}{\beta_1}} \right) \times \varepsilon_{cu} = A_{st} \times E_s \times \left(\frac{d - \frac{a}{\beta_1}}{\frac{a}{\beta_1}} \right) \times \varepsilon_{cu}$$

$$0.85 \times 20 \times \left(a \times 8 - 3 \times 0.79\right) + \left(3 \times 0.79\right) \times 6141 \times \left(\frac{\frac{a}{0.65} - 1.75}{\frac{a}{0.65}} \right) \times 0.015$$

$$= \left(5 \times 0.79\right) \times 6141 \times \left(\frac{5.35 - \frac{a}{0.65}}{\frac{a}{0.65}} \right) \times 0.015$$

Solving for *a*:

$a = 1.893$ in.

$$c = \frac{a}{\beta_1} = \frac{1.893}{0.65} = 2.91 \text{ in.}$$

Strain in tension longitudinal reinforcement is now:

$$\varepsilon_{st} = \frac{d - c}{c} \varepsilon_{cu} = \frac{5.35 - 2.91}{2.91} * 0.015 = 0.0126 < 0.024$$

Strain in extreme tension longitudinal reinforcement:

$$\varepsilon_{st,\max} = \frac{d_t - c}{c} \varepsilon_{cu} = \frac{6.25 - 2.91}{2.91} \times 0.015 = 0.0172 < 0.024$$

Strain in extreme compression longitudinal reinforcement:

$$\varepsilon_{sc} = \frac{c - d_c}{c} \varepsilon_{cu} = \frac{2.91 - 1.75}{2.91} \times 0.015 = 0.006 < 0.024$$

Stress in tension longitudinal reinforcement:

$$f_{st} = E_s \varepsilon_{st} = 6141 \times 0.0126 = 77.38 \text{ ksi}$$

Stress in extreme tension longitudinal reinforcement:

$$f_{st,\max} = E_s \varepsilon_{st} = 6141 \times 0.0172 = 105.63 \text{ ksi}$$

Stress in compression longitudinal reinforcement:

$$f_{sc} = E_s \varepsilon_{sc} = 6141 \times 0.006 = 36.85 \text{ ksi}$$

For compression and tension forces:

$$C_c = 0.85 f_c' \left(ab - A_{sc}\right) = 0.85 \times 20 \times \left(1.893 \times 8 - 3 \times .79\right) = 217.16 \text{ kips}$$

$$C_s = A_{sc} f_{sc} = \left(3 \times 0.79\right) \times 36.85 = 87.33 \text{ kips}$$

$$T = A_{st} f_{st} = 5 \times 0.79 \times 77.38 = 305.65 \text{ kips}$$

Nominal Moment:

$$M_n = C_c \left(d - \frac{a}{2} \right) + C_s \left(d - d_c \right)$$

$$M_n = 217.16 \times \left(5.35 - \frac{1.893}{2} \right) + 87.33 \times \left(5.35 - 1.75 \right)$$

$$M_n = 1270.65 \text{ kip-in.} = 105.89 \text{ kip-ft}$$

For development length *(ACI 440.1R-15:10.2b)*:

$$l_{bhf} = \frac{f_{fu}}{37.5} \frac{d_b}{\sqrt{f_c'}} \text{ for } 75000 \text{ psi} < f_{fu} < 150,000 \text{ psi}$$

$$l_{bhf} = \frac{105630}{37.5} \frac{1}{\sqrt{20000}} = 19.92 \text{ in.}$$

Considering a shear span to depth ratio of 4. For the effective length of the beam:

$$L = 4 \times 8 = 32 \text{ in.}$$

Taking the effective span as:

$$L = 34 \text{ in.}$$

Ultimate shear:

$$V_u = \frac{M_n}{L} = \frac{105.89 \text{ kip-ft}}{\frac{34}{12} \text{ ft}} = 37.37 \text{ kips}$$

Nominal shear strength provided by concrete:

$$\phi V_c = 0.75 \times 600 \text{ psi} \times bd = 0.75 \times 600 \times 8 \times 5.35 = 19.26 \text{ kips}$$

For the shear reinforcements, No. 4 BFRP rebars are used where:

$$f_{rupture} = 126 \text{ ksi}$$

Area of shear reinforcements:

$$A_v = 2 \times 0.196 = 0.392 \text{ in.}^2$$

For spacing (s) of shear reinforcements:

$$s = \frac{0.75 \times A_v \times f_y \times d}{V_u - \phi V_c} = \frac{0.75 \times 0.392 \times 126 \times 5.35}{37.37 - 19.26} = 10.94 \text{ in.}$$

According to ACI 318-14; Table 9.7.6.2.2 for maximum spacing of shear reinforcement:

$$4\sqrt{f_c'}\,b_w d = 4\times\sqrt{20000}\times 8\times 5.35 = 24.21 \text{ kips}$$

$$V_s = \frac{V_u - \phi V_c}{\phi} = \frac{37.37 - 28.8}{0.75} = 11.43 \text{ kips} < 4\sqrt{f_c'}\,b_w d = 24.21 \text{ kips}$$

Hence, maximum spacing:

$$s_{\max} = \frac{d}{2} = \frac{5.35}{2} = 2.675 \text{ in.} < 24 \text{ in.}$$

However, as the cross-sectional dimensions of the beam was small, a transverse reinforcement spacing of 6 in. was considered. Therefore, for transverse reinforcements #4 BFRP stirrups @ 6 in. o.c. was taken.

4.1.4. Specimen UHP-FRC #4 Design Calculations

The beam was designed with UHP-FRC with micro short steel fibers. The fiber content for the UHP-FRC beam was 3% by volume. High-strength GFRP (Glass, 104 ksi) rebars were used as flexural reinforcements. The design calculations are presented below:

$f_c' = 22$ ksi , $\beta_1 = 0.65$

$f_{fu} = 145.8$ ksi

$\varepsilon_{rupture} = 0.024$

$E_f = 6141$ ksi

$b = 8$ in.

$d = 5.35$ in.

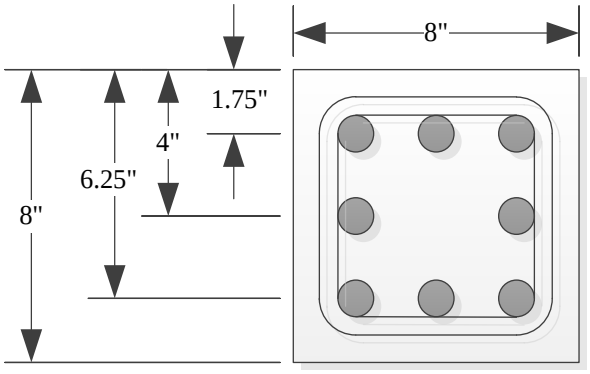

Figure 31. Cross section of UHP-FRC #4.

For the balanced reinforcement ratio *(ACI 440.1R-15: 7.2.1b)*:

$$\rho_{fb} = 0.85\beta_1 \frac{f_c'}{f_{fu}} \frac{E_f \varepsilon_{cu}}{E_f \varepsilon_{cu} + f_{fu}} = 0.85\times 0.65\times \frac{22000}{145800}\times \frac{6141\times 0.015}{6141\times 0.015 + 145.8}$$

$$\rho_{fb} = 0.0323$$

For compression control:

$$\rho_f > \rho_{fb} = 0.0323$$

Taking #8 BFRP rebars in a section as shown:

$$\rho_f = \frac{A_{st}}{bd} = \frac{5 \times 0.79}{8 \times 5.35} = 0.0923 > \rho_{fb} \text{ (Compression controlled)}$$

Based on strain compatibility:

$$a = \beta_1 c; \quad c = \frac{a}{\beta_1}$$

$$\frac{\varepsilon_{sc}}{\varepsilon_{cu}} = \frac{c - d_c}{c} \text{ or } \varepsilon_{sc} = \frac{c - d_c}{c} \times \varepsilon_{cu}$$

$$\frac{\varepsilon_{st}}{\varepsilon_{cu}} = \frac{d - c}{c} \text{ or } \varepsilon_{st} = \frac{d - c}{c} \times \varepsilon_{cu}$$

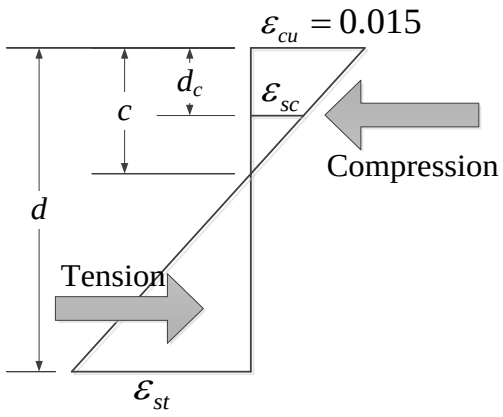

Figure 32. Strain compatibility diagram.

Compression force:

$$C = C_{concrete} + C_{reinforcement}$$

$$C_{concrete} = 0.85 f_c'(ab - A_{sc})$$

$$C_{reinforcement} = A_s f_{sc}$$

where:

$$f_{sc} = \min \begin{Bmatrix} f_{fu} \\ E_s \times \varepsilon_{sc} \end{Bmatrix}$$

Tension force:

$$T = A_{st} f_{st}$$

where:

$$f_{st} = \min \begin{Bmatrix} f_{fu} \\ E_s \times \varepsilon_{st} \end{Bmatrix}$$

Assuming that the BFRP rebars do not rupture in both tension and compression:

$$f_{sc} = E_s \times \varepsilon_{sc} = E_s \times \frac{c - d_c}{c} \times \varepsilon_{cu}$$

$$f_{st} = E_s \times \varepsilon_{st} = E_s \times \frac{d - c}{c} \times \varepsilon_{cu}$$

The compression force is now:

$$C = C_{concrete} + C_{reinforcement}$$

$$C = 0.85 f_c' \left(ab - A_s \right) + A_s f_{sc}$$

$$C = 0.85 f_c' \left(ab - A_s \right) + A_s \times E_s \times \left(\frac{c - d_c}{c} \right) \times \varepsilon_{cu}$$

$$C = 0.85 f_c' \left(ab - A_s \right) + A_s \times E_s \times \left(\frac{\frac{a}{\beta_1} - d_c}{\frac{a}{\beta_1}} \right) \times \varepsilon$$

Tension force:

$$T = A_{st} \times \varepsilon_{st} = A_{st} \times E_s \times \left(\frac{d - c}{c} \right) \times \varepsilon_{cu}$$

$$T = A_{st} \times E_s \times \left(\frac{d - \frac{a}{\beta_1}}{\frac{a}{\beta_1}} \right) \times \varepsilon_{cu}$$

Based of equilibrium of forces:

Compression force (C) = Tension force (T)

$$C_{concrete} + C_{reinforcement} = T$$

$$0.85 f_c' \left(ab - A_s \right) + A_s \times E_s \times \left(\frac{\frac{a}{\beta_1} - d_c}{\frac{a}{\beta_1}} \right) \times \varepsilon_{cu} = A_{st} \times E_s \times \left(\frac{d - \frac{a}{\beta_1}}{\frac{a}{\beta_1}} \right) \times \varepsilon_{cu}$$

$$0.85\times 22\times\left(a\times 8-3\times 0.79\right)+\left(3\times 0.79\right)\times 6141\times\left(\frac{\frac{a}{0.65}-1.75}{\frac{a}{0.65}}\right)\times 0.015$$

$$=\left(5\times 0.79\right)\times 6141\times\left(\frac{5.35-\frac{a}{0.65}}{\frac{a}{0.65}}\right)\times 0.015$$

Solving for *a*:

$$a=1.856 \text{ in.}$$

$$c=\frac{a}{\beta_1}=\frac{1.856}{0.65}=2.855 \text{ in.}$$

Strain in tension longitudinal reinforcement is now:

$$\varepsilon_{st}=\frac{d-c}{c}\varepsilon_{cu}=\frac{5.35-2.855}{2.855}\times 0.015=0.0131<0.024$$

Strain in extreme tension longitudinal reinforcement:

$$\varepsilon_{st,\max}=\frac{d_t-c}{c}\varepsilon_{cu}=\frac{6.25-2.855}{2.855}*0.015=0.0178<0.024$$

Strain in extreme compression longitudinal reinforcement:

$$\varepsilon_{sc}=\frac{c-d_c}{c}\varepsilon_{cu}=\frac{2.855-1.75}{2.855}*0.015=0.0058<0.024$$

Stress in tension longitudinal reinforcement:

$$f_{st}=E_s\varepsilon_{st}=6141\times 0.0131=80.45 \text{ ksi}$$

Stress in extreme tension longitudinal reinforcement:

$$f_{st,\max}=E_s\varepsilon_{st,\max}=6141\times 0.0178=109.31 \text{ ksi}$$

Stress in compression longitudinal reinforcement:

$$f_{sc}=E_s\varepsilon_{sc}=6141\times 0.0058=35.62 \text{ ksi}$$

For compression and tension forces:

$$C_c=0.85f_c'\left(ab-A_{sc}\right)=0.85\times 22\times\left(1.856\times 8-3\times .79\right)=233.34 \text{ kips}$$

$$C_s=A_{sc}f_{sc}=\left(3\times 0.79\right)\times 35.62=84.42 \text{ kips}$$

$$T=A_{st}f_{st}=5\times 0.79\times 80.45=317.78 \text{ kips}$$

Nominal Moment:

$$M_n = C_c\left(d - \frac{a}{2}\right) + C_s\left(d - d_c\right)$$

$$M_n = 233.34 \times \left(5.35 - \frac{1.856}{2}\right) + 84.42 \times \left(5.35 - 1.75\right)$$

$$M_n = 1335.74 \text{ kip-in.} = 111.31 \text{ kip-ft}$$

For development length *(ACI 440.1R-15:10.2b)*:

$$l_{bhf} = \frac{f_{fu}}{37.5}\frac{d_b}{\sqrt{f_c'}} f \text{ for } 75000 \text{ psi} < f_{fu} < 150{,}000 \text{ psi}$$

$$l_{bhf} = \frac{109310}{37.5}\frac{1}{\sqrt{22000}} = 19.65 \text{ in.}$$

Considering a shear span to depth ratio of 4. For the effective length of the beam:

$$L = 4 \times 8 = 32 \text{ in.}$$

Taking the effective span as:

$$L = 34 \text{ in.}$$

Ultimate shear:

$$V_u = \frac{M_n}{L} = \frac{111.31 \text{ kip-ft}}{\frac{34}{12} \text{ ft}} = 39.29 \text{ kips}$$

Nominal shear strength provided by concrete:

$$\phi V_c = 0.75 \times 600 \text{ psi} \times bd = 0.75 \times 600 \times 8 \times 5.35 = 19.26 \text{ kips}$$

For the shear reinforcements, No. 4 BFRP rebars are used where:

$$f_{rupture} = 126 \text{ ksi}$$

Area of shear reinforcements:

$$A_v = 2 \times 0.196 = 0.392 \text{ in.}^2$$

For spacing (s) of shear reinforcements:

$$s = \frac{0.75 \times A_v \times f_y \times d}{V_u - \phi V_c} = \frac{0.75 \times 0.392 \times 126 \times 5.35}{39.29 - 19.26} = 9.89 \text{ in.}$$

According to ACI 318-14; Table 9.7.6.2.2 for maximum spacing of shear reinforcement:

$$4\sqrt{f_c'} b_w d = 4 \times \sqrt{22000} \times 8 \times 5.35 = 25.39 \text{ kips}$$

$$V_s = \frac{V_u - \phi V_c}{\phi} = \frac{39.29 - 28.8}{0.75} = 13.99 \text{ kips} < 4\sqrt{f_c'} b_w d = 25.39 \text{ kips}$$

Hence, maximum spacing:

$$s_{max} = \frac{d}{2} = \frac{5.35}{2} = 2.675 \text{ in.} < 24 \text{ in.}$$

However, as the cross-sectional dimensions of the beam was small, a transverse reinforcement spacing of 6 in. was considered. Therefore, for transverse reinforcements #4 BFRP stirrups @ 6 in. o.c. was used.

4.2. Specimen Preparation

The specimens were constructed at the UT Arlington Civil Engineering Laboratory Building (CELB).

4.2.1 Strain Gauge Installation

Strain gauges were installed (Figure 33) on the flexural reinforcements near the interface of the reinforced concrete block and the cantilever UHP-FRC specimen. The exact locations of the strain gauges are depicted in Figures 34 to 37. The installation process includes marking, grinding, and sanding of the longitudinal reinforcements at the locations predetermined to obtain a flat, smooth surface for the strain gauges. A 400-grit sandpaper was used for sanding process. After that the strain gauges were glued to the surface and three layers of coating, polyurethane, nitrile, rubber mastic electrical tape and electric liquid, were applied to seal the moisture.

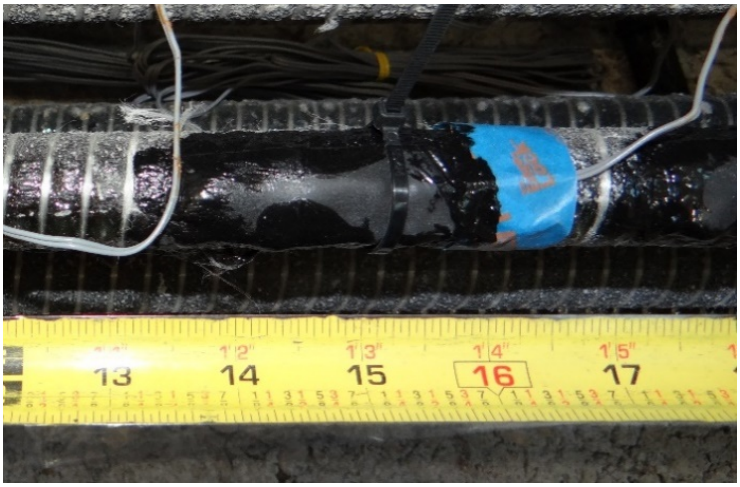

Figure 33. Strain gauge installed on a flexural reinforcement (BFRP).

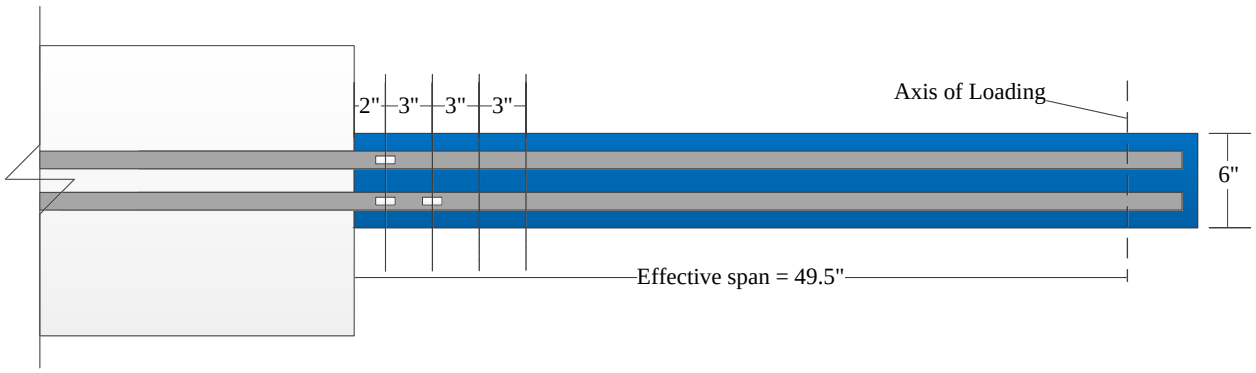

Figure 34. Strain gauge location for UHP-FRC #1.

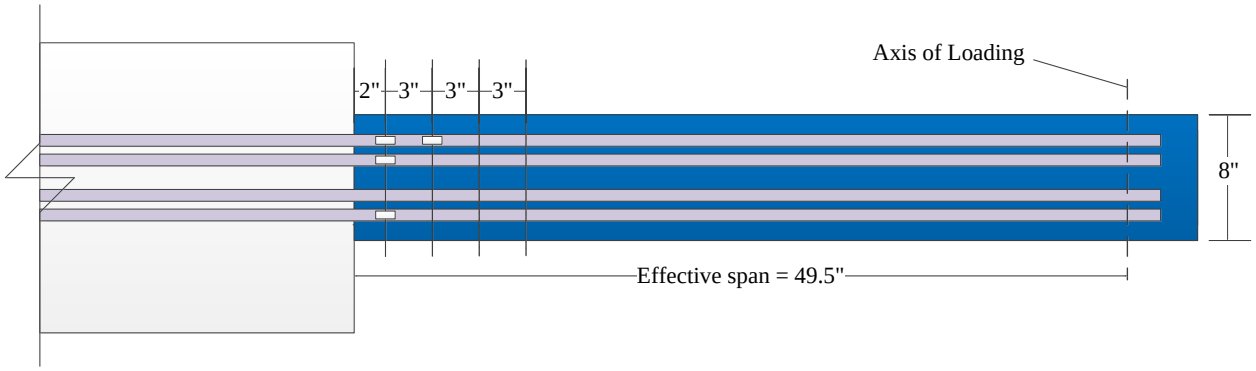

Figure 35. Strain gauge location for UHP-FRC #2.

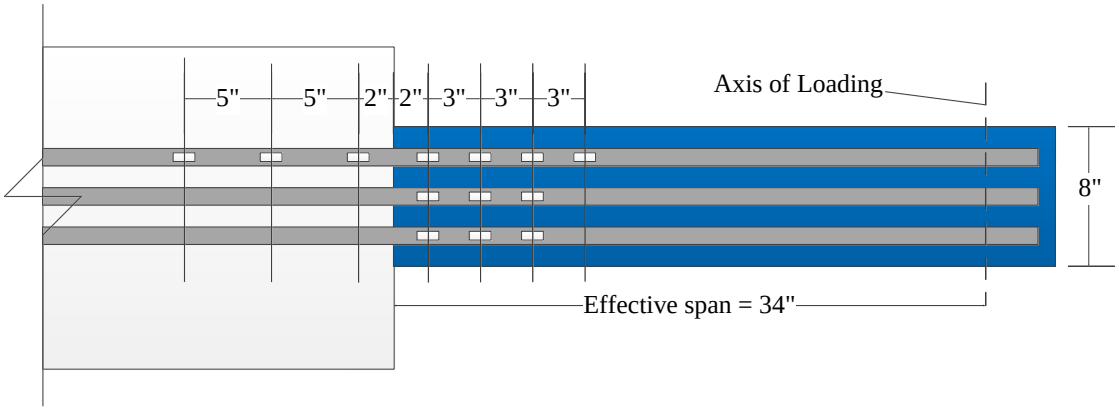

Figure 36. Strain gauge location for UHP-FRC #3.

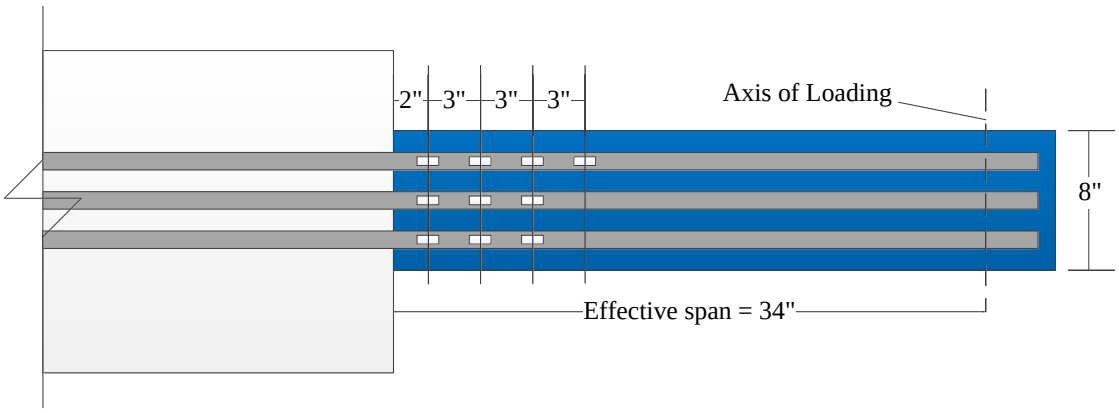

Figure 37. Strain gauge location for UHP-FRC #4.

4.2.2. Caging and Formwork Fabrication

Reinforcing bar cage for the UHP-FRC beam specimens as well as their supporting reinforced concrete block was prepared at the UT Arlington CELB. The preparation of the four specimens was conducted along with the preparation of a total of two supporting blocks (two specimens per support block). The reinforcement cage for the support block was prepared and placed in the formwork as shown in Figure 38. Additional reinforcements (Figure 39) were provided at the beam-block interface to prevent compression failure of the concrete of the support block. The reinforcements for the beam specimens were prepared (Figure 40). The prepared specimen reinforcements were inserted in the support cage as shown in Figure 41 and 42.

Figure 38. Preparation of support block cage and positioning inside the formwork.

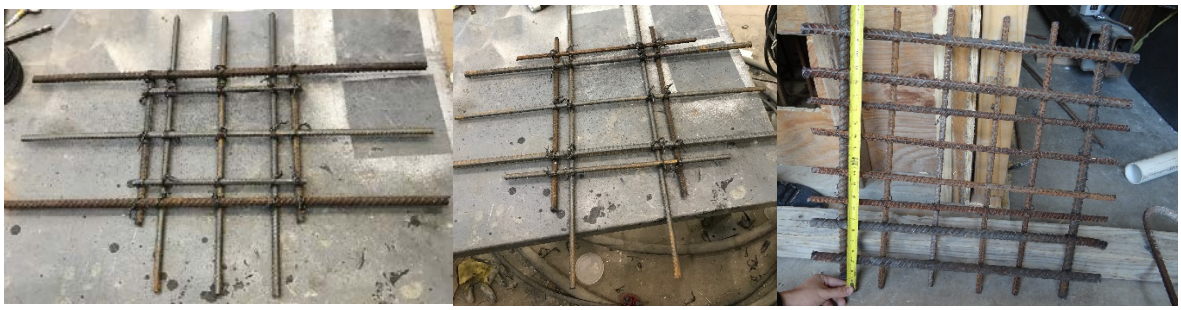

(a) (b) (c)

Figure 39. Additional reinforcements provided at the beam-block interface for (a) UHP-FRC #1 (b) UHP-FRC #2 (c) UHP-FRC #3 and #4.

(a) (b)

Figure 40. Reinforcement for specimens (a) UHP-FRC #1 and UHP-FRC #2 (b) UHP-FRC #3 and UHP-FRC #4.

Figure 41. Reinforcement for specimens UHP-FRC #1 (left) and UHP-FRC #2 (right).

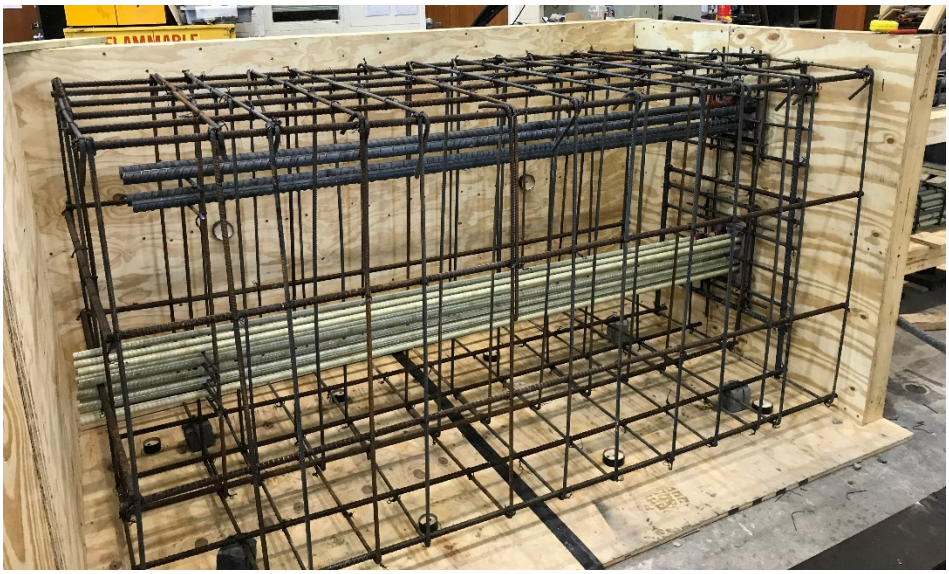

Figure 42. Reinforcements for the specimens inserted in the support reinforcement cage.

4.2.3. Mixing of Concrete, Casting and Curing of the UHP-FRC Specimens

Reinforced Concrete Support Block: A concrete with a design compressive strength of 5 ksi was poured in the support reinforced concrete block (Figure 43 and 44). The concrete was obtained from a local ready-mix truck with a specified slump of 5 inches. The concrete was initially poured on a wheelbarrow to check for consistency and slump prior to pouring concrete into the support block formwork. The concrete was then poured into the formwork and vibrated with a needle vibrator for compactness.

Figure 43. Concrete pouring of the support block.

Figure 44. The hardened concrete of the support block shown with the specimen (UHP-FRC #3 and UHP-FRC #4 specimen BFRP reinforcements).

UHP-FRC Specimens: The dry component materials of the UHP-FRC were weighed in pounds and collected as per the required proportion. It was then transferred to the pan mixer (Figure 45) for mixing and dry mixed initially. The water was added in gradual portions in order to get a good paste. After a uniform paste was ready, the fibers as per the required proportion were added and was mixed again for a few minutes till a consistent mix (Figure 46) was obtained. The UHP-FRC was then transferred from the mixer into the specimens (Figure 47 and 48) by using buckets. The specimen was cured in the strong floor room at a temperature of 77°F (25°C) and a relative humidity of 100% until the day of testing. Figure 49 shows the prepared final specimens UHP-FRC #3 and UHP-FRC #4 after the removal of the formwork.

(a) **(b)**

Figure 45. (a) Rotating pan mixer used for UHP-FRC (b) UHP-FRC preparation.

(a) **(b)**

Figure 46. (a) UHP-FRC preparation using a pan mixer (b) Consistent UHP-FRC mix showing uniform distribution of fibers.

Figure 47. UHP-FRC pouring for the specimens.

Figure 48. UHP-FRC pouring for the specimens.

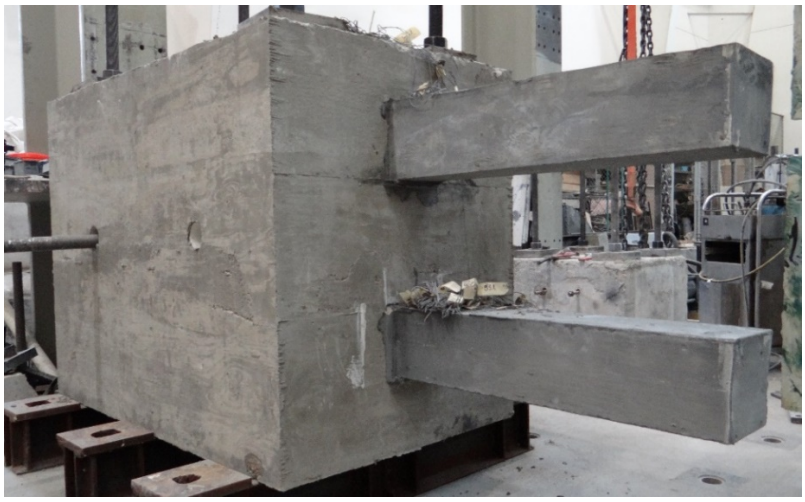

Figure 49. Prepared specimens UHP-FRC #3 and UHP-FRC #4.

4.2.4. Test Setup and Instrumentation

The loading of the specimen is achieved using a 400-kip Material Testing System (MTS) hydraulic actuator in the Civil Engineering Laboratory Building (CELB) at UTA using the loading protocol as shown in Figure 50. Displacement control was used for the loading of the specimens. The beams were loaded in the loading axis between two bearing plates of 6 in. wide along the length of the beam and 1 in. thick. The plates were spread along the entire width of the beam. A layer of grout was used at the contact surface between the UHP-FRC specimen and the loading plate to ensure a uniform interface contact. Lateral stiffeners were used on the lateral sides of the beam to prevent any torsional movement.

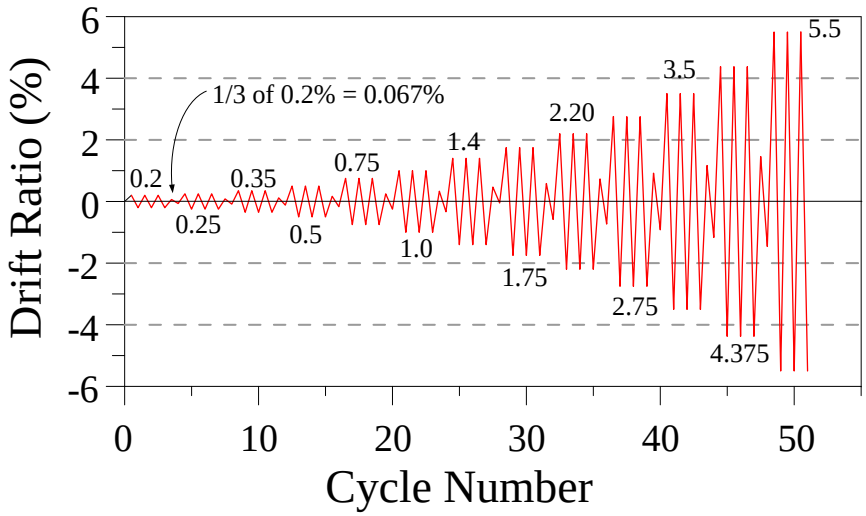

Figure 50. Loading protocol for reversed cyclic loading.

The test setup consists of a load application mechanism as shown in Figure 51 and Figure 52, four linear variable differential transformers (LVDTs) along with a string pot. The LVDTs and string pot was used to measure the vertical displacement and the strain gauges provide the

strain value of the flexural reinforcements in the specimen. All sensors were connected to the DAQ box and the data was recorded.

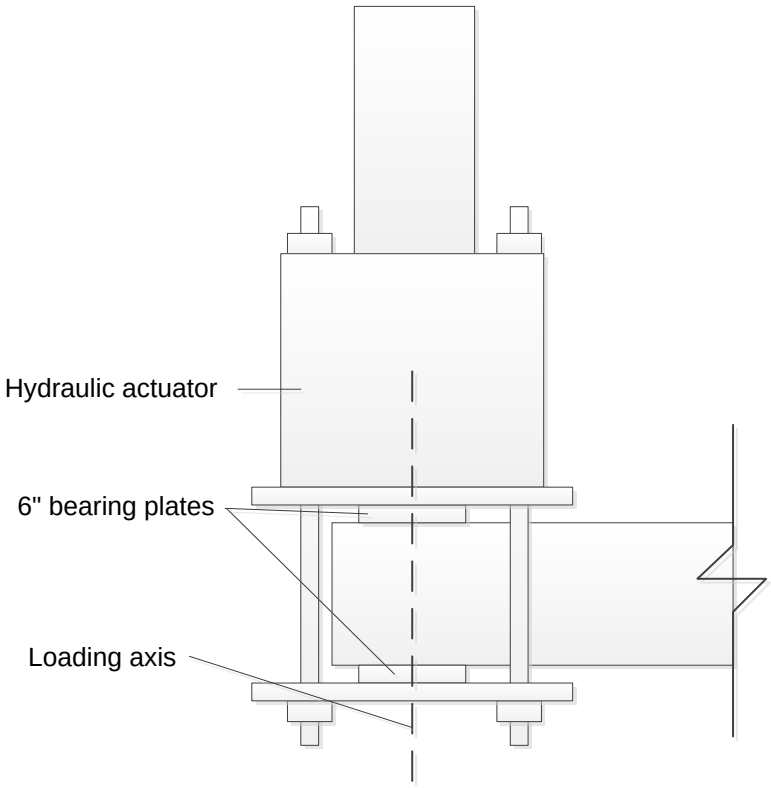

Figure 51. Cyclic load application mechanism on the cantilever specimen.

The drift ratio was calculated using the formula shown below. The shear stress was obtained from the recorded peak's longitudinal load using the formulae presented below:

$$D = \frac{V}{S} \times 100\% \qquad [7]$$

where:

D = Drift ratio (%)
V = Net vertical displacement of the specimen (in.)
S = Effective span (in.)

$$M = P \times \frac{S}{1000} \qquad [8]$$

where:

M = Applied moment (kips-in.)
P = Applied load (lbf)
S = Effective span (in.)

Figure 52. Figure showing the loading head setup of the cantilever specimen.

4.2.5. Material Testing

UHP-FRC Compressive Strength: The compressive strength is typically determined by testing standard 6×12 in. or 4×8 in. cylinders. However, using this method for very high strength concrete is difficult because of higher loading capacity of the machines and the need for the cylinders to have their ends fully smoothened *(26)*. In this research, 2.78 in. (70.7 mm) cubes were used to determine the compressive strength. Although some researchers believe cylinders have more accurate compressive strength, cubes are an acceptable alternative to the standard 4 in. (102 mm) cylinders. The main objective of the compressive strength is to obtain the compressive strength of UHP-FRC at the time of specimen testing.

5. ANALYSIS AND FINDINGS

Four pilot UHP-FRC reduced scale columns, one with corrosion resistant MMFX high-strength steel rebars (100 ksi as per ASTM A1035, 2016), one with non-corrosive high-strength GFRP (glass, 90 ksi) rebars, and two with non-corrosive high-strength BFRP (Basalt, 147 ksi) rebars were tested at UT Arlington under large displacement reversals to prove the proposed new DCSR design concept. All columns had a reinforcement ratio of 14%. The last two specimens were designed to have a smaller length-to-depth ratio to increase the shear force demand. UHMW polyethylene fibers (13 mm in length and 0.0015 mm in diameter with a tensile strength of 375 ksi) were used for specimen # 3 while micro steel fibers (13 mm in length and 0.2 mm in diameter with a tensile strength of 399 ksi) were used for the other three specimens.

All column specimens sustained very large cyclic displacements without major damage in the UHP-FRC material, which provided ample shear strength and confinement to the reinforcement throughout the testing. Even with the high amount of reinforcement, UHP-FRC's superior ductility provided a very stable cyclic behavior up to very large drift ratios. All specimens also exhibited a self-centering ability, which considerably reduces the residual displacement after being subject to large lateral displacements. This pilot testing also shows that the very high damage resistant and self-centering characteristics of the proposed columns made of high-performance materials and designed by the DCSR concept can provide excellent resilience (which requires no repair work after major earthquakes) for building structures in earthquake-prone areas.

5.1. UHP-FRC #1

A maximum moment of 840 kip-in. (95 kN-m) was recorded at a drift ratio of 8%. Moment versus drift ratio relationship of beam UHP-FRC #1 showed large cyclic deformation up to a drift ratio of 8% without significant damage to the UHP-FRC material. The specimen exhibited stable cyclic behavior up to very large drift ratios. From the Figure 53, it can be seen that there is minor residual deformation. Flexural cracking was seen to be the primary mode of cracking during the test. From the strain data, it was observed that the MMFX rebars slightly yielded at the interface. The moment and reinforcement strain relationship can be viewed in Figure 54. The test pictures of the specimen for different values of drift ratio can be viewed from Figure 55 to 69. The test was terminated before any strength deterioration because of limited space for further displacement.

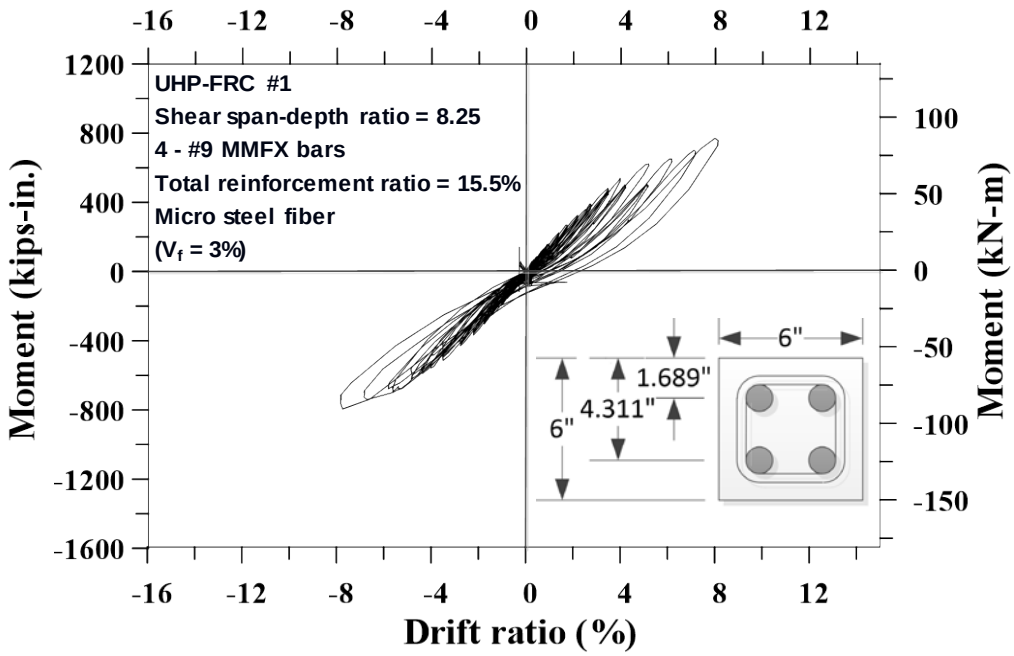

Figure 53. Moment vs Drift ratio for UHP-FRC #1 with steel fibers (MMFX bars).

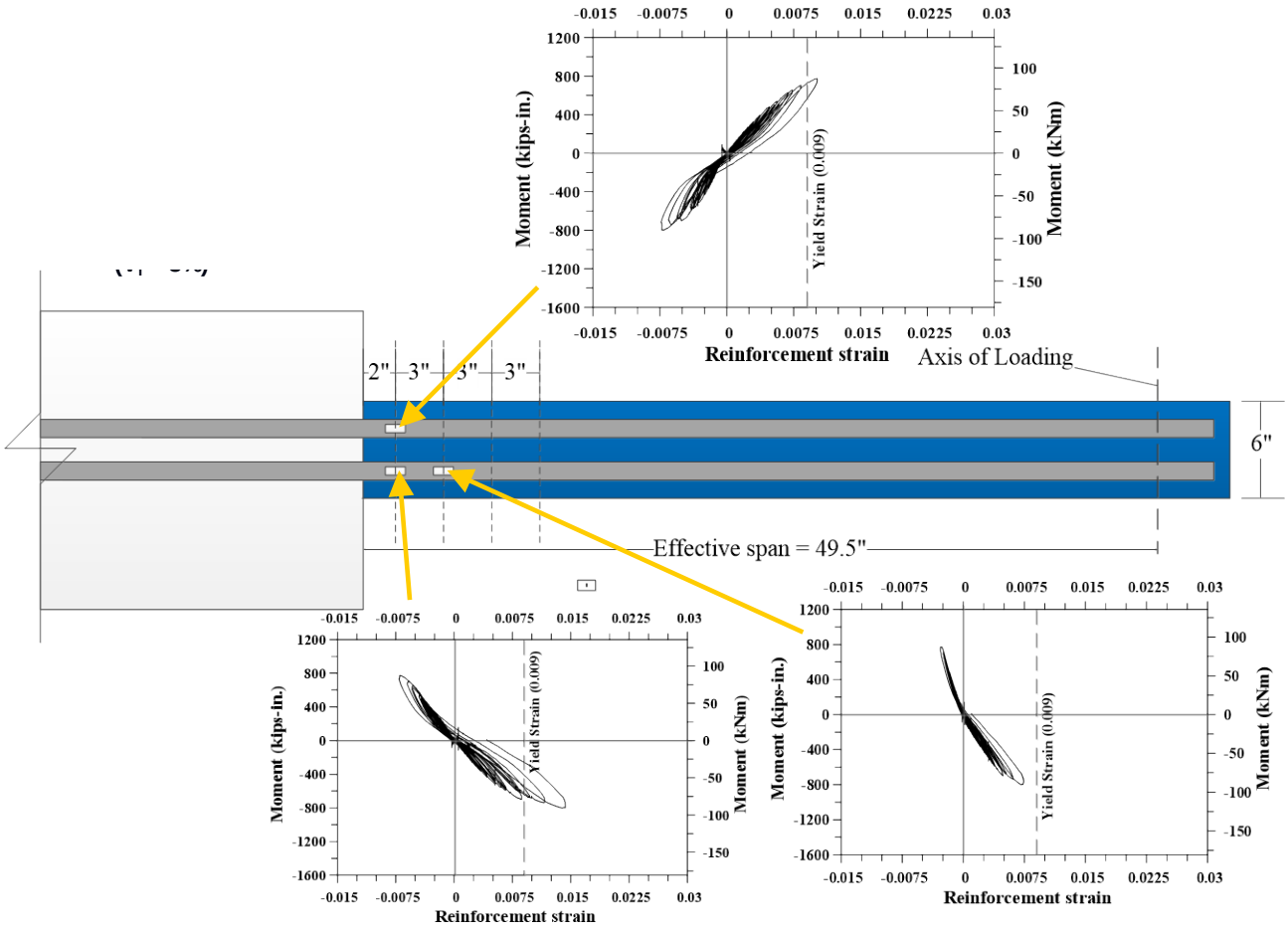

Figure 54. Moment vs reinforcement strain for UHP-FRC #1.

Figure 55. UHP-FRC #1 at 0.2% drift ratio.

Figure 56. UHP-FRC #1 at 0.25% drift ratio.

Figure 57. UHP-FRC #1 at 0.35% drift ratio.

Figure 58. UHP-FRC #1 at 0.5% drift ratio.

Figure 59. UHP-FRC #1 at 0.75% drift ratio.

Figure 60. UHP-FRC #1 at 1.0% drift ratio.

Figure 61. UHP-FRC #1 at 1.4% drift ratio.

Figure 62. UHP-FRC #1 at 1.75% drift ratio.

Figure 63. UHP-FRC #1 at 2.2% drift ratio.

Figure 64. UHP-FRC #1 at 2.75% drift ratio.

Figure 65. UHP-FRC #1 at 3.5% drift ratio.

Figure 66. UHP-FRC #1 at 4.0% drift ratio.

Figure 67. UHP-FRC #1 at 5.0% drift ratio.

Figure 68. UHP-FRC #1 at 7.0% drift ratio.

Figure 69. UHP-FRC #1 at 8.0% drift ratio.

5.2. UHP-FRC #2

A maximum moment of 1050 kip-in. (119 kN-m) was recorded at a drift ratio of 13%. Moment versus drift ratio relationship of beam UHP-FRC #2 showed large cyclic deformation up to a drift ratio of 10% without significant damage to the UHP-FRC material. Stable cyclic behavior was observed up to 13% drift ratio after which the moment started to decrease. From the Figure 70, it can be seen that there is minor residual deformation. Flexural cracking was seen to be the governing mode of cracking during the test. Strain data of flexural reinforcements (Figure 71) indicate that the rebars were fully elastic during the testing. The test pictures of the specimen for different values of drift ratio can be viewed from Figure 72 to 92. The test was terminated before any strength deterioration because of limited space for further displacement.

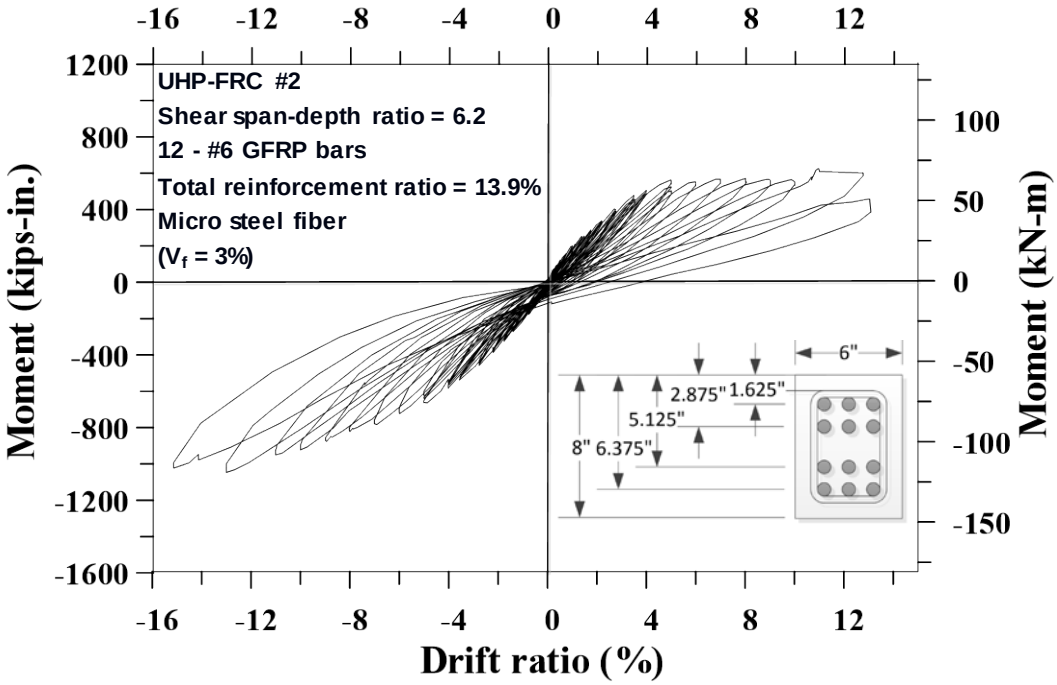

Figure 70. Moment vs Drift ratio for UHP-FRC #2 with steel fibers (GFRP bars).

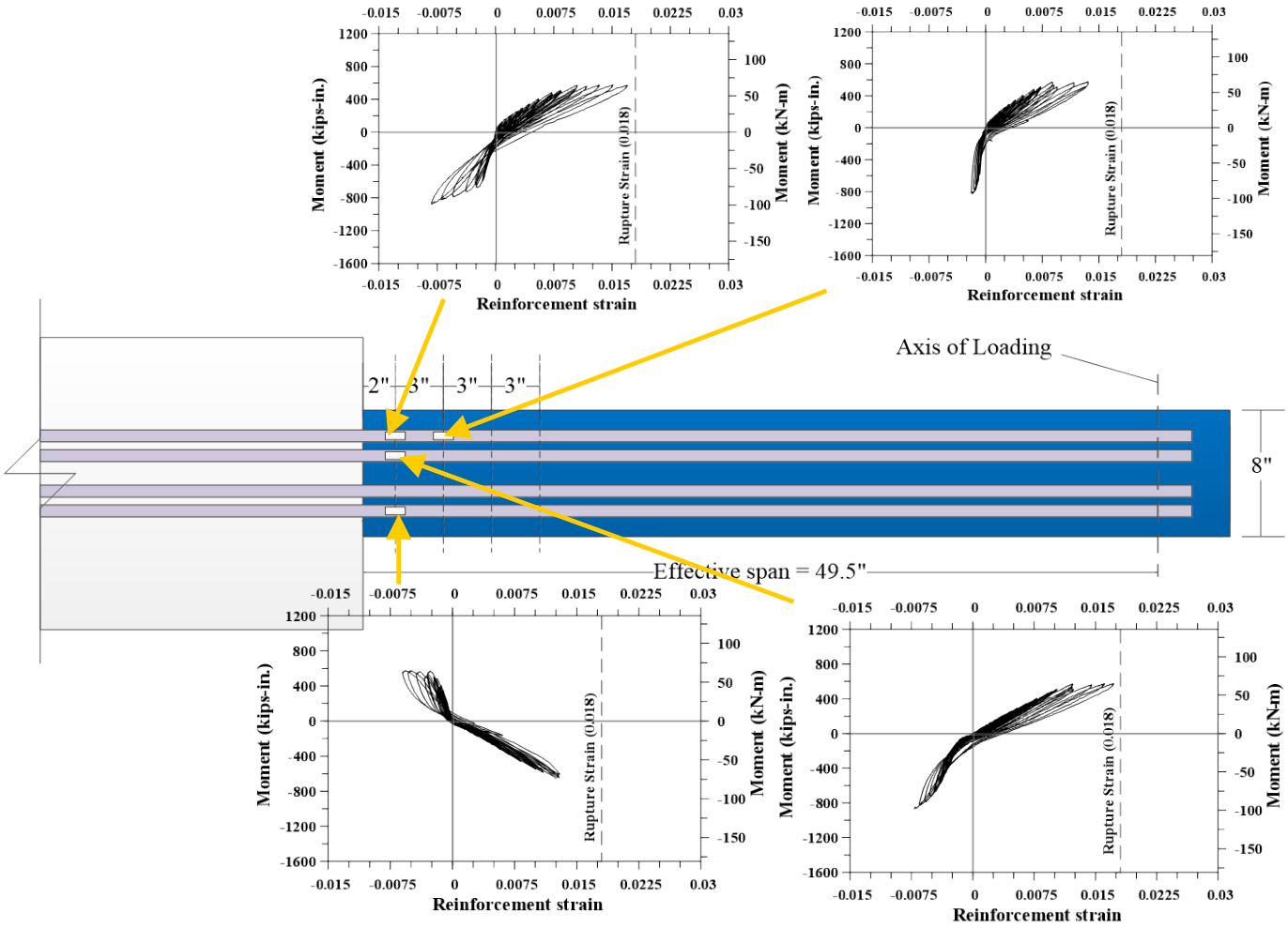

Figure 71. Moment vs reinforcement strain for UHP-FRC #2.

Figure 72. UHP-FRC #2 at 0.2% drift ratio.

Figure 73. UHP-FRC #2 at 0.25% drift ratio.

Figure 74. UHP-FRC #2 at 0.35% drift ratio.

Figure 75. UHP-FRC #2 at 0.5% drift ratio.

Figure 76. UHP-FRC #2 at 0.75% drift ratio.

Figure 77. UHP-FRC #2 at 1.0% drift ratio.

Figure 78. UHP-FRC #2 at 1.4% drift ratio.

Figure 79. UHP-FRC #2 at 1.75% drift ratio.

Figure 80. UHP-FRC #2 at 2.2% drift ratio.

Figure 81. UHP-FRC #2 at 2.75% drift ratio.

Figure 82. UHP-FRC #2 at 3.5% drift ratio.

Figure 83. UHP-FRC #2 at 4.0% drift ratio.

Figure 84. UHP-FRC #2 at 5.0% drift ratio.

Figure 85. UHP-FRC #2 at 6.0% drift ratio.

Figure 86. UHP-FRC #2 at 7.0% drift ratio.

Figure 87. UHP-FRC #2 at 8.0% drift ratio.

Figure 88. UHP-FRC #2 at 9.0% drift ratio.

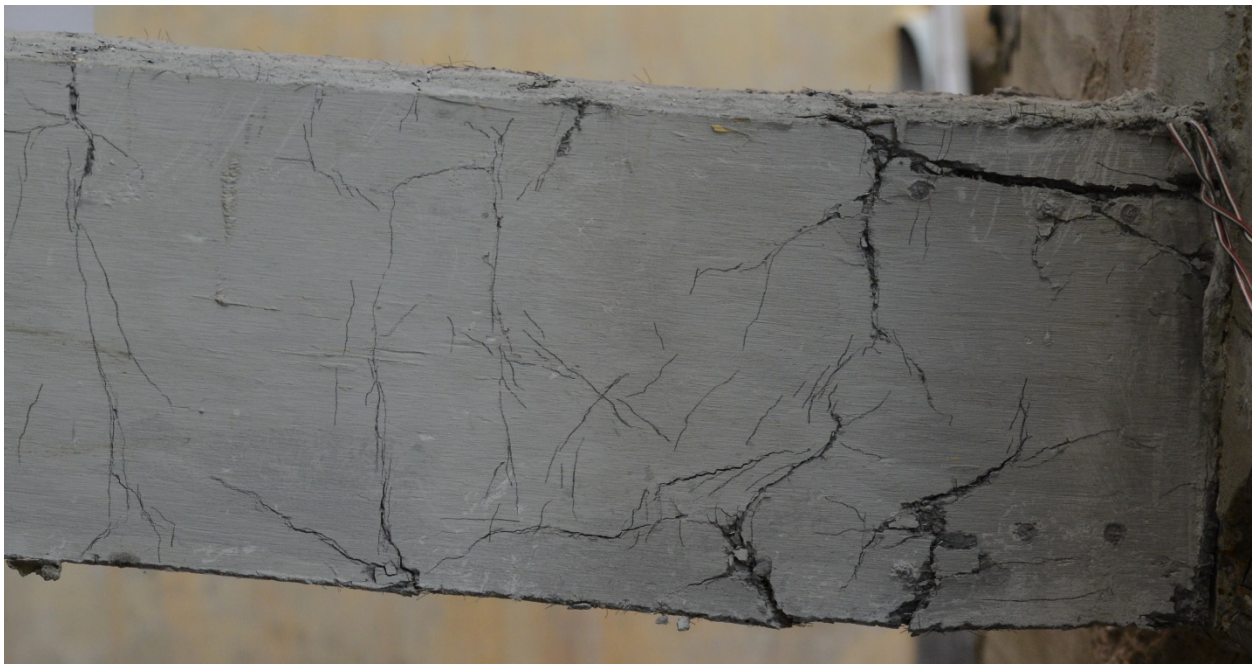

Figure 89. UHP-FRC #2 at 10.0% drift ratio.

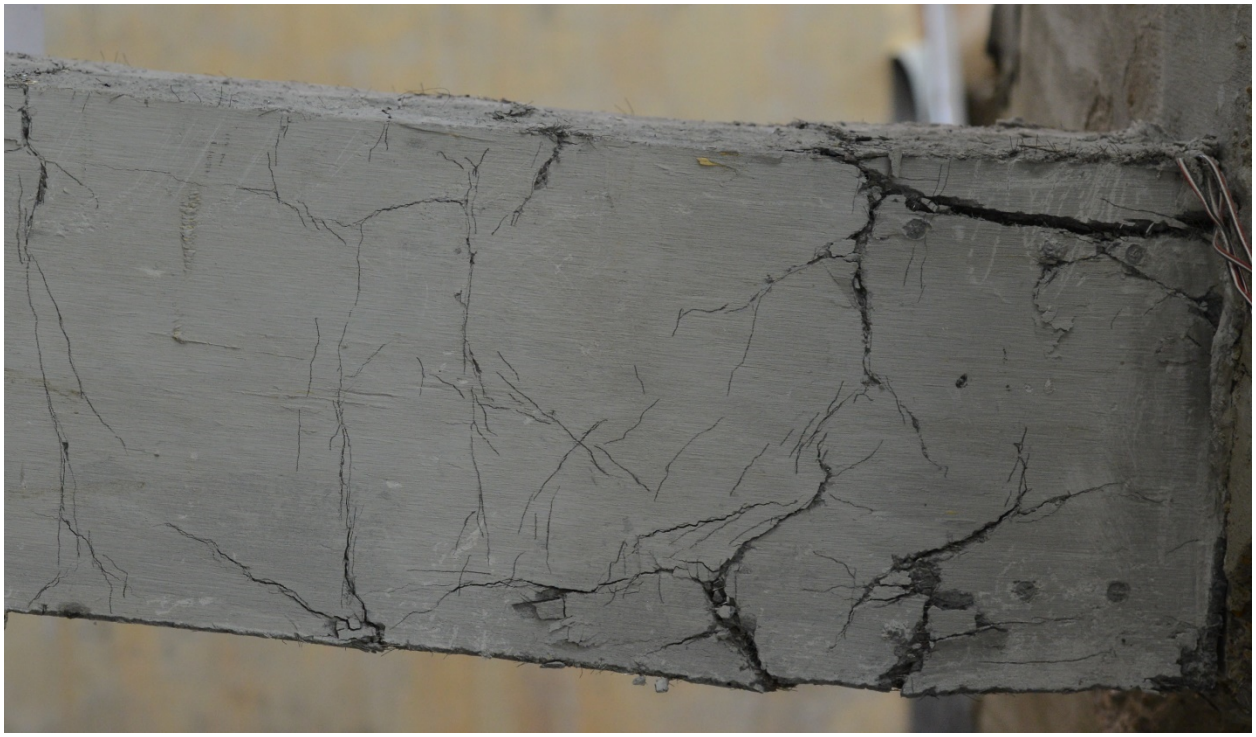

Figure 90. UHP-FRC #2 at 10.0% drift ratio.

Figure 91. UHP-FRC #2 at 13.0% drift ratio.

Figure 92. UHP-FRC #2 at 15.0% drift ratio.

5.3. UHP-FRC #3

A maximum moment of 1470 kip-in. (166 kN-m) was recorded at a drift ratio of 10%. Moment versus drift ratio relationship of beam UHP-FRC #3 showed large cyclic without significant damage to the UHP-FRC material. Stable cyclic behavior was observed up to 9% drift ratio after which the moment started to decrease. From the Figure 93, it can be seen that there is minor residual deformation. Despite having a shear span to depth ratio of 4.25, flexural cracking was seen to be the governing mode of cracking during the test. It was seen that the flexural reinforcements had ruptured at the interface of the support block and the specimen resulting to excessive drift ratios. Strain data of flexural reinforcements are presented from Figure 94 to 96**.** The test pictures of the specimen for different values of drift ratio can be viewed from Figure 97 to 115.

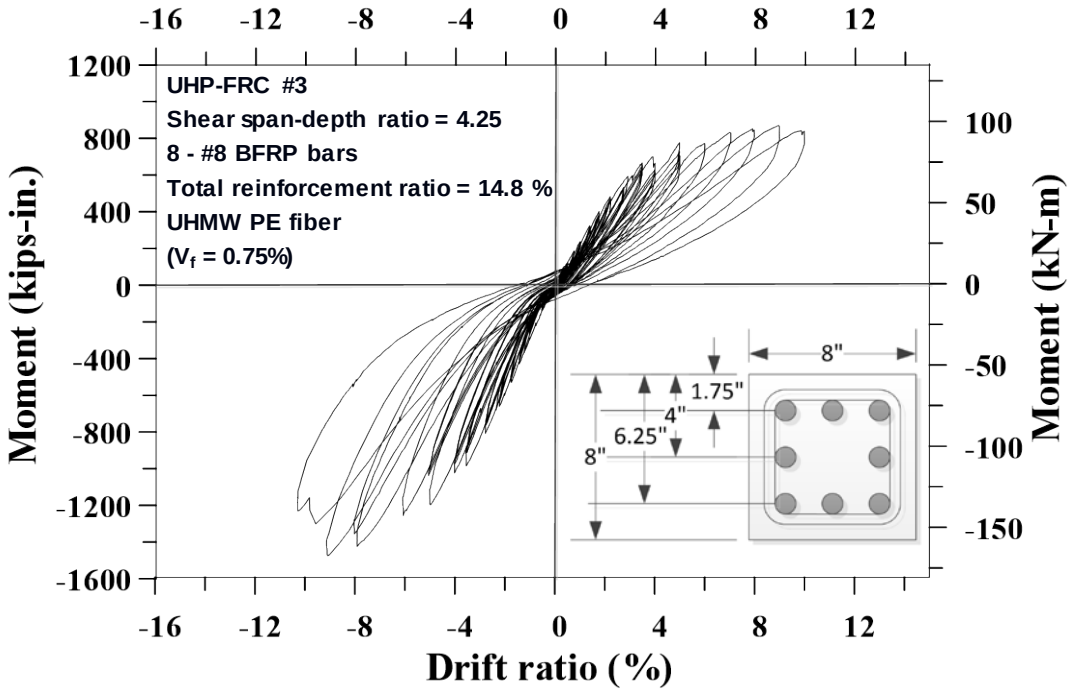

Figure 93. Moment vs Drift ratio for UHP-FRC #3 with PE fibers (BFRP bars).

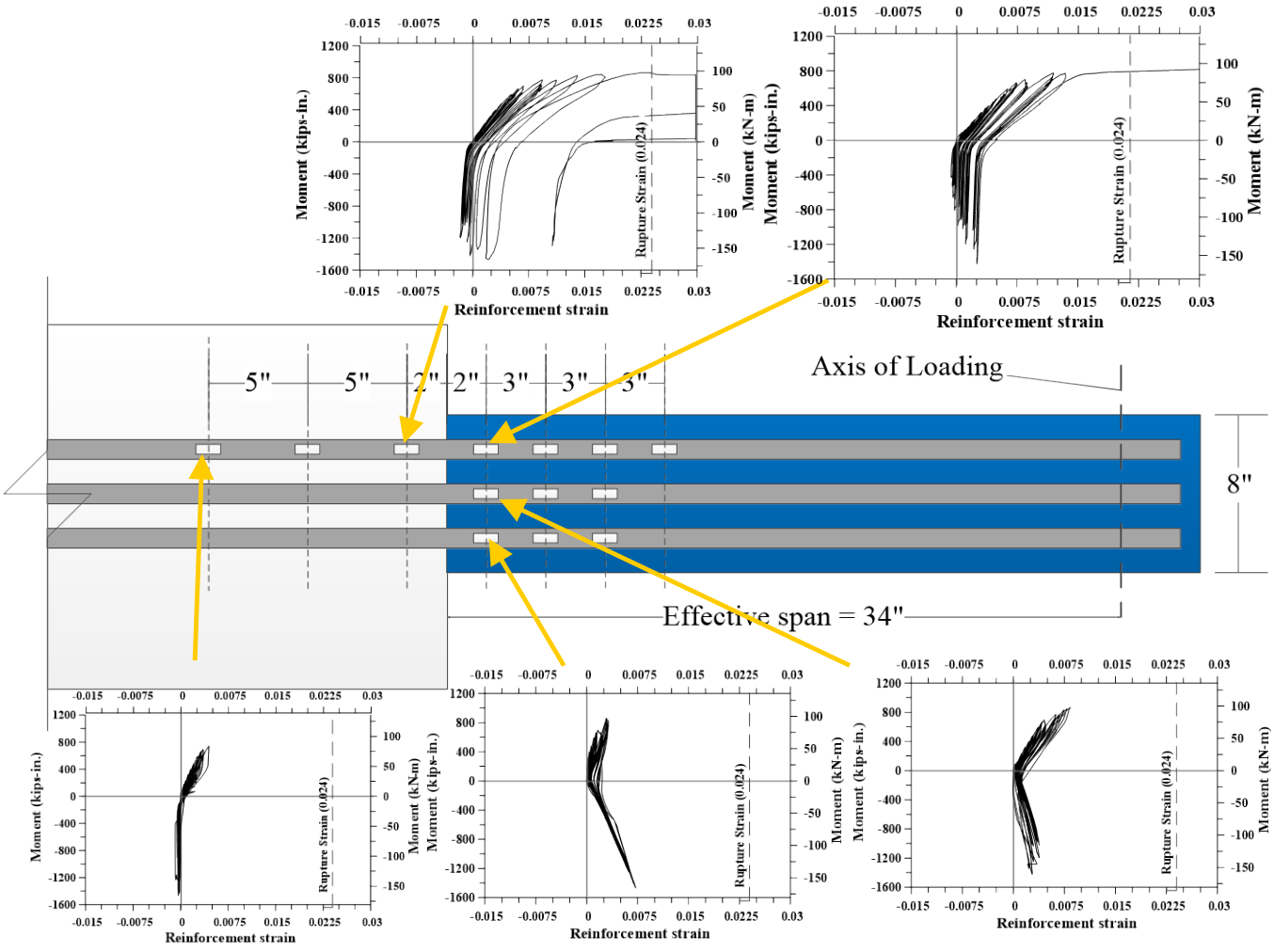

Figure 94. Moment vs reinforcement strain for UHP-FRC #3.

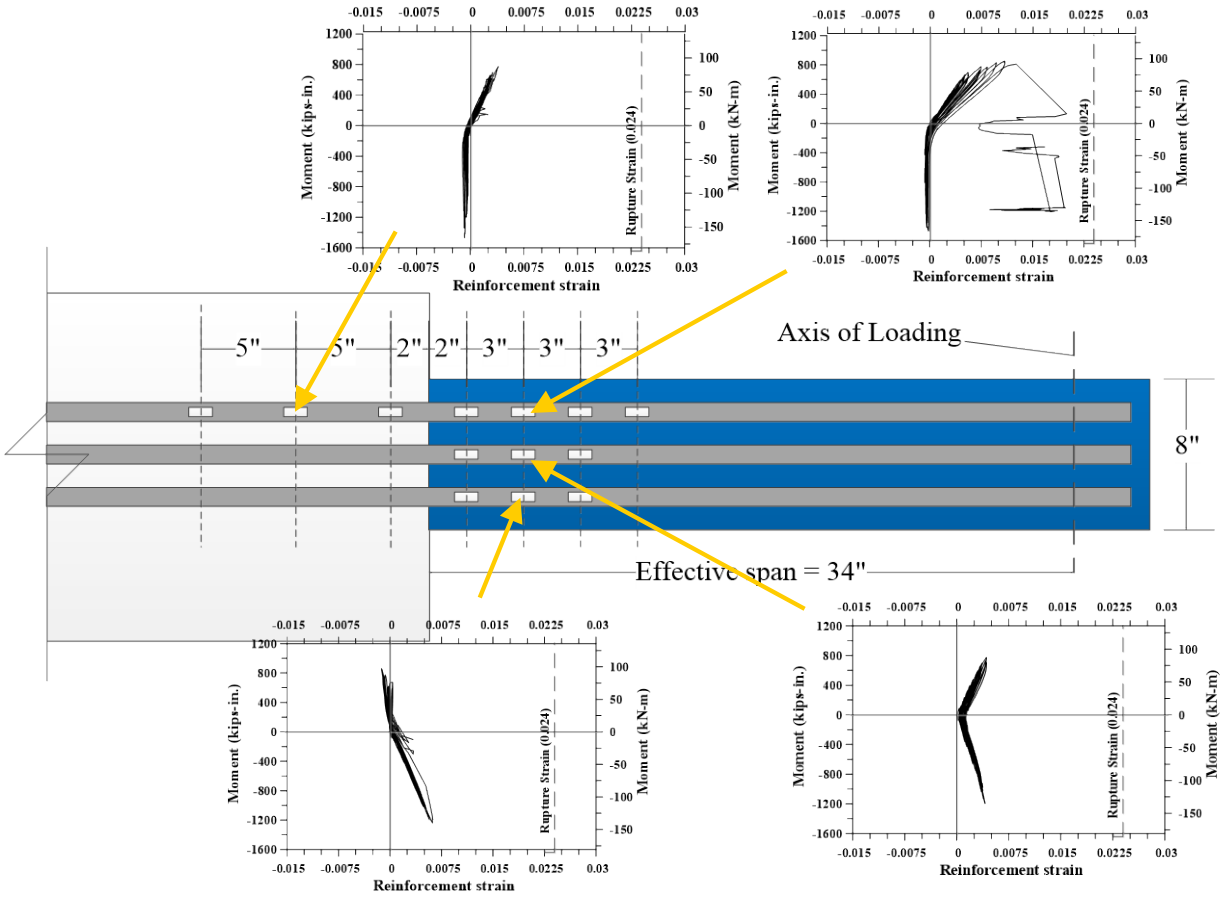

Figure 95. Moment vs reinforcement strain for UHP-FRC #3.

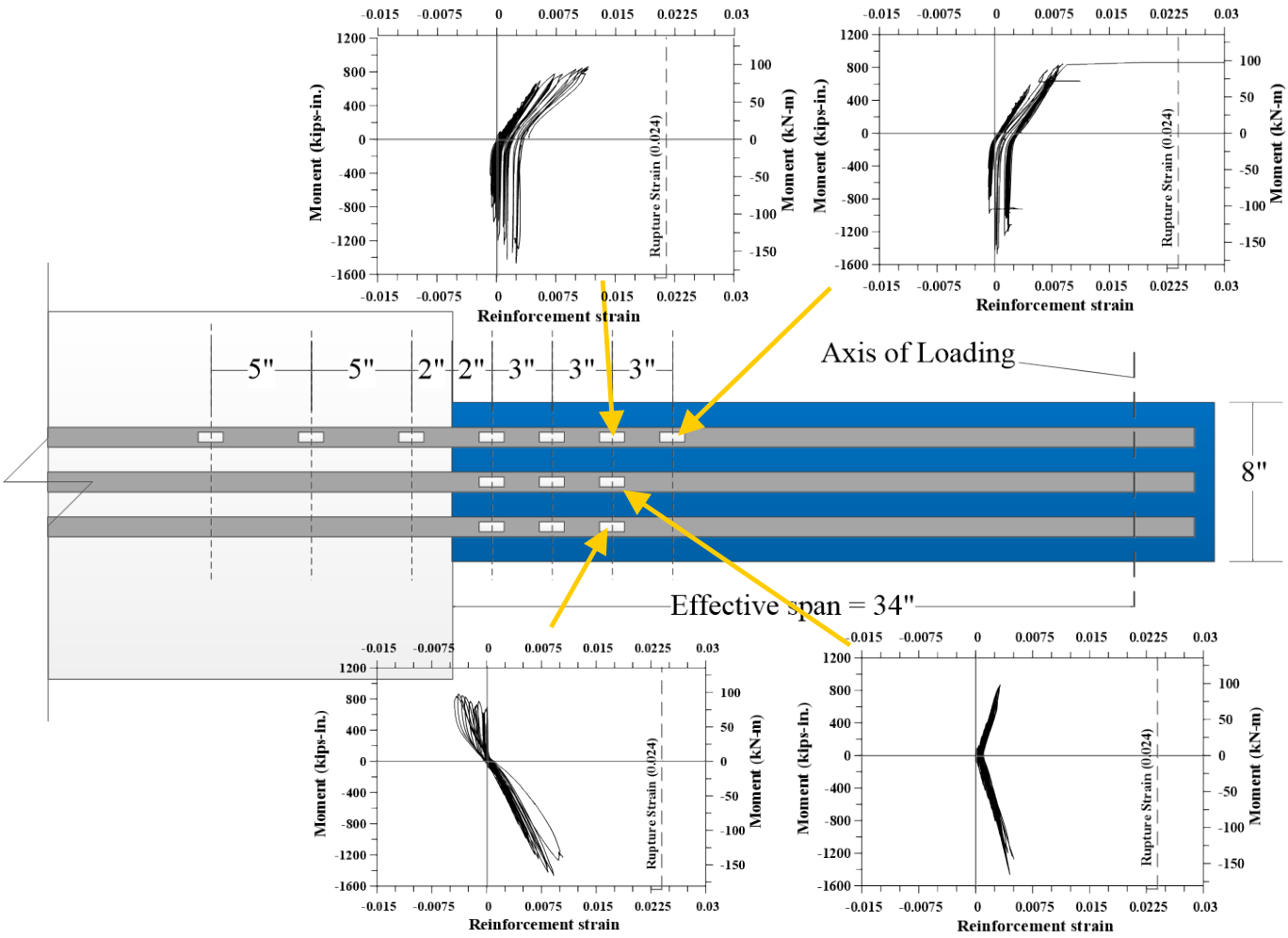

Figure 96. Moment vs reinforcement strain for UHP-FRC #3.

Figure 97. UHP-FRC #3 at 0% drift ratio.

Figure 98. UHP-FRC #3 at 0.2% drift ratio.

Figure 99. UHP-FRC #3 at 0.25% drift ratio.

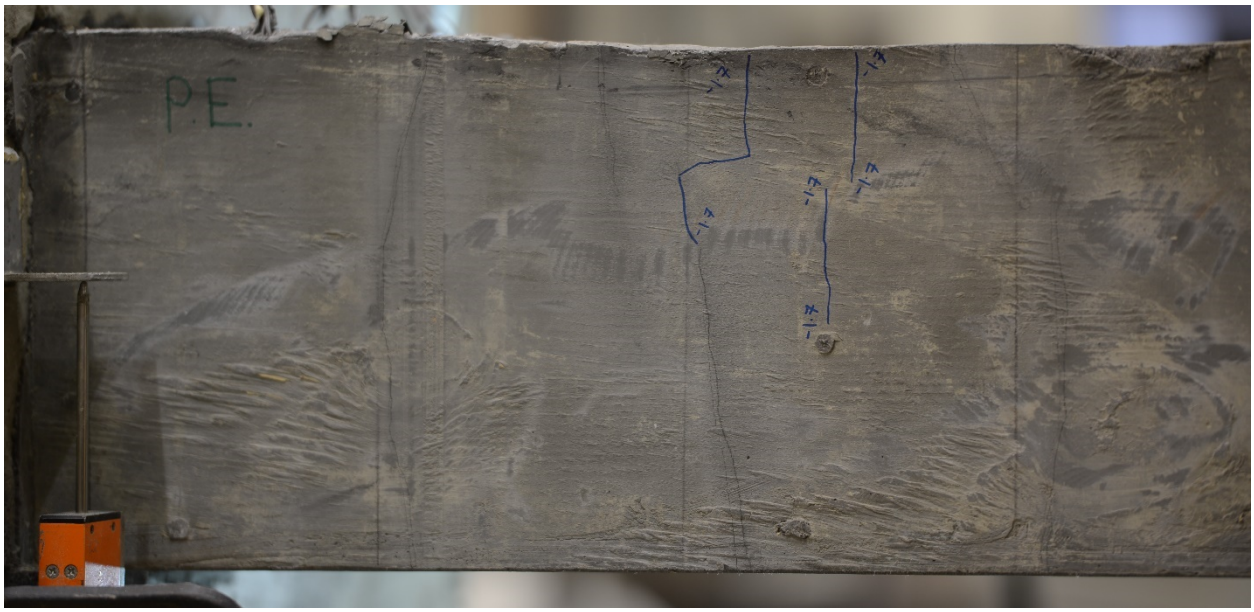

Figure 100. UHP-FRC #3 at 0.35% drift ratio.

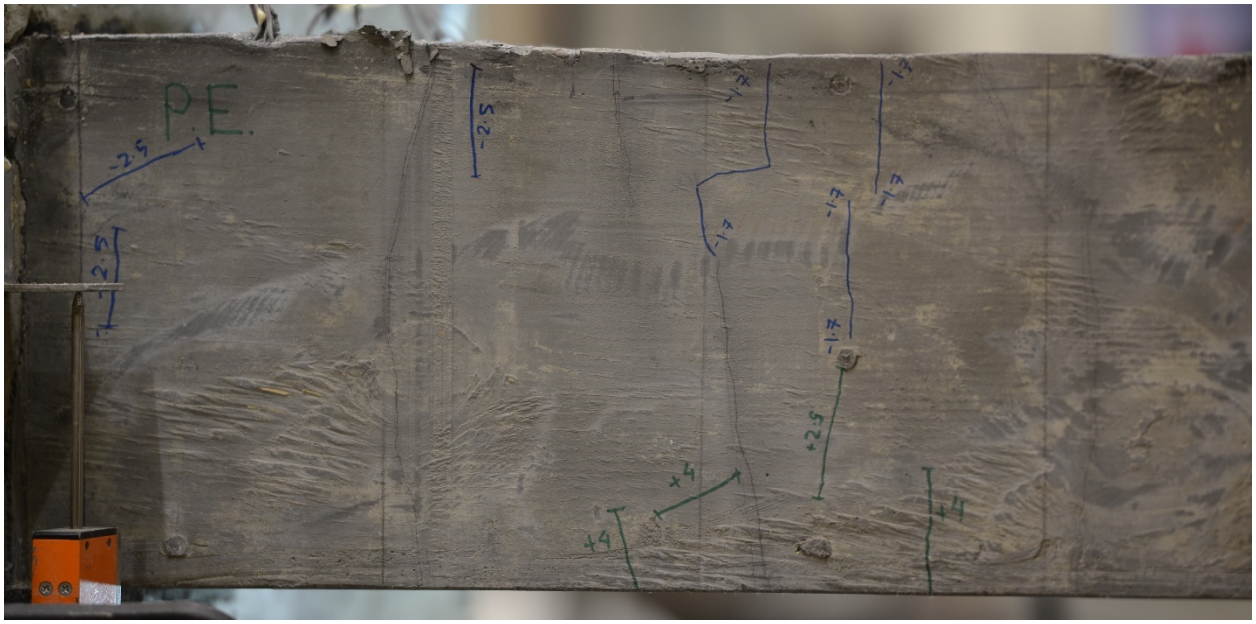

Figure 101. UHP-FRC #3 at 0.5% drift ratio.

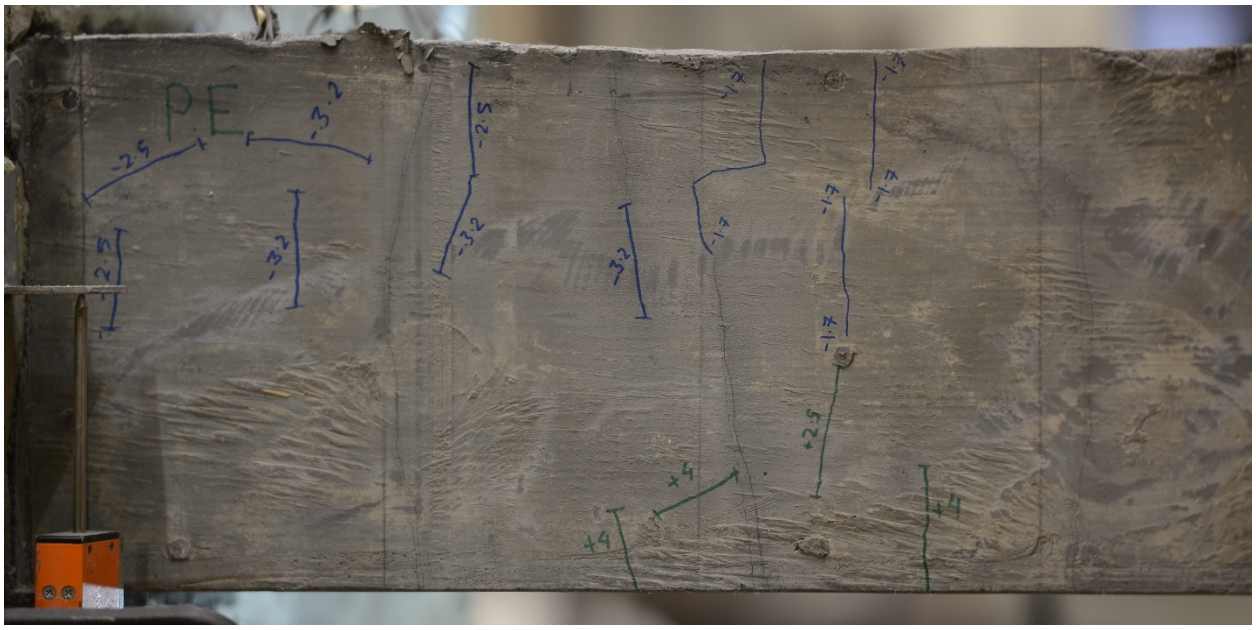

Figure 102. UHP-FRC #3 at 0.75% drift ratio.

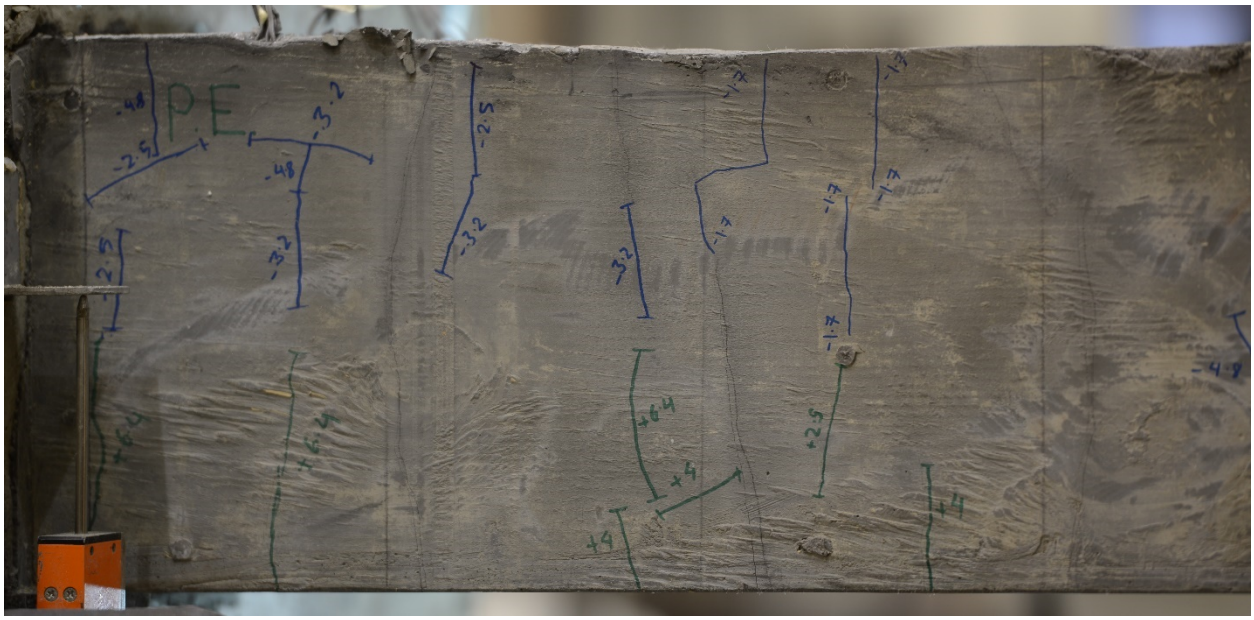

Figure 103. UHP-FRC #3 at 1.0% drift ratio.

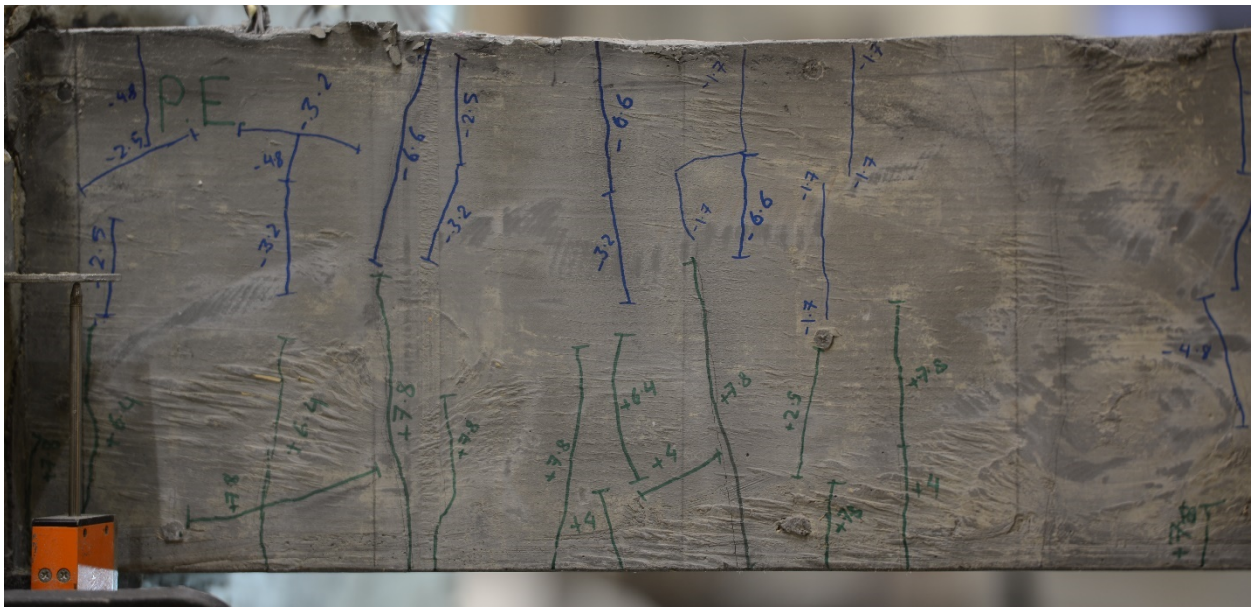

Figure 104. UHP-FRC #3 at 1.4% drift ratio.

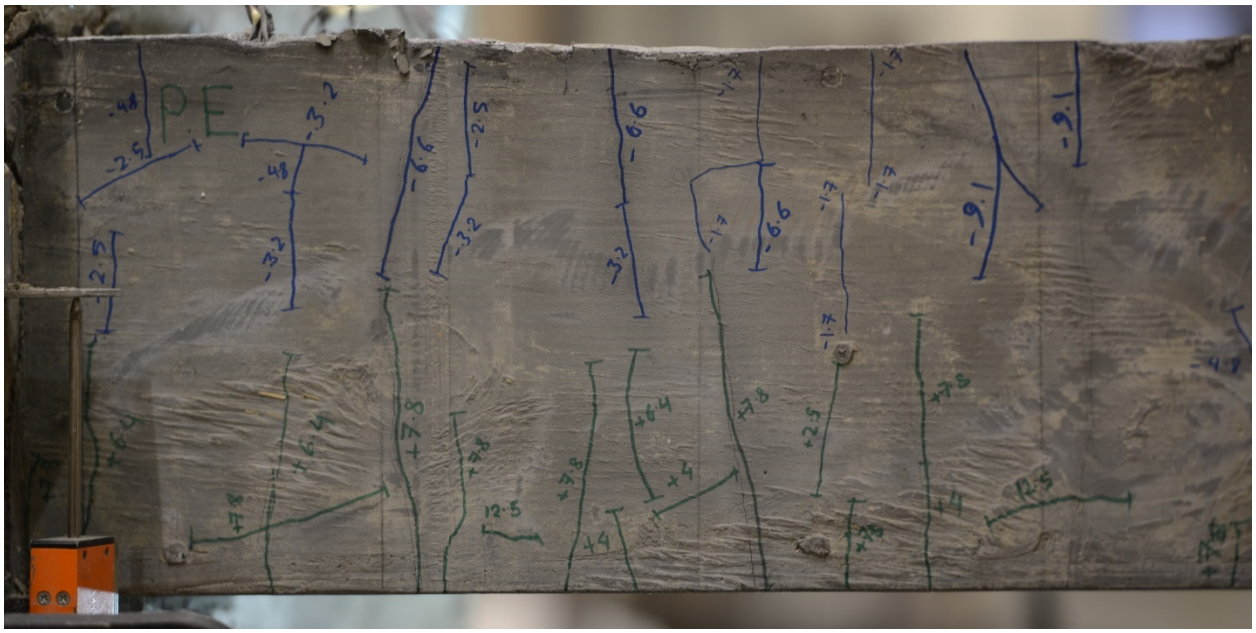

Figure 105. UHP-FRC #3 at 1.75% drift ratio.

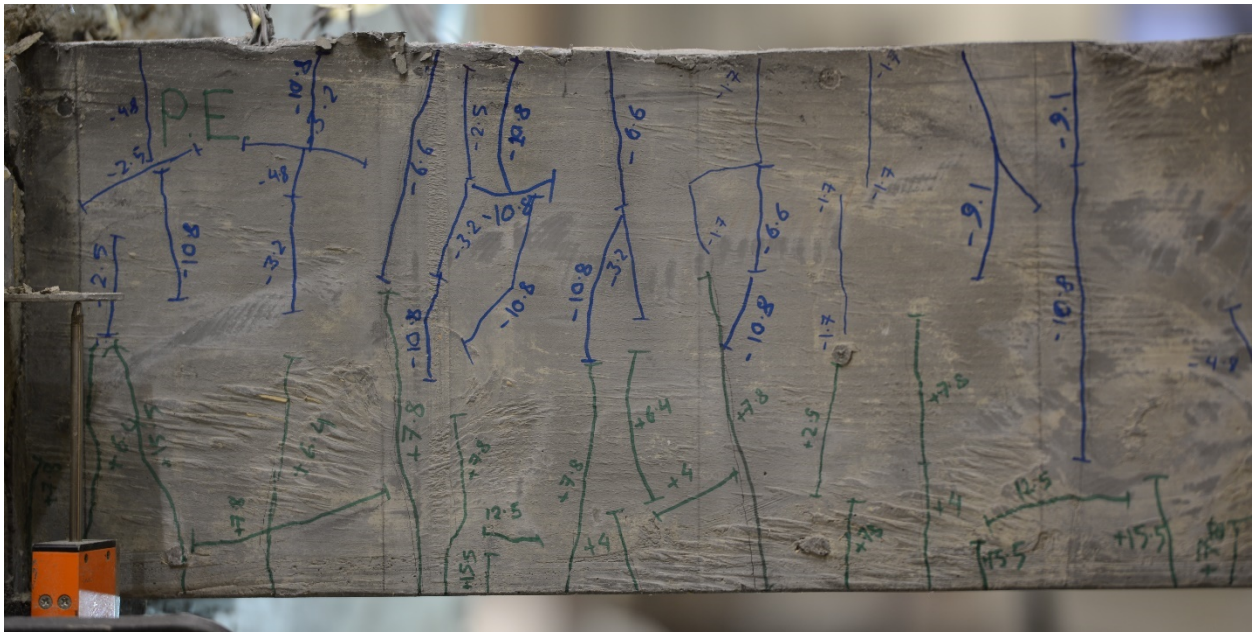

Figure 106. UHP-FRC #3 at 2.2% drift ratio.

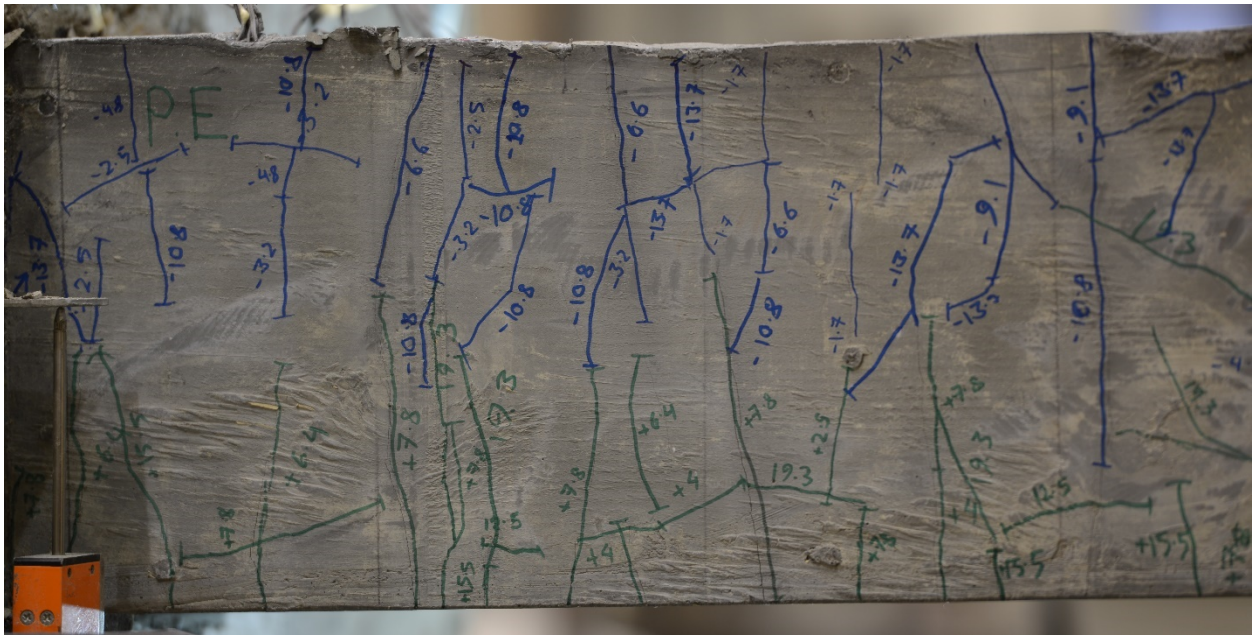

Figure 107. UHP-FRC #3 at 2.75% drift ratio.

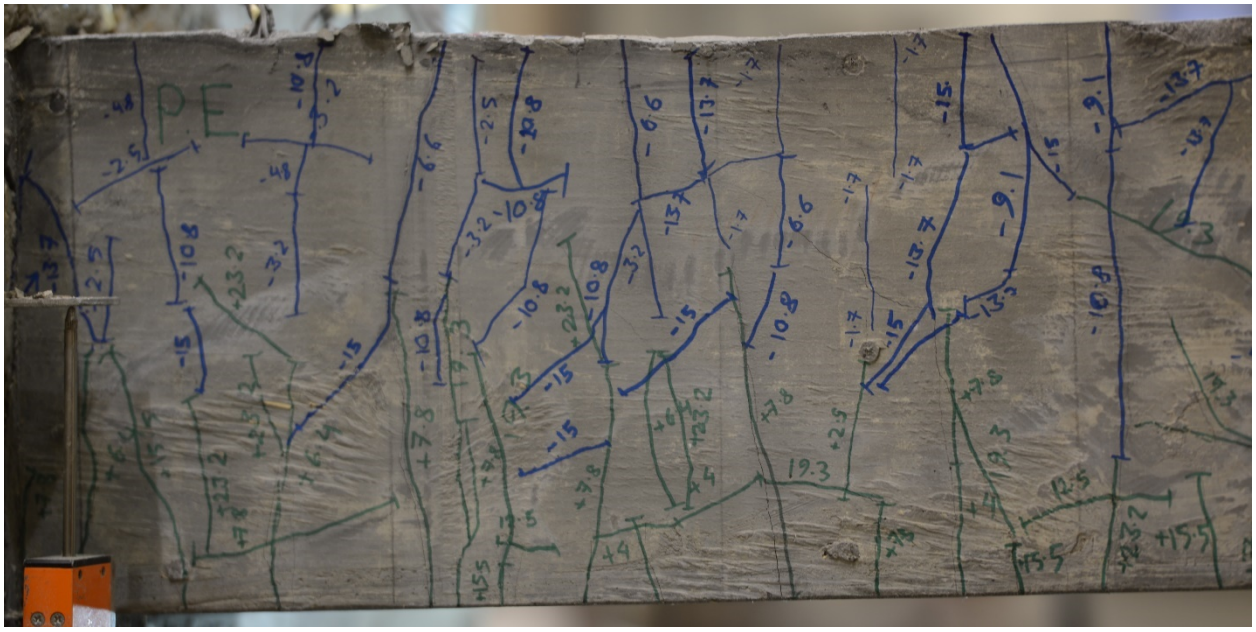

Figure 108. UHP-FRC #3 at 3.5% drift ratio.

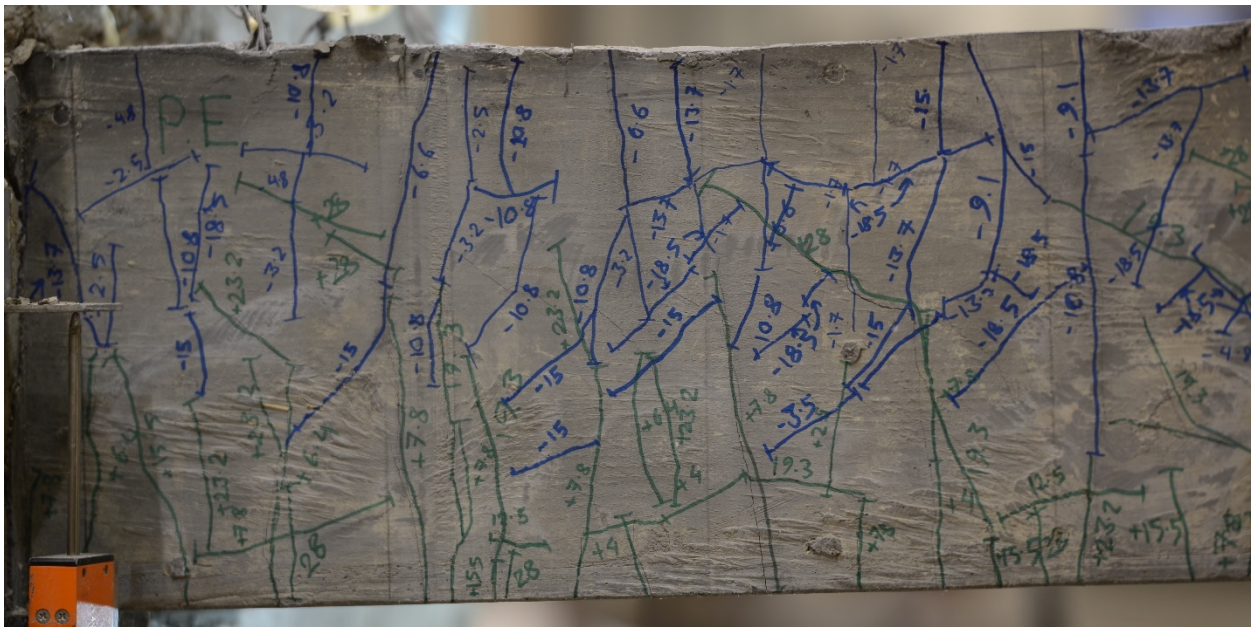

Figure 109. UHP-FRC #3 at 4.0% drift ratio.

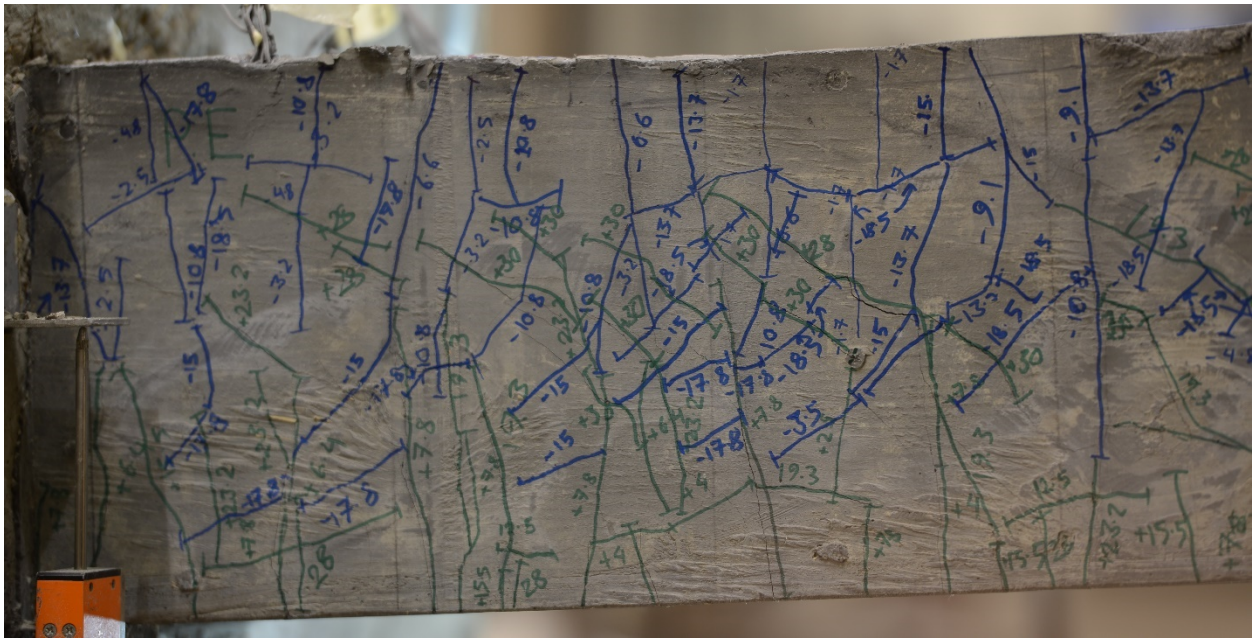

Figure 110. UHP-FRC #3 at 5.0% drift ratio.

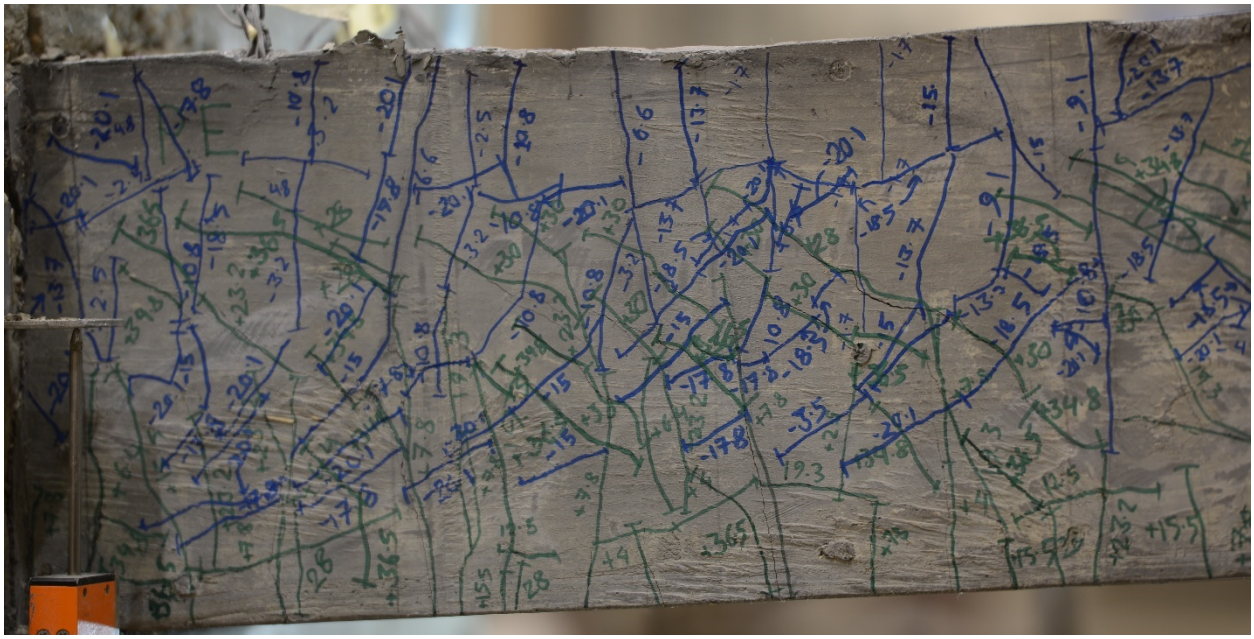

Figure 111. UHP-FRC #3 at 6.0% drift ratio.

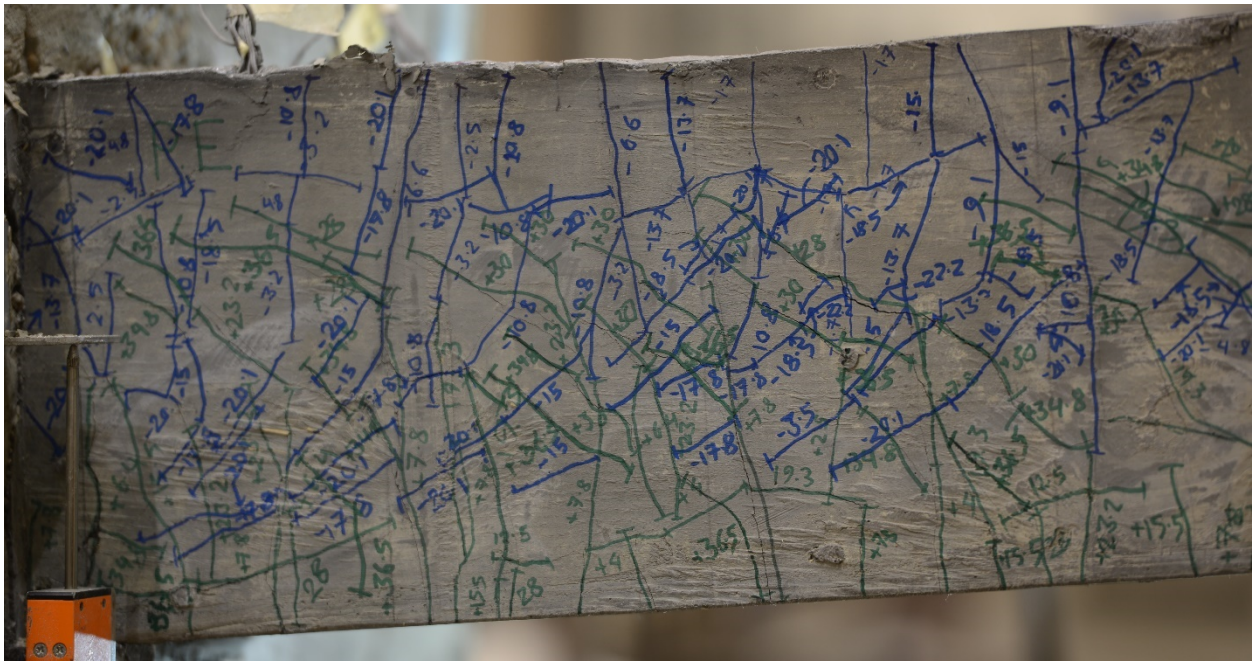

Figure 112. UHP-FRC #3 at 7.0% drift ratio.

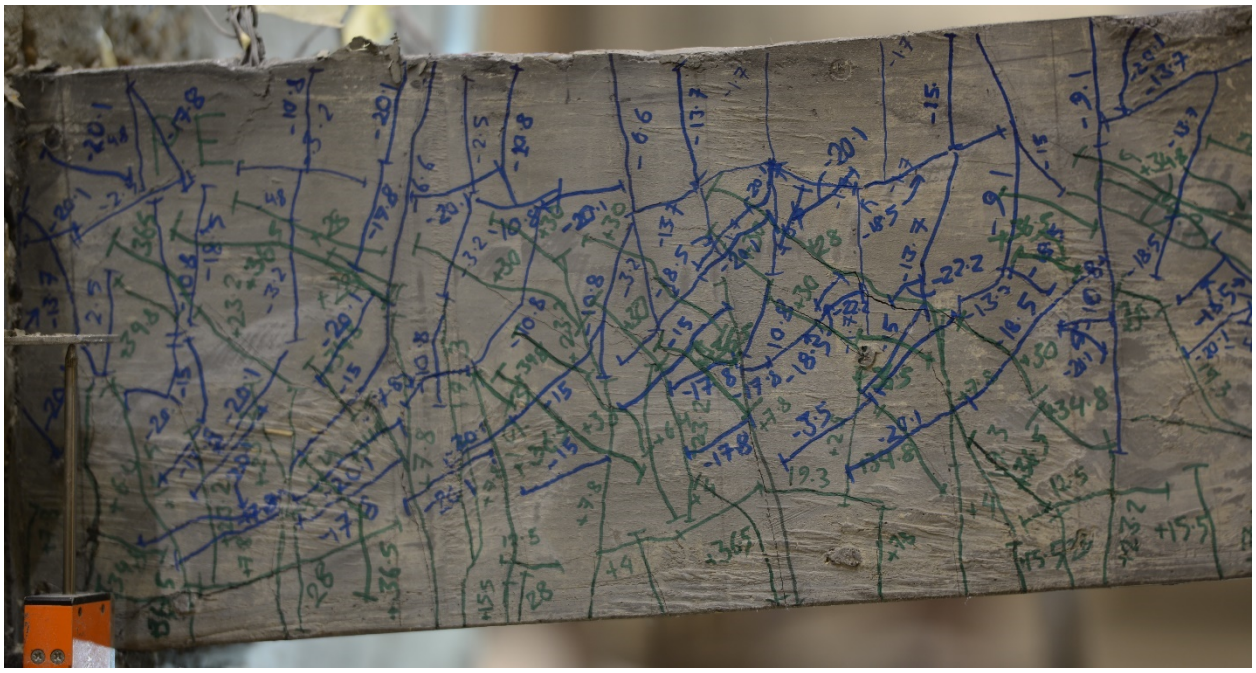

Figure 113. UHP-FRC #3 at 8.0% drift ratio.

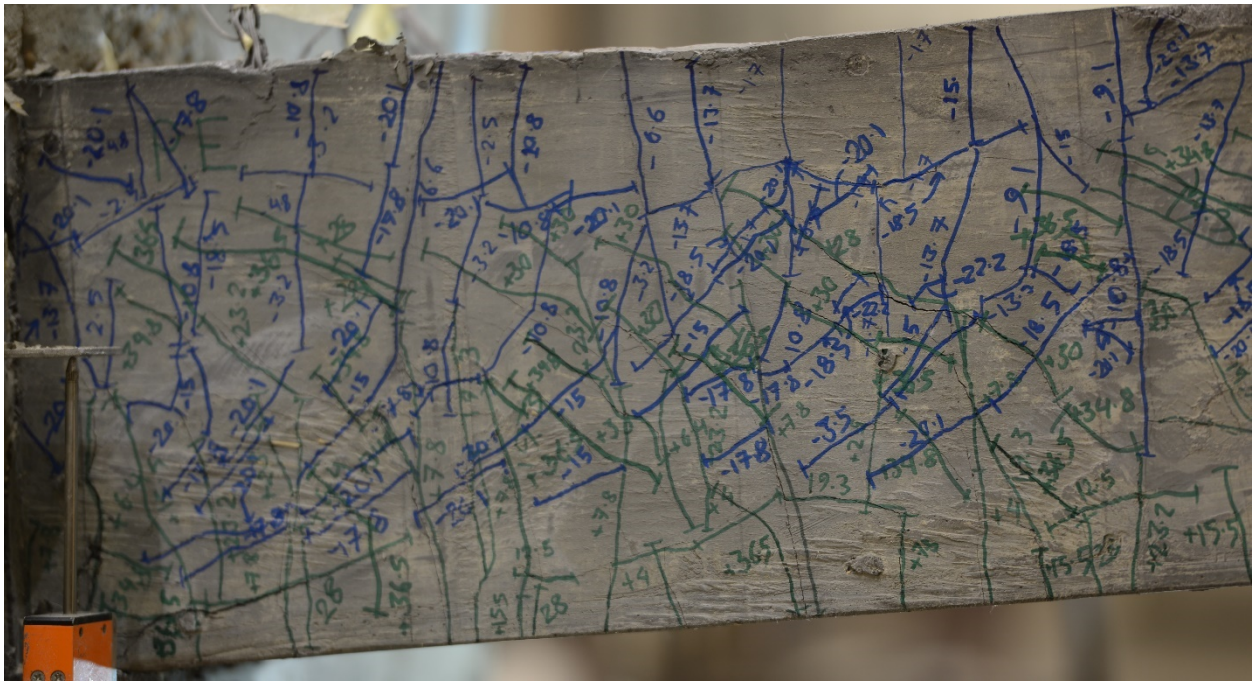

Figure 114. UHP-FRC #3 at 9.0% drift ratio.

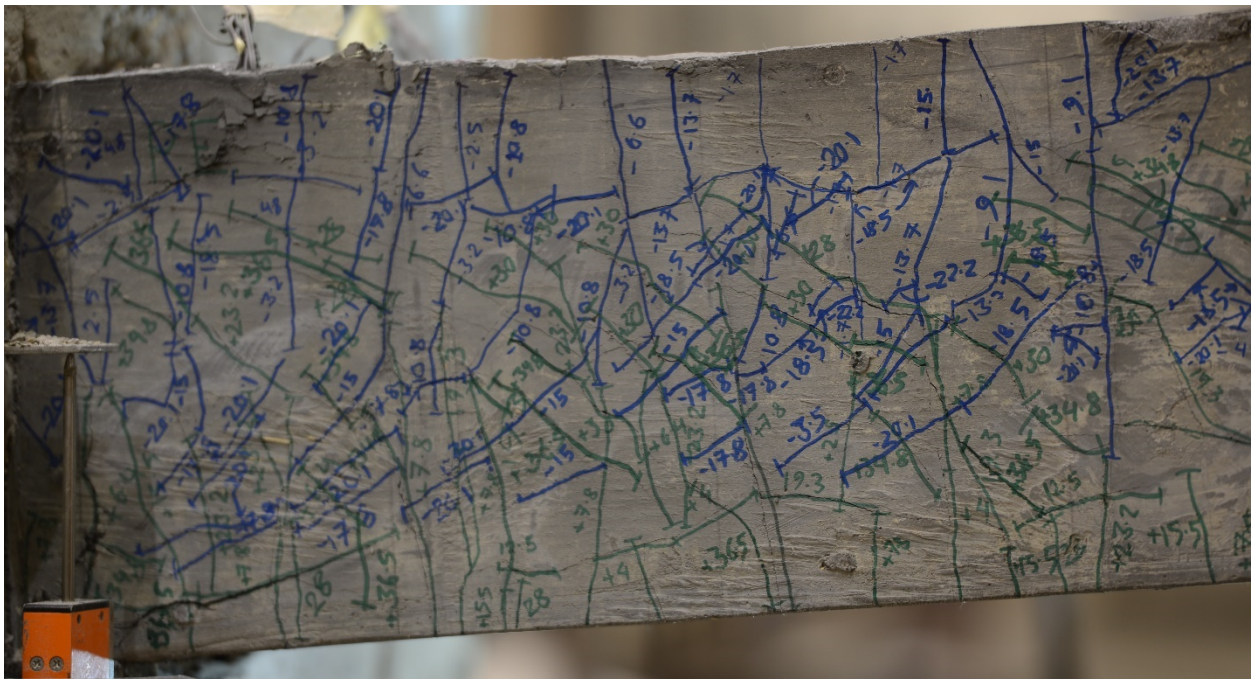

Figure 115. UHP-FRC #3 at 10.0% drift ratio.

5.4. UHP-FRC #4

A maximum moment of 1430 kip-in. (162 kN-m) was recorded at a drift ratio of 8%. Moment versus drift ratio relationship of beam UHP-FRC #4 showed large cyclic without significant damage to the UHP-FRC material. Stable cyclic behavior was observed up to 8% drift ratio after which the moment started to decrease. From the Figure 116, it can be seen that there is minor residual deformation. Despite having a shear span to depth ratio of 4.25, flexural cracking was seen to be the governing mode of cracking during the test similar to specimen UHP-FRC #3. Flexural reinforcements remained elastic throughout the testing. Strain data of flexural reinforcements are presented from Figure 117 and 118. The test pictures of the specimen for different values of drift ratio can be viewed from Figure 119 to 137.

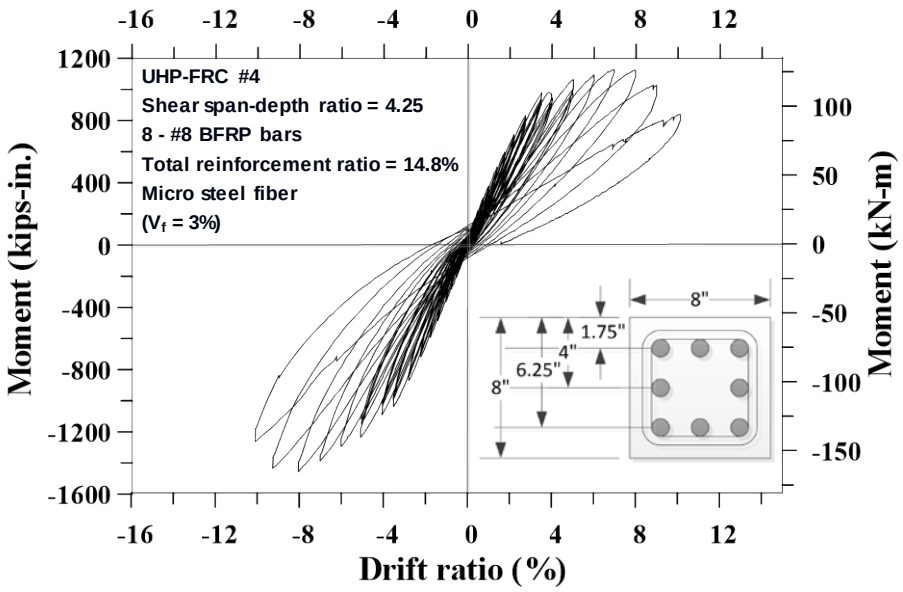

Figure 116. Moment vs drift ratio for UHP-FRC #4 with steel fibers (BFRP bars).

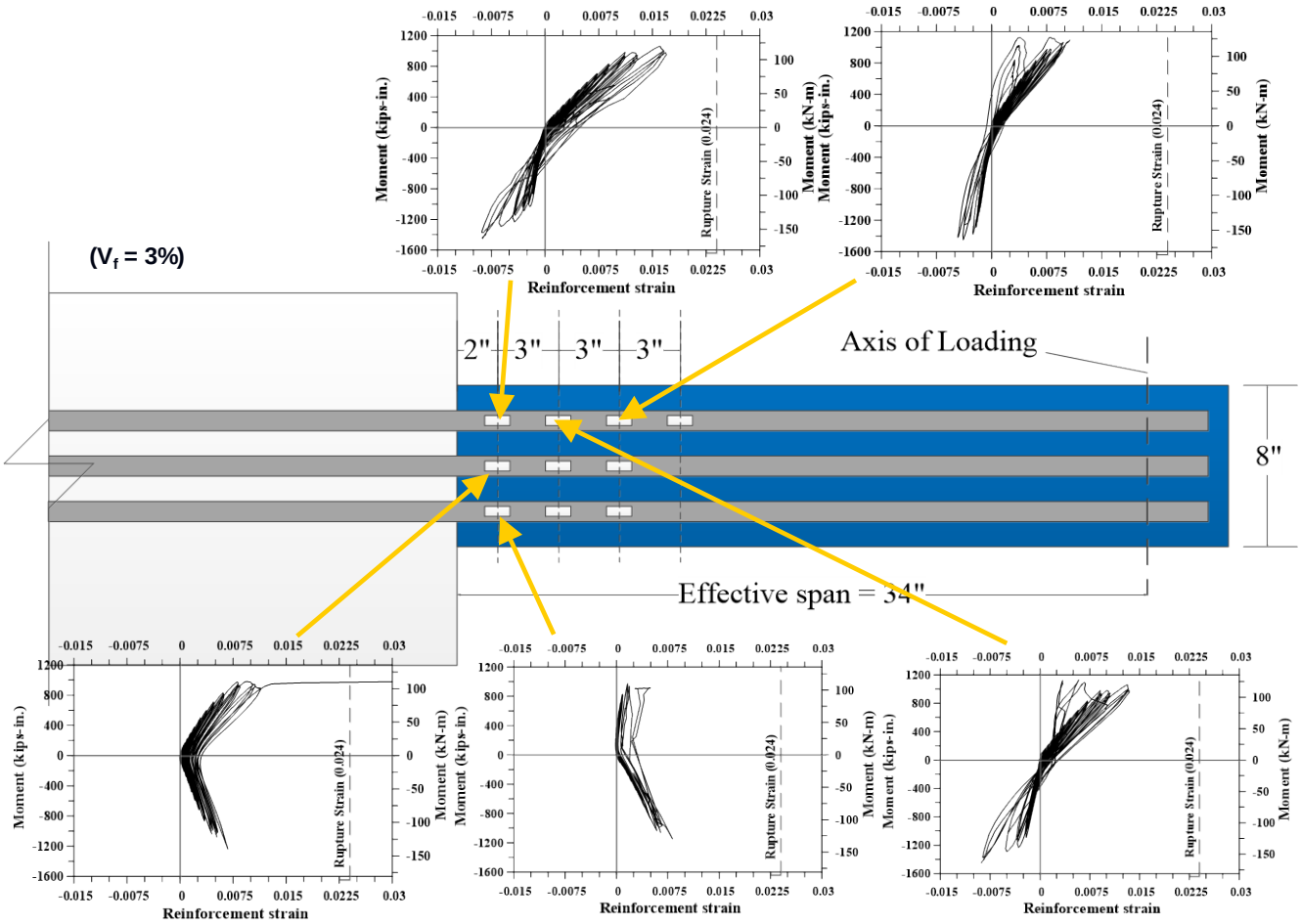

Figure 117. Moment vs reinforcement strain for UHP-FRC #4.

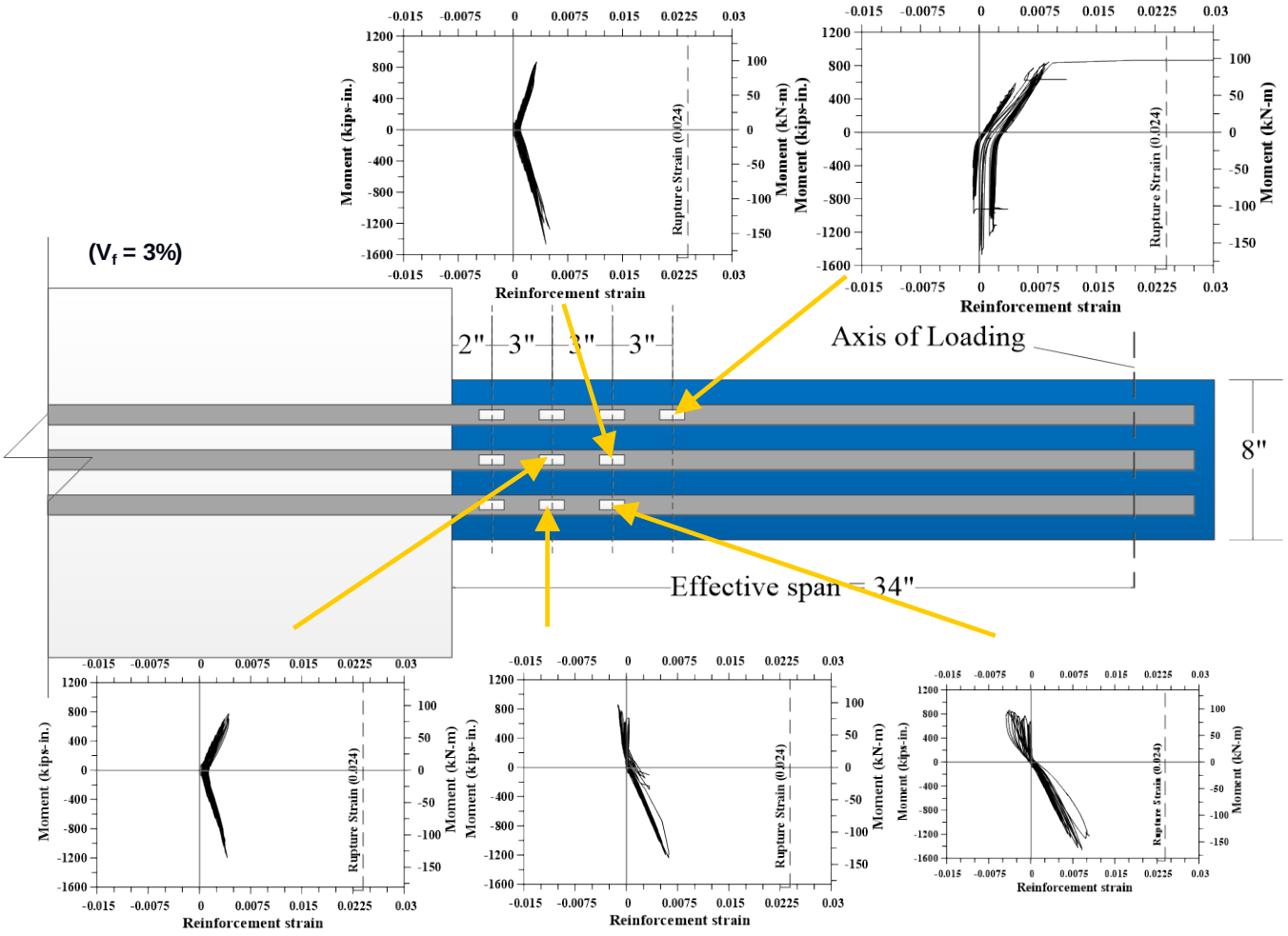

Figure 118. Moment vs reinforcement strain for UHP-FRC #4.

Figure 119. UHP-FRC #4 at 0% drift ratio.

Figure 120. UHP-FRC #4 at 0.2% drift ratio.

Figure 121. UHP-FRC #4 at 0.25% drift ratio.

Figure 122. UHP-FRC #4 at 0.35% drift ratio.

Figure 123. UHP-FRC #4 at 0.5% drift ratio.

Figure 124. UHP-FRC #4 at 0.75% drift ratio.

Figure 125. UHP-FRC #4 at 1.0% drift ratio.

Figure 126. UHP-FRC #4 at 1.4% drift ratio.

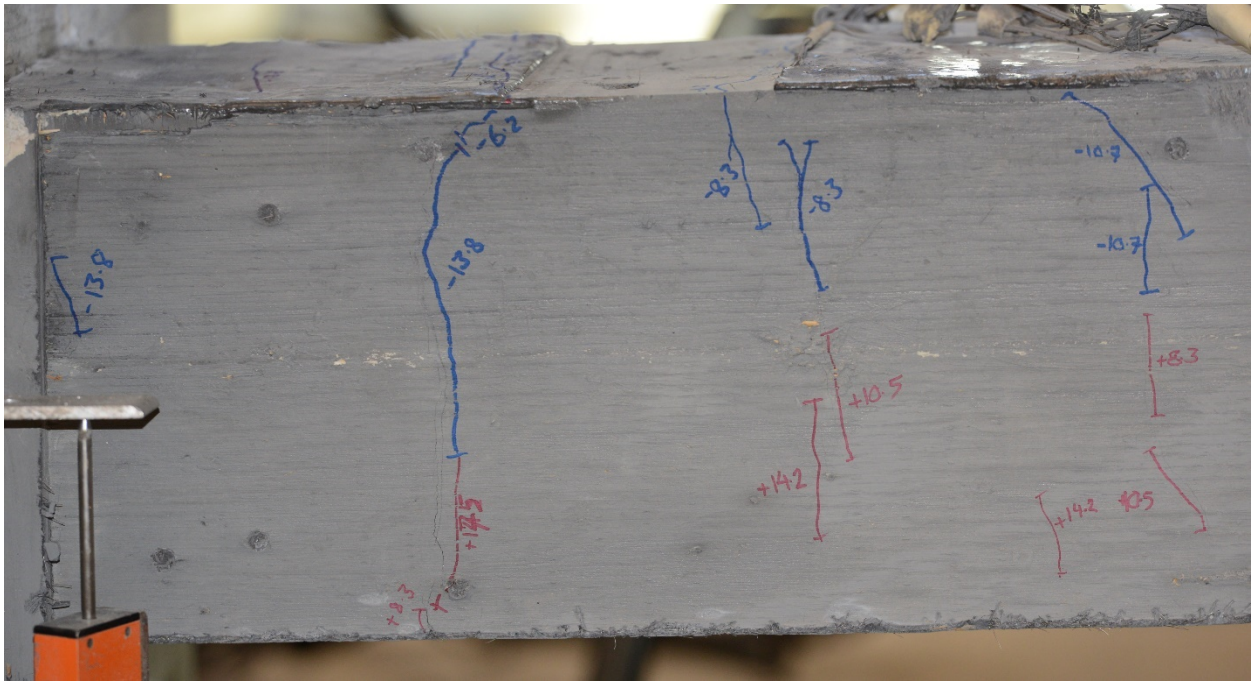

Figure 127. UHP-FRC #4 at 1.75% drift ratio.

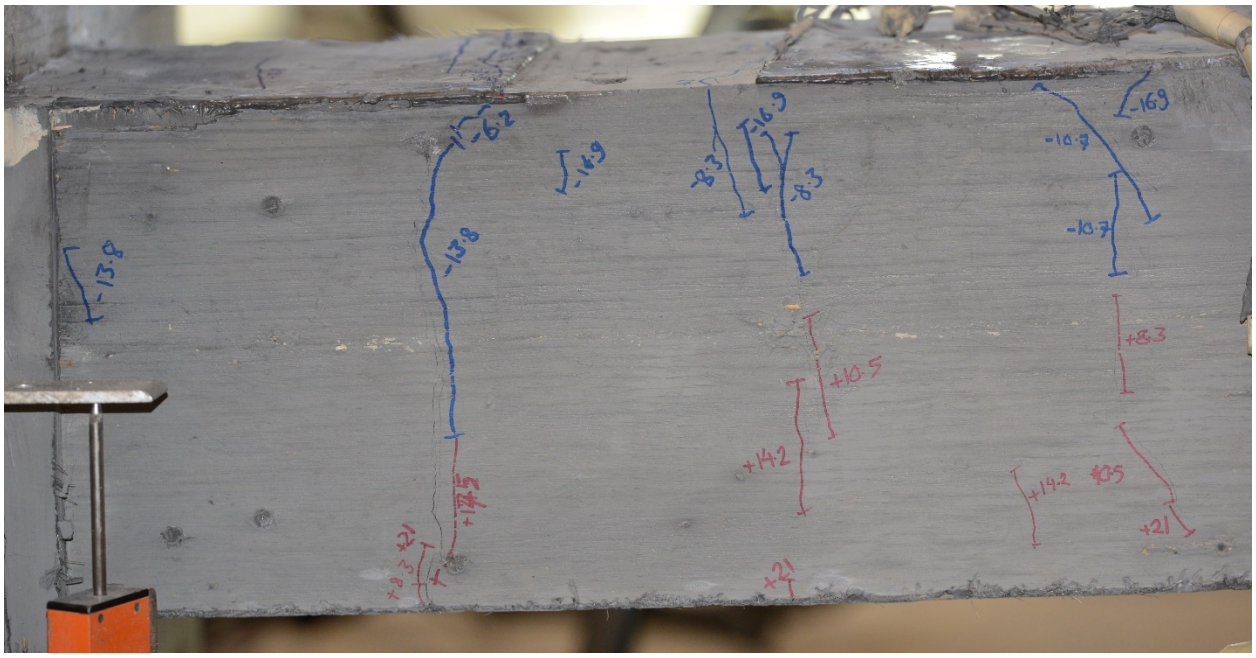

Figure 128. UHP-FRC #4 at 2.2% drift ratio.

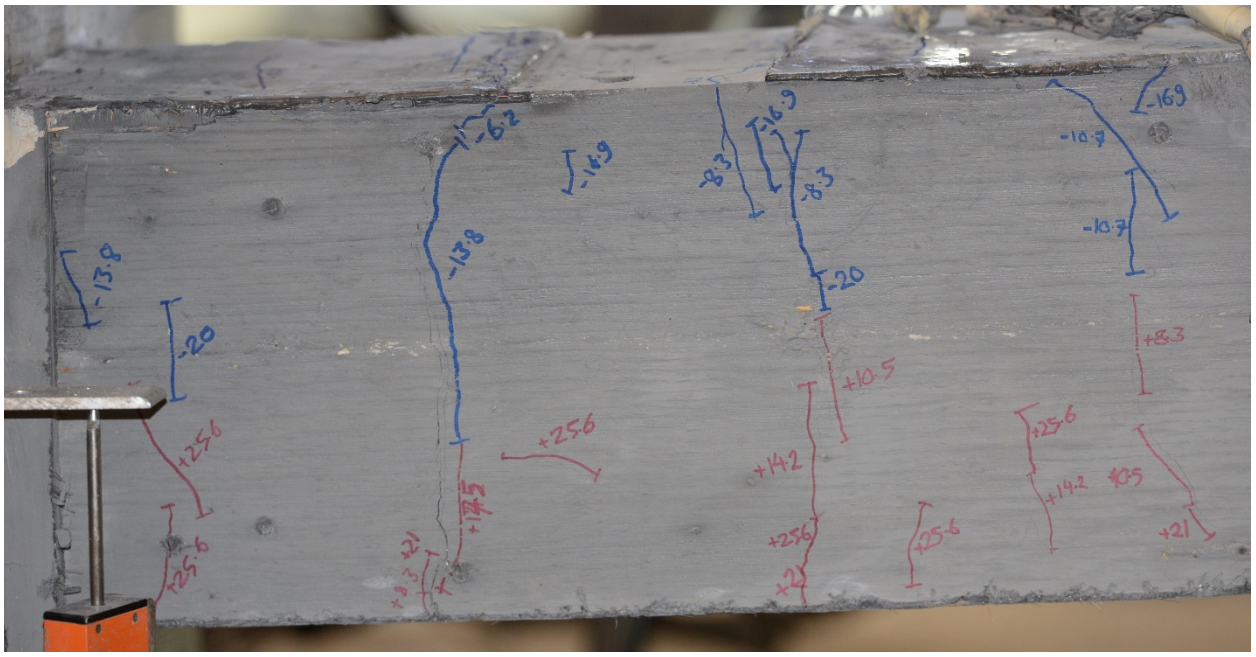

Figure 129. UHP-FRC #4 at 2.75% drift ratio.

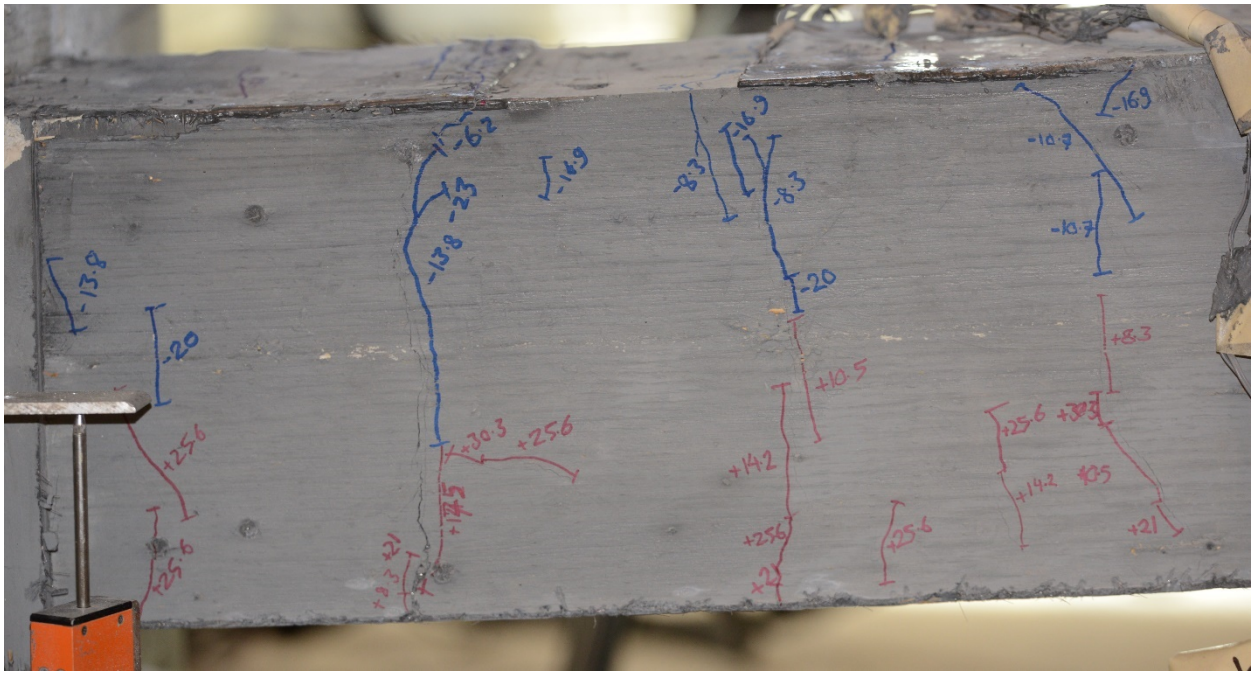

Figure 130. UHP-FRC #4 at 3.5% drift ratio.

Figure 131. UHP-FRC #4 at 4.0% drift ratio.

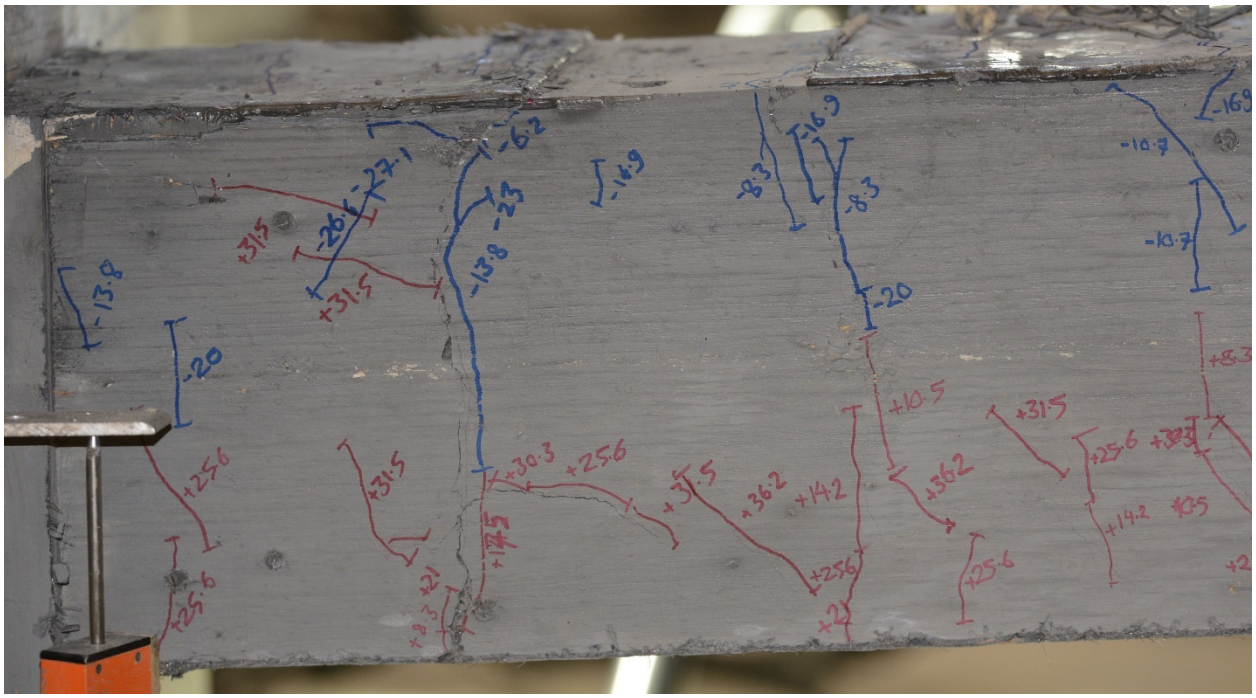

Figure 132. UHP-FRC #4 at 5.0% drift ratio.

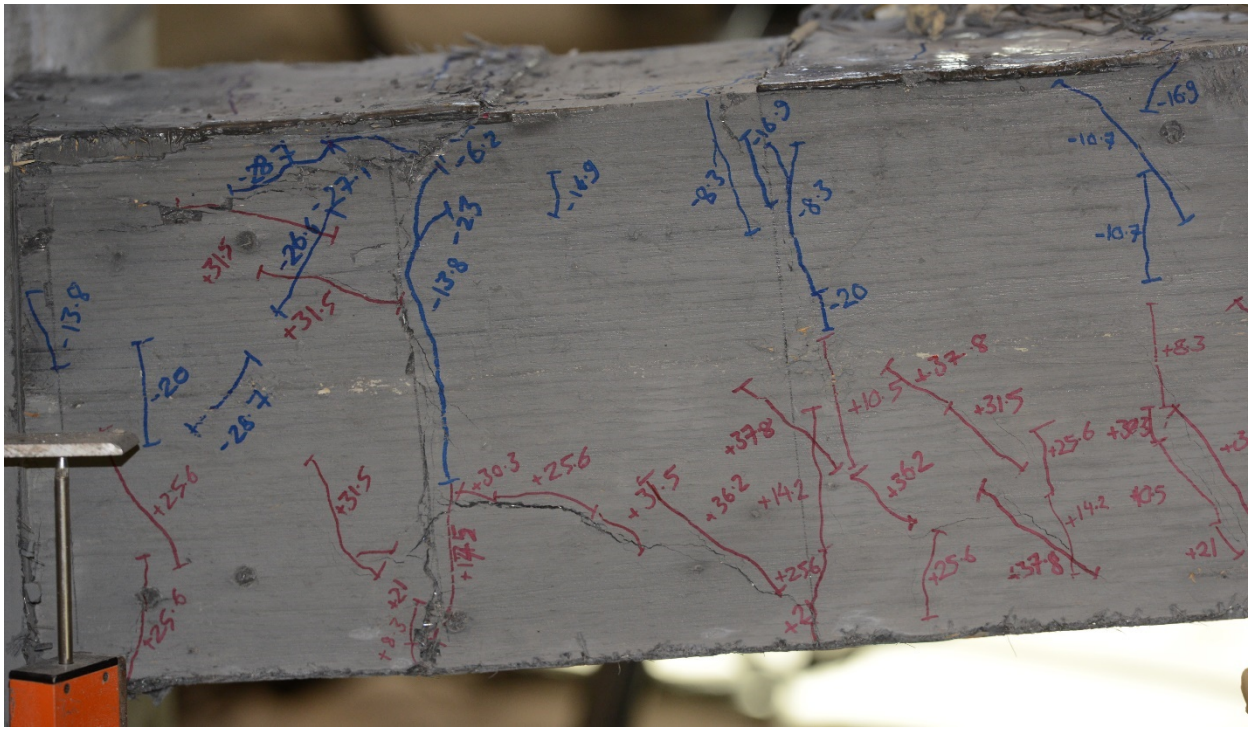

Figure 133. UHP-FRC #4 at 6.0% drift ratio.

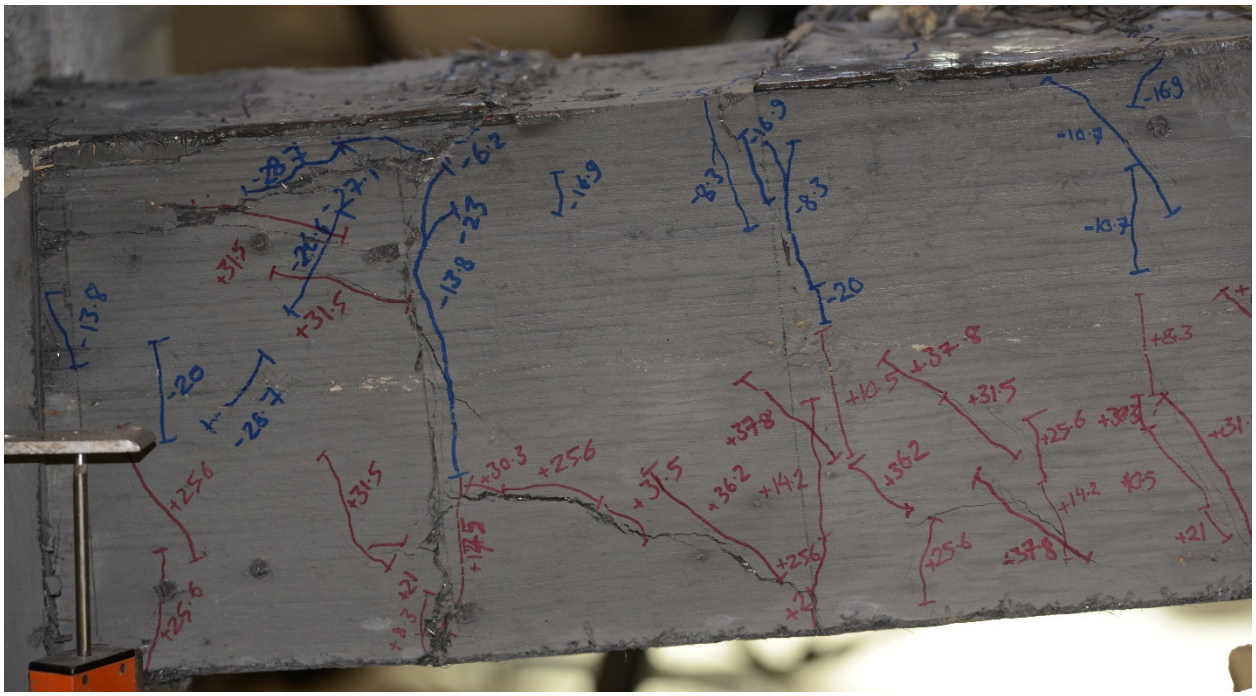

Figure 134. UHP-FRC #4 at 7.0% drift ratio.

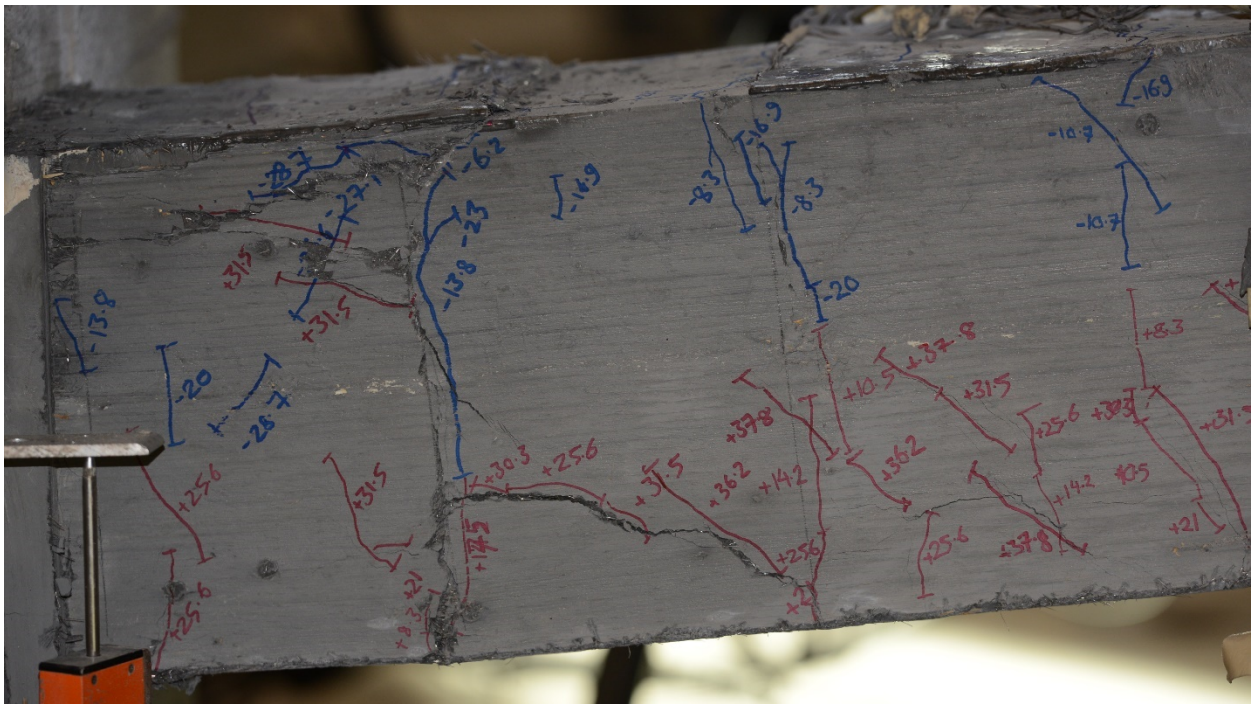

Figure 135. UHP-FRC #4 at 8.0% drift ratio.

Figure 136. UHP-FRC #4 at 9.0% drift ratio.

Figure 137. UHP-FRC #4 at 10.0% drift ratio.

The test pictures of the specimens at different values of drift ratio can be viewed from Figure 138 to Figure 140.

(a) **(b)**

Figure 138. Cracking in: (a) UHP-FRC #1 with high-strength steel at 5% (top) and 8% drift ratio (bottom) and (b) UHP-FRC #2 specimen with GFRP bars at 5% (top) and 10% (bottom) drift ratio.

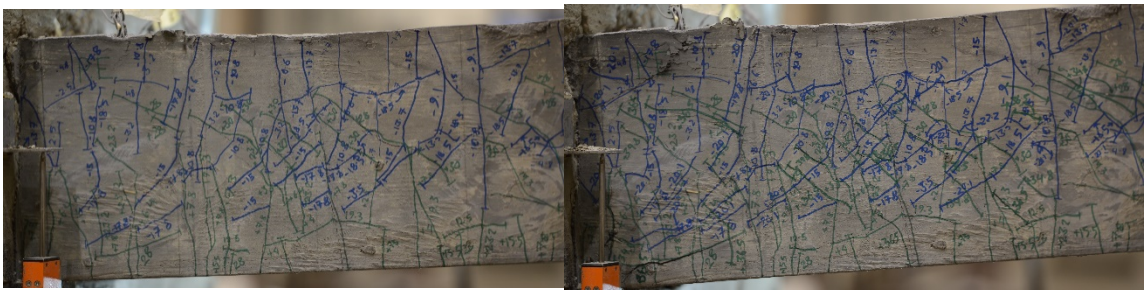

Figure 139. Cracking in UHP-FRC #3 specimen (PE fibers) with BFRP bars at 5% drift ratio(left) and 10% drift ratio (right).

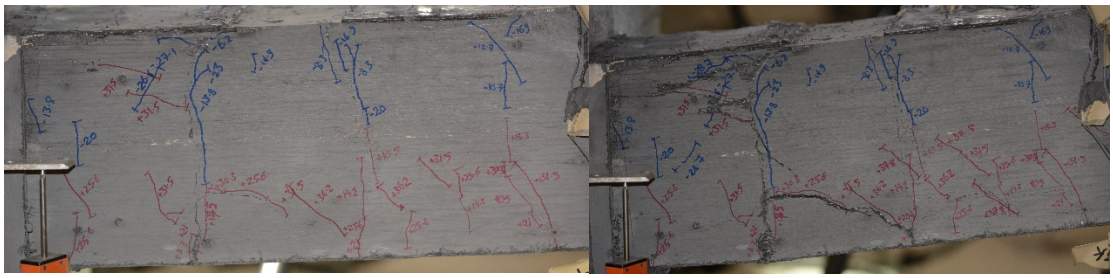

Figure 140. Cracking in UHP-FRC #4 specimen (steel fibers) with BFRP bars at 5% drift ratio (left) and 9% drift ratio (right).

A comparison between the maximum moment and the nominal moments are presented in Table 11. Figure 141 shows the combined Moment vs. drift ratios for all the specimens for comparison.

Table 11. Comparison between the calculated design nominal moment and the maximum recorded moment values.

Specimen	f_c' [a] ksi (MPa)	M_n [b] kip-in. (kN-m)	f_{cm}' [c] ksi (MPa)	M_n' [d] kip-in. (kN-m)	Maximum moment kip-in. (kN-m)	Design nominal moment vs. maximum moment	Modified nominal moment vs. maximum moment
UHP-FRC #1	22 (152)	792 (89)	18.7 (129)	768 (87)	840 (95)	6% higher	9% higher
UHP-FRC #2	22 (152)	1128 (116)	20.9 (144)	1060 (120)	1050 (119)	7% lower	1% lower
UHP-FRC #3	20 (138)	1271 (144)	15.2 (105)	1103 (125)	1470 (166)	16% higher	33% higher
UHP-FRC #4	22 (152)	1336 (151)	19.8 (137)	1263 (143)	1430 (162)	7% higher	13% higher

[a] Target compressive strength
[b] Design nominal moment
[c] Actual compressive strength
[d] Modified nominal moment

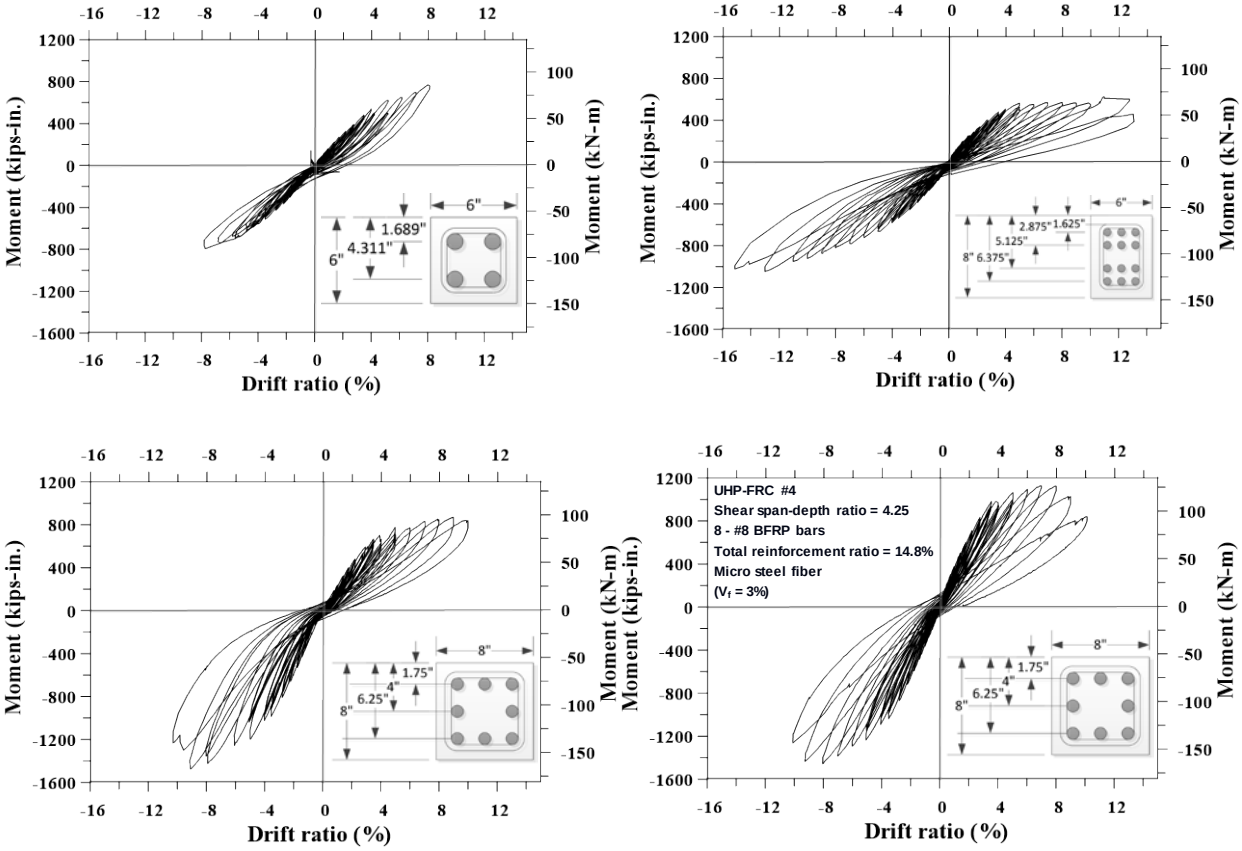

Figure 141. Combined moment vs. drift ratio for all the four specimens.

6. CONCLUSIONS

This pilot research investigated a new type of structural members made with ultra-high-performance materials including ultra-high-performance fiber-reinforced concrete (UHP-FRC), high-strength noncorrosive FRP rebars, and high-strength high corrosion resistant MMFX steel rebars. Two phases of experimental tests were carried out: Four specimens were prepared and tested under fully reversed cyclic loading. These beams were designed based on a newly developed design concept–the ductile-concrete strong-reinforcement (DCSR), in which UHP-FRC serves as the ductile component and reinforcement serves as the elastic components. Specimen designs followed the DCSR concept, and these design procedures are described in Sections 4.1.1, 4.1.2, 4.1.3, and 4.1.4.

The four UHP-FRC specimens represent reduced scale columns—one with corrosion resistant MMFX high-strength steel rebars (100 ksi as per ASTM A1035, 2016), one with non-corrosive high-strength GFRP (90 ksi) rebars, and two with non-corrosive high-strength BFRP (147 ksi) rebars—all of which were tested at UT Arlington under large displacement reversals to prove the proposed new DCSR design concept. All columns had a reinforcement ratio of 14%. The last two specimens were designed to have a smaller length-to-depth ratio to increase the shear force demand. UHMW polyethylene fibers (13 mm in length with a diameter of 0.0015 mm and a tensile strength of 375 ksi) were used for Specimen 3 while micro steel fibers (13 mm in length with a diameter of 0.2 mm and a tensile strength of 399 ksi) were used for Specimens 1,2, and 4.

Test results clearly indicated that the proposed structural members have a much larger stiffness, strength, and damage resistance compared to conventional reinforced concrete members. The proposed flexural members can also sustain very large cyclic displacements without major damage to the UHP-FRC material, which provided ample shear strength and confinement to the reinforcement throughout testing. Even with the high amount of reinforcement, UHP-FRC's superior ductility provided a very stable cyclic behavior up to very large drift ratios. The specimens also exhibited a self-centering ability, which considerably reduces the residual displacement after being subject to large displacements. The strain gauge reading of the flexural reinforcement shows, at a very large drift ratio, rupture occurred near the beam-support block interface along with the spreading of the elongation along the length of the rebar due to FRP's low axial stiffness. This makes the use of FRP reinforcements more suitable to UHP-FRC as it permits the distribution of deformation throughout the flexural reinforcement. This helps to avoid the regions of strain concentration and localized failure leading to the premature failure of specimens that can happen in UHP-FRC members with steel rebars. This premature rebar failure due to the strong bond between reinforcement and UHP-FRC has been observed in other research. From the test results, it is observed that the recorded maximum values of moment correspond to the design nominal moment beam specimens (Table 11). The test results (Figures 143, 144 and 145) also show that the high damage resistance and self-centering characteristics of the proposed UHP-FRC columns can provide excellent resilience for future infrastructures. Further analytical study is warranted to investigate the structural responses of building and bridge structures using the proposed structural members under severe ground motions.

REFERENCES

1. Horii, H., and Nemat-Nasser, S. Compression-Induced Microcrack Growth in Brittle Solids: Axial Splitting and Shear Failure. *Journal of Geophysical Research*, 1985. Volume: 90, No. B4, pp. 3105-3125.

2. Federal Highway Administration (FHWA). Ultra-High Performance Concrete. TechNote, FHWA-HRT-11-038, Federal Highway Administration, 2011. 8 pages.

3. Ahlborn, T., Harris, D., Misson, D., and Peuse, E. Characterization of Strength and Durability of Ultra-High-Performance Concrete Under Variable Curing Conditions. Transportation Research Record: Journal of the Transportation Research Board, No. 2251. Transportation Research Board of the National Academies, Washington, D.C., 2011. pp. 68–75. DOI: 10.3141/2251-07.

4. Aghdasi, P., Heid A.E., and Chao, S.-H. Developing Ultra-High-Performance Fiber-Reinforced Concrete for Large-Scale Structural Applications. *ACI Materials Journal*, September-October 2016. Volume: 113, No. 5, pp. 559-570.

5. Aviram, A., Stojadinovic, B., Parra-Montesinos, G. J., and Mackie, K. R. Structural response and cost characterization of bridge construction using seismic performance enhancement strategies. PEER Report No. 2010/01, 2010.

6. Bae, S. Seismic Performance of Full-Scale Reinforced Concrete Columns. Department of Civil, Architectural and Environmental Engineering, the University of Texas at Austin, Austin, TX, Dec. 2005, 312 pp.

7. ACI Innovation Task Group 6. Design Guide for the Use of ASTM A1035/A1035M Grade 100 (690) Steel Bars for Structural Concrete (ACI ITG-6R-10). American Concrete Institute, 2010.

8. Seliem, H.M., Hosny, A., Rizkalla, S., Zia, P., Briggs, M., Miller, S., Darwin, D., Browning, J., Glass, G.M., Hoyt, K., Donnelly, K., and Jirsa, J.O. Bond Characteristics of ASTM A1035 Steel Reinforcing Bars. *ACI Structural Journal*, 2009. V. 106, No. 4, pp. 530-539.

9. Wiss, Janney, Elstner Associates, Inc. (WJE) Mechanical Properties of ASTM A1035/A1035M High Strength Steel Bar Reinforcement. Chicago, IL, 2008. *Final Report*, WJE No. 2008.9901.0, 47 pp.

10. Mast, R.F., Dawood, M., Rizkalla, S.H., and Zia, P. Flexural Strength Design of Concrete Beams Reinforced with High-Strength Bars. *ACI Structural Journal*, 2008. V. 105, No. 5, Sept.-Oct., pp. 570-577.

11. National Cooperative Highway Research Program (NCHRP). Use of Fiber-Reinforced Polymers in Highway Infrastructure. NCHRP Synthesis 512, 2017. 159 pages.

12. SP Systems Guide to Composites. Composite Engineering Materials - Systems

13. ACI Committee 440. Guide for the Design and Construction of Structural Concrete Reinforced with Fiber-Reinforced Polymer (FRP) Bars (ACI 440.1R-15). American Concrete Institute, 2015.

14. Naani, A. Flexural Behavior and Design of RC Members Using FRP Reinforcement. *Journal of Structural Engineering*, 1993. Volume: 119, No. 1, pp. 3344-3359. DOI: 10.1061/(ASCE)0733-9445(1993).119:11(3344)

15. ACI Committee 318. Building Code Requirements for Structural Concrete (ACI 318-14) and Commentary (ACI 318R-14). American Concrete Institute, Farmington Hills, MI, 2014. 519 pp.

16. Nagasaka, T., Fukuyums, H., and Tanigaki, M. Shear Performance of Concrete Beams Reinforced with FRP Stirrups. Fiber-Reinforced-Plastic Reinforcement for Concrete Structures-International Symposium, SP-138, American Concrete Institute, Farmington Hills, MI, 1993. pp. 789-811.

17. Sonobe, Y., Fukuyama, H., Okamoto, T., Kani, N., Kimura, K., Kobayashi, K., Masuda, Y., Matsuzaki, Y., Mochizuki, S., Nagasaka, T., Shimizu, A., Tanano, H., Tanigaki, M., and Tenshigawara, M. Design Guidelines of FRP Reinforced Concrete Building Strcutures. *Journal of Composites for Construction*, 1997. Volume: 1, No. 3, pp.90-115. DOI: 10.1061/(ASCE)1090-0268(1997)1:3(90)

18. Michaluk, C.R., Rizkalla, S., Tardros, G., and Benmokrane, B. Flexural Behavior of One-Way Concrete Slabs Reinforced by Fiber Reinforced Plastic Reinforcement. *ACI Structural Journal*, 1998. Volume:95, No. 3, pp. 353-364.

19. Tureyen, A.K., and Frosch, R.J. Shear Tests of FRP Reinforced Concrete Beams without Stirrups. *ACI Structural Journal*, 2002. Volume: 99, No. 4, pp. 427-434.

20. Chao, S.H., Kaka, V., Palacios, G., Kim, J., Choi, Y.J., Aghdasi, P., Nojavan, A., and Schultz, A.E. Seismic Behavior of Ultra-High-Performance Fiber-Reinforced Concrete Moment Frame Members. First International Interactive Symposium On UHPC, Des Moines, Iowa, 2016.

21. Palacios, G., Liu, X., Chao, S.H., Nojavan, A., and Schultz, A.E. Seismic Performance of a Highly Damage-Tolerant Ultra-High-Performance Fiber-Reinforced Concrete Column. 16th World Conference on Earthquake (16WCEE), Santiago Chile, 2017. Paper No. 2833.

22. ACI Committee 374. ACI 374.2R-13: Guide for Testing Reinforced Concrete Structural Elements under Slowly Applied Simulated Seismic Loads. American Concrete Institute, Farmington Hills, Michigan, 2013.

23. Choi, H., Palacios, G., Popovics, J.S., and Chao, S.H. Monitoring Damage in Concrete Columns Using Ultrasonic Tomography. *ACI Structural Journal*, 2018.

24. AASHTO. LRFD Bridge Design Specifications. 7th edition, American Association of State Highway and Transportation Officials (AASHTO), Washington, D.C., 2017.

25. Kaka V. Applications of Ultra-High-Performance Fiber-Reinforced Concrete (UHP-FRC) on Flexural Structural and Architectural Members. Master's Thesis, The University of Texas at Arlington, 2017.

26. Graybeal, B.A., and Davis, M. Cylinder or Cube: Strength Testing of 80 to 200 MPa (11.6 to 29 ksi) Ultra-High Performance Fiber-Reinforced Concrete. *ACI Materials Journal*, 2008. Volume: 105, No. 6, pp. 603-609.